January 2009

Multi-element isotopic analyses of presolar graphite grains from the Orgueil meteorite

Manavi Jadhav
Washington University in St. Louis

WASHINGTON UNIVERSITY

Department of Earth and Planetary Sciences

Dissertation Examination Committee:
Ernst K. Zinner, Co-chair
Frank A. Podosek, Co-chair
Thomas J. Bernatowicz
Charles M. Hohenberg
Frédéric Moynier
Jill D. Pasteris

MULTI-ELEMENT ISOTOPIC ANALYSES OF PRESOLAR GRAPHITE GRAINS FROM THE ORGUEIL METEORITE

by

Manavi Jadhav

A dissertation presented to the
Graduate School of Arts and Sciences
of Washington University in
partial fulfillment of the
requirements for the degree
of Doctor of Philosophy

August 2009

Saint Louis, Missouri

ABSTRACT OF THE DISSERTATION

Multi-Element Isotopic Analyses of Presolar Graphite Grains from the Orgueil Meteorite

by

Manavi Jadhav

Doctor of Philosophy in Earth and Planetary Sciences

Washington University in St. Louis, 2009

Professor Ernst K. Zinner, Co-chair

Professor Frank A. Podosek, Co-chair

This dissertation presents the results and implications of the isotopic analyses of presolar graphite grains from the primitive carbonaceous chondrite, Orgueil. Graphite grains from low- and high-density fractions were analyzed for C, N, O, Si, Al-Mg, K, Ca, and Ti isotopes. These analyses indicate that isotopic properties are density dependent. Most low-density grains come from supernovae as indicated by large ^{18}O, ^{15}N, ^{28}Si excesses, high inferred ^{26}Al/^{27}Al and ^{41}Ca/^{40}Ca ratios, and the initial presence of the short-lived radionuclide ^{44}Ti in some grains. Some high-density grains also show supernovae signatures, but a majority seems to originate from low-metallicity asymptotic giant branch stars. Evidence for this comes from correlated ^{12}C and ^{30}Si enrichments. In low-metallicity asymptotic giant branch stars, ^{12}C and ^{29,30}Si that are produced in the He shell are mixed into the envelope by the third dredge-up during the thermally pulsing phase. This scenario also increases the C/O ratio of the envelope and favours the condensation of graphite grains over SiC grains. A

minor fraction of high-density graphite grains exhibits very low $^{12}C/^{13}C$ ratios and extremely large $^{42,43}Ca$ and $^{46,47,49,50}Ti$ excesses. These excesses are much larger than those expected in the envelopes of asymptotic giant branch stars and are as large as those predicted for pure He-shell material in those stars and the interior, O-rich zones of type II supernovae. However, these zones have almost pure ^{12}C, making the low $^{12}C/^{13}C$ ratios enigmatic. We propose that born-again, asymptotic giant branch stars that have undergone a very late thermal pulse, such as Sakurai's object, might be the stellar source for these grains. In such stars, limited mixing of the He-burning intershell with the thin, residual hydrogen envelope leads to the production of ^{13}C and enables material with s-process enrichments and low $^{12}C/^{13}C$ ratios to occur on the surface simultaneously. This study concludes that low-density graphite grains originate from supernovae while high-density graphite grains have multiple stellar sources: low-metallicity and born-again asymptotic giant branch stars, as well as supernovae.

Acknowledgements

To leave graduate school with ones enthusiasm for science and academia completely intact and, in fact, greatly enhanced, is a rare occurence. I am one such lucky graduate student. I am greatly indebted to my advisor and mentor, Ernst Zinner, for making this possible. Thank you, Ernst, for teaching me everything I know. It has been an honour to learn from one of the pioneers of our research field and I feel privileged to be your "scientific daughter". I am grateful for the patience and encouragement with which you have helped me identify my weaknesses and worked with me to overcome them. Thank you for all your help in trying to tame the beast of a NanoSIMS! I learnt more than science from you and will cherish our chats about travelling, photography, mountains, hiking, music, and so much more. I always walk away from your office having learnt something new everyday.

Sachiko Amari graciously shared her knowledge and taught me everything I know about presolar graphite grains. I am eternally grateful to you, Sachiko, for helping me, a complete novice to a laboratory, especially a chemistry lab, learn all the skills required for this dissertation. I am very fortunate to have had the opportunity to learn the chemical separation technique from the person who played a major role in developing it. You have been such a tremendous source of moral support. Apart from being a great co-advisor, you have been a very special friend, mentor, and guide.

I would like to thank Frank Podosek for agreeing to be my official advisor at the Department of Earth and Planetary Sciences and for his extremely informative classes on Meteorites, Radiogenic Isotopes and Methods of Geochemistry. I also thank the

rest of my committee members: Tom Bernatowicz, Jill Pasteris, Charles Hohenberg, and Fred Moynier, for agreeing to be on my commitee and for their valuable comments on this thesis.

The chemical and physical separation of graphite grains from Orgueil was carried out by Teruyuki Maruoka. I am extremely grateful for his endeavour without which this dissertation might have taken a completely different path. I thank Roberto Gallino for providing us with the AGB nucleosynthesis models used in this dissertation. Roberto's enthusiasm for science and life, in general, is so infectious – it has always been a great pleasure to work with him. I had a chance to work with Mike Savina at Argonne National Lab. Thank you, Mike, for taking the time to explain the intricacies of CHARISMA. Above all, thanks for helping me view the trials and tribulations of experimental science in a positive light. I am also grateful to Kuljeet Marhas for teaching me a lot about the NanoSIMS. I am very fortunate to have had the opportunity to work with and learn from her.

I thank Frank Stadermann and Christine Floss for their help with using the NanoSIMS, Auger Nanoprobe and the SEM. I am grateful to Kevin Croat for helping me deal with micromanipulator problems. My colleague, Frank Gyngard was a great help during NanoSIMS measurements.

Tim Smolar was extremely helpful in keeping all the machines running. I deeply appreciate him being available to replace/clean the ion sources on weekends. I am indebted to Hugh Chou for helping me deal with my love-hate relationship with computers – if not for him I would be turning in a handwritten dissertation! Also, Jan Foster went out of her way to spoil our research group by tackling all the bureaucracy for us. I do not know what I would have done without her help and guidance.

I am very grateful to Doug Green, my former advisor at Ohio University. Thank you for giving me a shot at graduate school and explaining the bull dog's bite-phenomenon to me. Your mentorship has had a major role in making this disser-

tation possible. I would also like to thank my very first Astronomy advisor, Arvind Paranjpye, for introducing me to the wonders of planetary science and astronomy.

Without the support of all my friends, this dissertation would not have been possible. I thank all my friends in graduate school for being such great buddies and making everything so much more tolerable. I love Maitrayee for spoiling me and cooking Indian food for me. Thank you, Cyn, for making the last few months of "dissertating" so much more tolerable by writing with me. I am extremely fortunate to have friendships that have lasted decades – Mohit and Vayu, thank you for always being there for me. Vayu, thanks for all your help with LaTeX and good-naturedly humouring my obssession to write in LaTeX without knowing much about it.

My best friend, Ryan, deserves a lot of credit for this dissertation. You have helped me through times that I thought I would never recover from, and you also taught me to find humour in all situations. I doubt I can ever repay you for this. I am so grateful for all your help with meeting deadlines over the years and putting up with all my mind-numbing formatting demands. Those late-night tuna casseroles, shrimp scampi, and all the home-cooked meals have kept me alive all these years! And, thank you for Gauge.

Without my family, none of this could have been possible. My parents and brother have been my pillars of support and, have had to sacrifice a lot to help me pursue my dreams and turn them into reality. I thank them from the bottom of my heart for their unconditional love and encouragement over the years. This dissertation is as much your achievement, Ma, Baba and Adit, as it is mine.

In memory of Mary Stoertz

..... like the brightest star in the sky your life was short

but you left us all with what we need to shine .....

Contents

Abstract of the Dissertation **ii**

Acknowledgements **iv**

List of Figures **xii**

List of Tables **xiii**

1 INTRODUCTION AND BACKGROUND **1**

1.1 Discovery of presolar grains 2

1.2 Studying presolar grains 5

1.3 Types of presolar grains 6

1.4 Presolar graphite grains 10

1.5 Overview of the presented research and dissertation 17

1.6 Statement of Labor 17

2 ISOTOPIC ANALYSIS OF PRESOLAR GRAPHITE GRAINS FROM ORGUEIL **25**

2.1 Introduction 26

2.2 Experimental procedure and methods 27

2.3 Results 28

2.4 Discussion 32

2.5 Conclusions 33

3 NEW STELLAR SOURCES FOR HIGH-DENSITY, PRESOLAR GRAPHITE GRAINS 36

3.1 Introduction . . . 37

3.2 Experimental Methods . . . 38

3.3 Results . . . 40

3.4 Discussion . . . 42

3.5 Conclusions . . . 51

4 MULTI-ELEMENT ISOTOPIC ANALYSES OF PRESOLAR GRAPHITE GRAINS FROM ORGUEIL 56

4.1 Introduction . . . 57

4.2 Experimental Methods . . . 60

4.2.1 Chemical and physical separation of the graphite grains . . . 60

4.2.2 Grain-mount nomenclature . . . 61

4.2.3 Sample preparation . . . 61

4.2.4 EDX analyses and grain mount documentation . . . 63

4.2.5 NanoSIMS analyses . . . 64

4.3 Results . . . 68

4.3.1 Isotopic compositions of the grains . . . 68

4.4 Discussion . . . 79

4.4.1 Nucleosynthetic Sources for Orgueil graphite . . . 80

4.4.2 Comparison with Murchison graphite . . . 95

4.4.3 Unresolved issues . . . 96

4.5 Summary . . . 97

5 SUMMARY AND FUTURE PERSPECTIVES 147

List of Figures

1.1 Schematic representation of the life of presolar grains. 2
1.2 Stellar sources of presolar grains. 3
1.3 Exotic noble gas components in presolar grains. 4
1.4 Bulk abundances of presolar grains in carbonaceous chondrites. 7
1.5 SEM images of presolar graphite from Murchison. 11
1.6 TEM images of slices of presolar graphites 12
1.7 Carbon and nitrogen isotopic ratios in Murchison graphites. 13
1.8 Carbon and oxygen isotopic ratios in Murchison graphites. 15
1.9 Silicon isotopic ratios in Murchison graphites. 16

2.1 Carbon, nitrogen and oxygen isotopes in Orgueil graphite grains . . . 29
2.2 Silicon isotopic ratios of Orgueil graphite grains 31
2.3 Carbon isotopes and δ^{30}Si in Orgueil graphite grains 32

3.1 Ca and Ti isotopic patterns of 3 HD graphite grains from SNe 43
3.2 Ca and Ti isotopic patterns of HD graphite grain, g-9 45
3.3 Ca isotopic pattern of HD graphite grain, g-34 47
3.4 Ca isotopic patterns in HD graphite grains, g-29 and g-40 49

4.1 SE images of presolar graphite grains from Orgueil 108
4.2 Distribution of C isotopic ratios in presolar graphite grains 109
4.3 Carbon and nitrogen isotopic ratios in presolar graphite grains 110
4.4 Carbon and oxygen isotopic ratios in presolar graphite grains 111

4.5 Silicon isotopic ratios in presolar graphite grains 112
4.6 Carbon isotopic ratio and $\delta^{30}Si/^{28}Si$ in HD presolar graphites 113
4.7 Mg isotopic ratios in LD graphites 114
4.8 Mg isotopic ratios in HD graphites 115
4.9 Inferred values of $^{26}Al/^{27}Al$ in presolar graphite grains 116
4.10 Inferred values of $^{41}Ca/^{40}Ca$ in presolar graphite grains 117
4.11 Ca isotopic ratios in LD graphites from Orgueil 118
4.12 Ca isotopic ratios in HD graphites from Orgueil 119
4.13 Depth profile of various ion signals showing ^{44}Ca and ^{48}Ti signal correlations 120
4.14 Ti isotopic ratios in LD graphites 121
4.15 Ti isotopic ratios in HD graphites from Orgueil 122
4.16 Ca isotopic patterns of grains with ^{44}Ca excesses 123
4.17 Supernova structure and important isotopic abundances in SN layers 124
4.18 Inferred $^{44}Ti/^{48}Ti$ ratios in graphite grains from Orgueil 125
4.19 Model abundances of $^{40,41,42,43,44}Ca$ and the $^{41}Ca/^{40}Ca$ ratio in the interior of a type II SN 126
4.20 Model abundances of $^{44,46,47,48,49,50}Ti$ isotopes in the interior of a type II SN 127
4.21 Mixing calculation results for grain OR1d4m-3 128
4.22 Mixing calculation results for grain OR1d1m-11 129
4.23 Ti isotopic pattern in grain with large ^{47}Ti anomaly 130
4.24 Mixing calculation results for grain OR1f(1,2)m-o67 131
4.25 Ca isotopic patterns of grains with extreme anomalies that match He shell values 132
4.26 Mixing calculation results for grain OR1f2m-25 133
4.27 Ti isotopic pattern of ^{12}C-enriched HD graphites 134

4.28 Ca and Ti isotopic patterns of HD grains 135

List of Tables

2.1 Density fractions of presolar graphite from Orgueil 28

3.1 C, N, O, Si, Al-Mg, K, Ca, and Ti isotopic Ratios of HD graphite grains with $^{12}C/^{12}C < 20$ 41

4.1 Density fractions of Orgueil presolar graphites 136

4.2 Measurement phases for NanoSIMS measurements 137

4.3 C, N, O, and Si isotopic ratios of presolar graphite grains from Orgueil 138

4.4 Mg isotopic ratios and inferred $^{26}Al/^{27}Al$ ratios for Orgueil graphites 140

4.5 K isotopic ratios and inferred $^{41}Ca/^{40}Ca$ ratios of graphite grains . . . 142

4.6 C, Ca, and Ti isotopic ratios of LD graphite grains 143

4.7 Ca isotopic ratios and inferred $^{44}Ti/^{48}Ti$ ratios of graphite grains . . . 144

4.8 C, Ca, and Ti isotopic ratios of HD graphite grains 145

4.9 Results of mixing calculations 146

Chapter 1

INTRODUCTION AND BACKGROUND

At the end of a star's life, the elements that it has produced are ejected into the interstellar medium (ISM). This material modifies the composition of the ISM and new stars are formed from this ISM. Thus, material is continuously recycled in the universe. Presolar grains are tiny pieces of such material that were ejected into the ISM through stellar outflows or explosions. Some of these grains became incorporated in the protosolar nebula and remained unaltered during the entire process of solar system formation. As the solar system continued to evolve, these grains were incorporated via accretion, into solar system objects, like meteorites. Consequently, primitive meteorites that fall to Earth carry presolar grains in them. Figure 1.1 is a schematic representation of the life of presolar grains. These grains condensed in the atmospheres of evolved stars and supernova ejecta, and preserve the original compositions of their parent stars. Figure 1.2 shows images of some stellar environments in which presolar grains formed.

These grains provide us with an excellent opportunity to study a wide range of astrophysical and cosmochemical problems in the laboratory. Prior to the discovery of presolar grains, most of the information on stars and their chemical compositions came from telescopic observations. The properties of interstellar grains initially were studied indirectly, through the effect they had on light traveling from the stars to the telescopes. Presolar grains are bona fide pieces of this same material that can

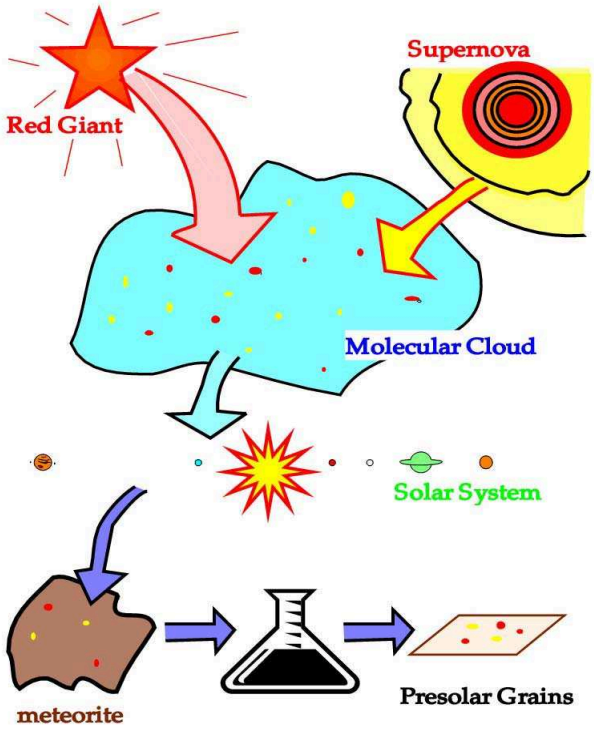

Figure 1.1 A schematic representation of the life of presolar grains (Courtesy: Larry Nittler).

now be analyzed with amazing precision in a modern geochemical laboratory. These studies, combined with astronomical observations, can provide information on stellar nucleosynthesis and evolution, the formation of dust in stellar environments, and its processing in the interstellar medium, the formation of the solar system, and galactic chemical evolution.

1.1 Discovery of presolar grains

For a long time it was believed that early solar system material was entirely homogenized in the hot solar nebula (Cameron, 1962). Under this assumption, the isotopic compositions of solar system materials should be uniform everywhere. Physical and chemical processes in the early solar system, like mass-dependent fractionation and radioactive decay, were capable of changing the isotopic composition of solar system materials by not more than a few parts per thousand. However, the discovery of large

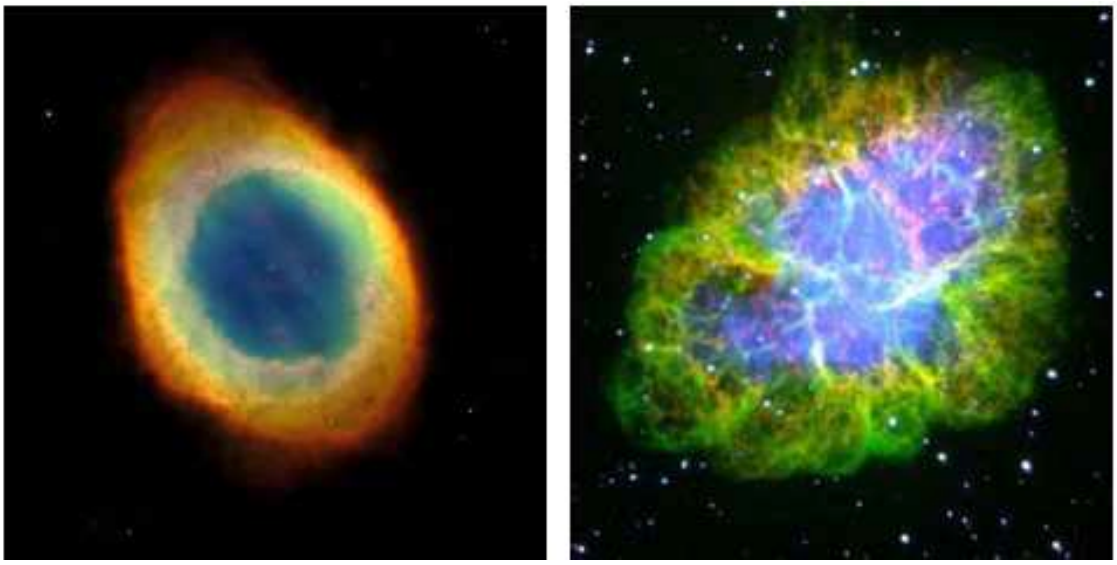

Figure 1.2 Left panel- Hubble Space Telescope image of the Ring Nebula (M57): This is an image of a planetary nebula whose central dying star had the same mass as that of the sun. Such stars release gas and dust into the ISM at the ends of their lives. Right Panel- Chandra X-ray Observatory image of the Crab Nebula (M1): This is an optical image of a supernova remnant of a massive star ($> 8\ M_{\odot}$) that exploded and released material into the ISM on a much larger scale. Such environments are the likely stellar sources of presolar grains. (Sources: http://hubblesite.org/ and http://chandra.harvard.edu/).

isotopic 'anomalies' (departure from solar system values) in primitive meteorites challenged the idea of a completely homogenized solar nebula (e.g., Reynolds and Turner, 1964; Black and Pepin 1969; Clayton et al., 1973; Lewis et al., 1983; Halbout et al., 1986). There was now a possibility that primitive meteorites host interstellar particles that had different histories compared to objects in the solar system. The large magnitudes of these anomalies can only be explained by nuclear reactions (that occur at millions of degrees), which alone are capable of changing nuclear structure. Thus, presolar material can be identified by the presence of large isotopic anomalies.

It was the discovery of unusual xenon and neon components with extreme isotopic compositions in carbonaceous chondrites by Reynolds and Turner (1964) and Black and Pepin (1969) that initiated the idea of an isotopically heterogeneous solar nebula. Black and Pepin (1969) found a Ne component that was enriched in ^{22}Ne

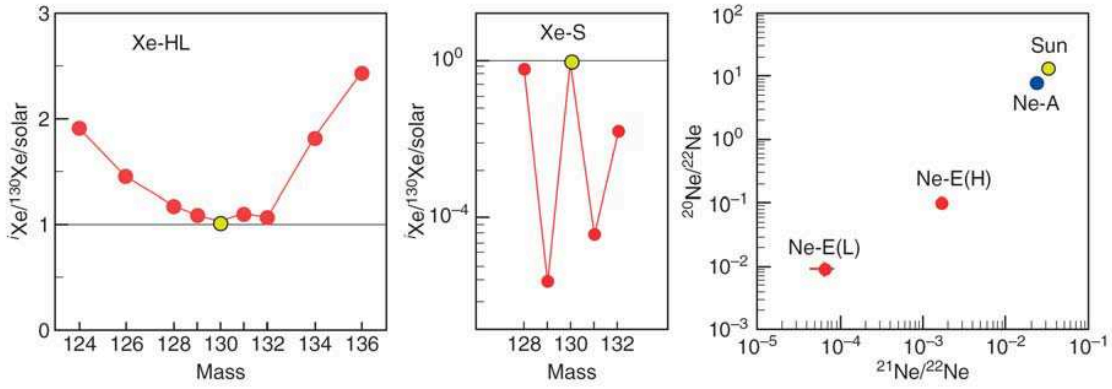

Figure 1.3 The exotic components of Xe and Ne that led to the discovery of presolar grains. (Source: Zinner, 2004).

and had $^{20}Ne/^{22}Ne < 3.4$ in C-chondrites. The $^{20}Ne/^{22}Ne$ and $^{21}Ne/^{22}Ne$ ratios observed in these meteorites are almost 10^{-3} times the solar value (Figure 1.3). This ^{22}Ne-rich component was released between 900 °C and 1000 °C and named Ne-E by Black (1972). Later, studies of different density fractions of Orgueil and Murchison by Eberhardt et al. (1979), Lewis et al. (1979), and Jungck (1982) led to the discovery of two types of Ne-E during step-wise heating: Ne-E(L) is released at low temperatures (500 – 800 °C) and Ne-E(H) is released at temperatures of about 1100 – 1500 °C. The low-(2.2 – 2.5 g cm^{-3}) and high-(2.5 – 3.1 g cm^{-3}) density fractions of silicate-free residues of carbonaceous chondrites were found to contain the low- and high-temperature components, respectively. Low values of $^{20}Ne/^{22}Ne$ indicated the presence of nearly "pure" ^{22}Ne in the density fractions and suggested a stellar origin for Ne-E. Black (1972), Clayton (1975), Eberhardt et al. (1981), and Jungck (1982) suggested that the decay of ^{22}Na could be the possible source of ^{22}Ne in the meteorites. This ^{22}Na would have to have been incorporated into the grains within the very short time span of less than 2.6 years, i.e., the half life of ^{22}Na. Reynolds and Turner (1964) found two exotic components of Xe while studying the chondrite, Renazzo. It was found that the light isotopes, ^{124}Xe and ^{126}Xe, and the heavy isotopes, ^{134}Xe and ^{136}Xe, were all highly enhanced with respect to the solar value. This component was

called Xe-HL or Xe-heavy and light (Figure 1.3). The Xe-L component is produced by proton capture (p-process) or photodisintegration, whereas the Xe-H component is a product of the rapid neutron capture process (r-process). A second component of Xe was discovered by Srinivasan and Anders (1978) while studying Murchison. They found ^{128}Xe and ^{130}Xe to be enhanced, and attributed their production to the slow neutron capture process (s-process). This component was called Xe-S (Figure 1.3).

The quest to isolate the carriers of these exotic noble gas components led to the first isolation of presolar grains from primitive meteorites by the Anders group at the University of Chicago. Through a series of physical and harsh chemical separation procedures pioneered by Tang et al. (1988) and Amari et al. (1994), the first interstellar grains were isolated. Lewis et al. (1987) found nanodiamonds to be the carriers of Xe-HL. Silicon carbide (SiC) grains were the carriers of the Xe-S and Ne-E(H) components (Bernatowicz et al., 1987; Tang and Anders, 1988). Also, Amari et al. (1990) established the carrier of the low-temperature Ne component [Ne-E(L)] to be interstellar graphite. All of these presolar phases are fairly resistant to the chemical separation processes, simplifying their isolation, but their microscopic (and sometimes sub-microscopic) nature and their low abundances make studying these grains a challenge.

1.2 Studying presolar grains

New chemical and microanalytical tools had to be developed and adapted to study the newly discovered presolar grains. Different techniques are used to analyze various aspects of these grains. Their morphologies and chemical compositions are studied with scanning electron microscopes (SEM). Raman spectroscopy and electron diffraction analysis in a transmission electron microscope (TEM) are used to obtain the crystallographic structure of the grains. TEM studies are also able to find and analyze internal subgrains in presolar grains. Bulk isotopic analyses of noble gases on presolar

material are carried out with gas mass spectrometry (GMS). High-precision isotopic measurements of heavy elements like Sr, Ba, Nd, and Sm from grain aggregates can be obtained by thermal ionization mass spectrometry (TIMS), inductively coupled plasma mass spectrometry (ICP-MS), and secondary ion mass spectrometry (SIMS). Bulk analyses provide average isotopic compositions over many grains. Single-grain noble gas measurements can also be carried out with laser heating (Nichols et al. 1995; Heck et al. 2005). Since every grain carries unique information about its parent star, it has become increasingly important to be able to carry out single-grain isotopic analysis.

Conventional SIMS machines (e.g., CAMECA IMS-3f) were able to provide reasonably precise isotopic measurements for several elements in grains of sizes ≥ 1 μm and ones that had relatively high elemental abundances. However, the new CAMECA NanoSIMS-50 and 50L are capable of achieving very high spatial resolutions (30 – 200 nm). They also have high sensitivity at high mass resolutions and multidetection systems. Due to its unique ion optical design, the NanoSIMS can achieve 30 times higher secondary ion transmission at mass resolving powers of $\sim$ 5000 (needed for most measurements, e.g., O isotopes, in order to separate atomic ions from molecular interferences), compared to the CAMECA IMS-3f. Much smaller presolar grains can now be analysed because of this multidetection capability and the increased spatial resolution, which increase overall sensitivity. Heavy-element isotopes in single grains can be analyzed with laser ablation and resonant ionization mass spectrometry (RIMS) (Savina et al., 2003). This technique enables heavy-element isotopic analyses without any isobaric interference.

1.3 Types of presolar grains

Figure 1.4 shows the types of presolar grains discovered in primitive meteorites and their respective abundances. Presolar grains have been found in the matrices of

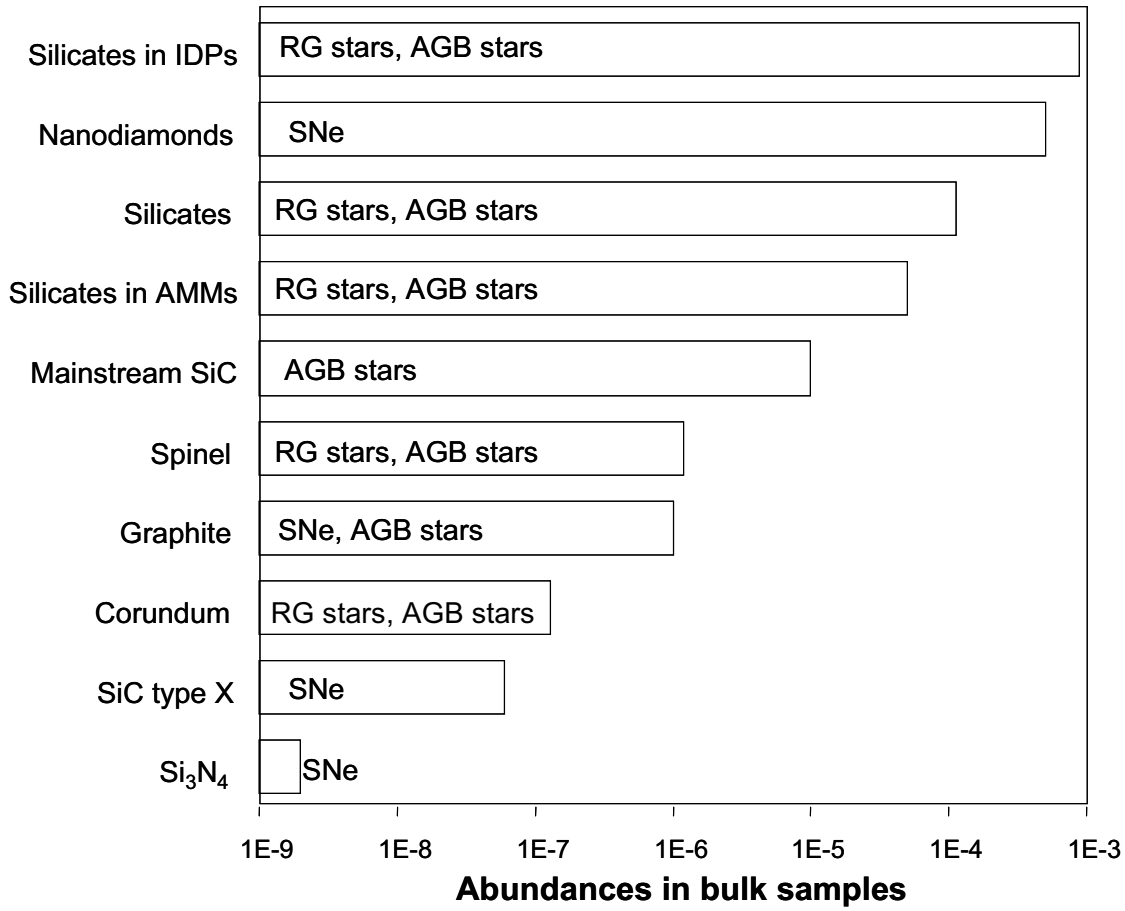

Figure 1.4 Bulk abundances of the different types of presolar grains identified in primitive chondrites. (Source: Nyugen, 2005).

all classes of primitive meteorites or chondrites. Their matrix-content-normalized abundances depend on the degree of metamorphism that the meteorite has been subjected to. The type and extent of metamorphism affect different presolar grains differently. Carbonaceous chondrites are the least thermally metamorphosed, and their chemical compositions are identical to those observed in the solar photosphere (except the volatile elements). The CI (e.g., Orgueil) and CM2 (e.g., Murchison) carbonaceous chondrites are such meteorites. These meteorites naturally contain the largest absolute number of presolar grains and thus, would be the most obvious searching grounds for presolar grains.

Nanodiamonds were the first presolar grains to be isolated (Lewis et al., 1987).

They are the most abundant type ($\sim$ 500 ppm) but, unfortunately, the least understood. This is because nanodiamonds are very small ($\sim$ 2.5 nm in diameter) and therefore, impossible to study individually. The only available evidence of their presolar nature is from the presence of the Xe-HL component (Lewis et al., 1987), and anomalies in Te and Pd isotopic ratios (Richter et al., 1998; Maas et al., 2001). All these signatures indicate a supernova origin. The carbon isotopic ratios are close to solar, which could be due to an averaging effect, since these measurements were made on diamond aggregates and not individual grains. The $^{14}N/^{15}N$ ratio is about 35 % higher than the solar value but has been shown to agree with the ratio observed in Jupiter (Owen et al., 2001). It remains to be verified which fractions of nanodiamonds are actually presolar.

Presolar SiC grains are the most extensively studied presolar material. This is principally because they are relatively easy to extract and their sizes range from $\sim$ 0.5 μm in diameter to over 30 μm, making them easier to study individually. They have an abundance of $\sim$ 10 ppm (Huss and Lewis, 1995) in carbonaceous, ordinary, and enstatite chondrites. They are carriers of the Xe-S and Ne-E(H) components. Almost every major, minor, and trace element shows isotopic anomalies. SiC grains are classified into seven populations according to their C, N, and Si compositions. Mainstream SiC grains ($\sim$ 93% of all grains) have $^{12}C/^{13}C$ ratios that range from 10 to $\sim$ 100 (i.e., solar value). Their N isotopic ratios also vary from just below solar ($^{14}N/^{15}N \sim 200$) to highly ^{14}N-enriched ($^{14}N/^{15}N \sim 20{,}000$). These signatures indicate an origin in asymptotic giant branch (AGB) stars (Hoppe et al., 1994). Type X SiC grains (1% of all SiC grains) are depleted in ^{29}Si and ^{30}Si (Amari et al., 1992), which indicates they originated in supernovae (SNe). Most of these grains exhibit excesses in ^{12}C and ^{15}N. Type Y (Amari et al., 2001a) and Z grains (Hoppe et al., 1997) have $^{12}C/^{13}C \sim 100 - 400$ and $4 - 90$, respectively, and ^{30}Si enrichments relative to the mainstream correlation line. Type A+B grains have $^{12}C/^{13}C < 10$ but Si ratios

similar to those of mainstream grains (Amari et al., 2001b). The Y and Z grains might originate from low-mass and -metallicity (lower than solar) AGB stars as suggested by Amari et al. (2001a) and Hoppe et al. (1997). The origin of A+B grains is still under debate but, J-type stars seem to be a likely source (Lambert et al., 1986). A few nova SiC grains are known (Amari et al., 2001c; José et al., 2004; Nittler and Hoppe, 2004 a;b). These grains have $^{12}C/^{13}C = 4 - 9$, $^{14}N/^{15}N = 5 - 20$ and ^{30}Si excesses. Their $^{29}Si/^{28}Si$ ratios are close-to-solar values.

Presolar oxide grains in meteorites have also been identified. Their oxygen isotopic compositions have been used to classify them into four groups (Nittler et al., 1997): Group 1 grains are depleted in ^{18}O and have large ^{17}O excesses. They originate from red giant and AGB stars. Group 2 grains are highly depleted in ^{18}O and have large ^{17}O excesses. These depletions have been explained by extra-mixing (cool bottom processing (CBP) in low-mass, AGB stars wherein material from the convective envelope is transported to the underlying, outer boundaries of the H-burning region. This results in partial H burning of the envelope material (Wasserburg et al., 1995). Group 3 oxide grains are believed to have originated from low-metallicity red giant and AGB stars, because they are depleted in ^{17}O and ^{18}O. However, some group 3 grains were recently thought to contain SN signatures (Nittler et al., 2008). Group 4 grains exhibit enrichments in both ^{17}O and ^{18}O, and could originate from metal-rich stars and type II SNe (Choi et al. 1998).

Presolar silicates were discovered in IDPs (Messenger et al., 2003) and in the Acfer 094 carbonaceous chondrite (Nguyen and Zinner, 2004). Silicates in CI chondrites are easily transformed by aqueous alteration into hydrous silicates. This process erases the presolar signatures in oxygen from these grains. Therefore, pristine silicates are only likely to be found in the least aqueously altered meteorites. Furthermore, the presolar silicates are very small ($\sim 0.2 - 0.9$ μm) and were, until recently, impossible to find in meteorites, which are dominated by solar system silicates. But with the

advent of new isotopic imaging capabilities, these silicates were finally discovered and analyzed. Presolar silicates have oxygen isotopic properties similar to those of presolar oxides.

Silicon nitride grains are the least abundant presolar grain type. Like Type X SiC grains, they exhibit excesses in ^{28}Si, ^{15}N, and ^{13}C and, have high ^{26}Al/^{27}Al ratios. They are thought to have originated from type II SNe (Nittler et al., 1995).

Presolar phases are also found within other presolar grains during TEM studies. Tiny subgrains of Ti-, Fe-, Zr-, Mo-carbides, kamacite (Fe-Ni), cohenite ($(Fe,Ni)_3C$), metallic osmium, and elemental iron have been found in presolar graphite grains. Presolar graphite grains, which are the focus of this dissertation, are discussed in detail in the following section.

1.4 Presolar graphite grains

Presolar graphite was first isolated from the Murchison meteorite as the carrier of Ne-E(L) (almost pure ^{22}Ne) by Amari et al. (1990). Since then these grains have been extensively studied in Murchison, and almost everything we know about presolar graphite is based on these studies (Amari et al., 1990; 1995; Zinner et al., 1995; Hoppe et al., 1995; Travaglio et al. 1999). Although graphite can be found in the most primitive meteorites (Huss and Lewis, 1995), it has a low abundance compared to SiC (Huss and Lewis, 1995) and the separation procedure for graphite is far more complicated than that for SiC (Amari et al., 1994). Complications in separation arise because graphite is not as chemically resistant as SiC or the oxides, and because it needs to be isolated from other carbonaceous material in the meteorite that has chemical properties similar to graphite's. The separation procedure (Amari et al., 1994) consisted of dissolution of silicates, removal of sulphur, mild oxidation to remove the peripheral abundant, amorphous, and disordered carbonaceous material, eventually followed by density separation in order to study graphite of various densities.

Presolar graphite grains exhibit a low degree of crystallinity compared to terrestrial graphite. However, they are fairly well-ordered and exhibit a range of densities. The density of presolar graphite is an important parameter to determine because it reflects the degree of crystallinity and the presence of trace elements. Thus, most work done on presolar graphite is carried out on narrow aliquots of density fractions.

Most of the studies were carried out on the Murchison density fractions: KE1 and KE3 (1.6 – 2.05 g cm^{-3}), KFA1 (2.05 – 2.10 g cm^{-3}), KFB1 (2.10 – 2.15 g cm^{-3}), and KFC1 (2.15 – 2.20 g cm^{-3}). All isotopically identified presolar graphite grains seem to be spherical with diameters > 1 μm (ranging up to ~ 20 μm). Structural and isotopic properties of Murchison presolar graphite vary with density (Amari et al., 1995; Hoppe et al., 1995).

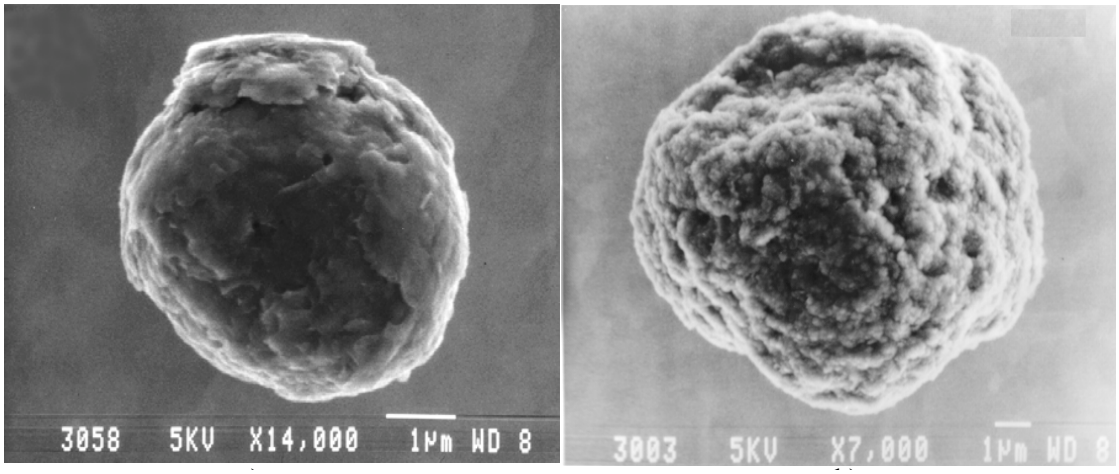

Figure 1.5 Different morphologies of presolar graphite grains from Murchison Left panel: onion-type, Right panel: cauliflower-type. (Courtesy: Sachiko Amari)

The low-density presolar graphite grains in Murchison are large and exhibit typical "cauliflower" morphology (Hoppe et al., 1995). These cauliflower grains are concentrically packed aggregates of small scales of poorly graphitized carbon. The high-density presolar grains show another distinct morphology dubbed the "onion" structure (Hoppe et al., 1995). These grains are smaller and have a smoother texture than that of cauliflower grains. They have shell-like, concentric platy layers of well-

crystallized carbon (Figure 1.5). The surface textures of these graphite spherules are manifestations of distinct internal structures (Bernatowicz et al., 1991, 1996). TEM studies have also revealed that most cauliflower and onion grains contain refractory grains (Figure 1.6). These grains condensed independently and some of them probably acted as condensation nuclei for the graphite grains. Small (20 – 500 nm) TiC grains have been found in both onion and cauliflower spherules (Bernatowicz et al., 1991). Some spherules have zirconium- and molybdenum-rich carbides (Bernatowicz et al., 1996), whereas the grains that demonstrate SN origins have, in addition to TiC, kamacite, cohenite, iron grains, iron carbides, and metallic osmium (Bernatowicz et al., 1999; Croat et al., 2003; Croat et al. 2005). These refractory inclusions provide information on the physical and chemical compositions of the gas from which the graphite grains condensed.

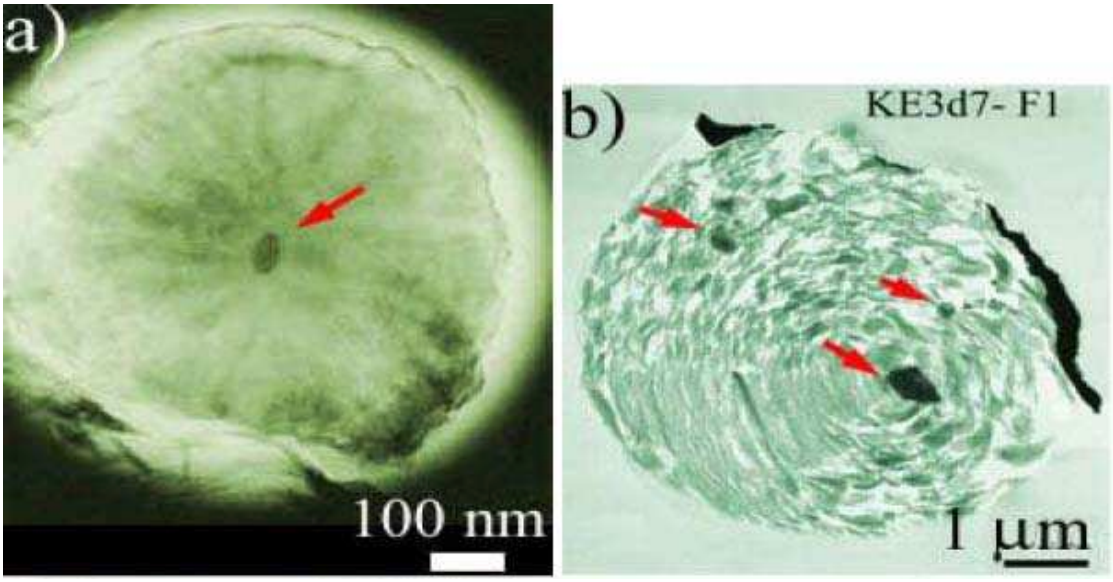

Figure 1.6 TEM images of slices of presolar graphites. Red arrows indicate internal refractory carbide grains. a) onion-type graphite (dense) grain containing a central (Ti, Zr, Mo) carbide. b) Cauliflower-type graphite (less dense) grain contains multiple titanium carbides.(Source: http://presolar.wustl.edu/work/grains.html)

The isotopic properties of graphite also correlate with density. The $^{12}C/^{13}C$ ratios in Murchison graphite vary over a large range (2 – 7000) demonstrating their presolar

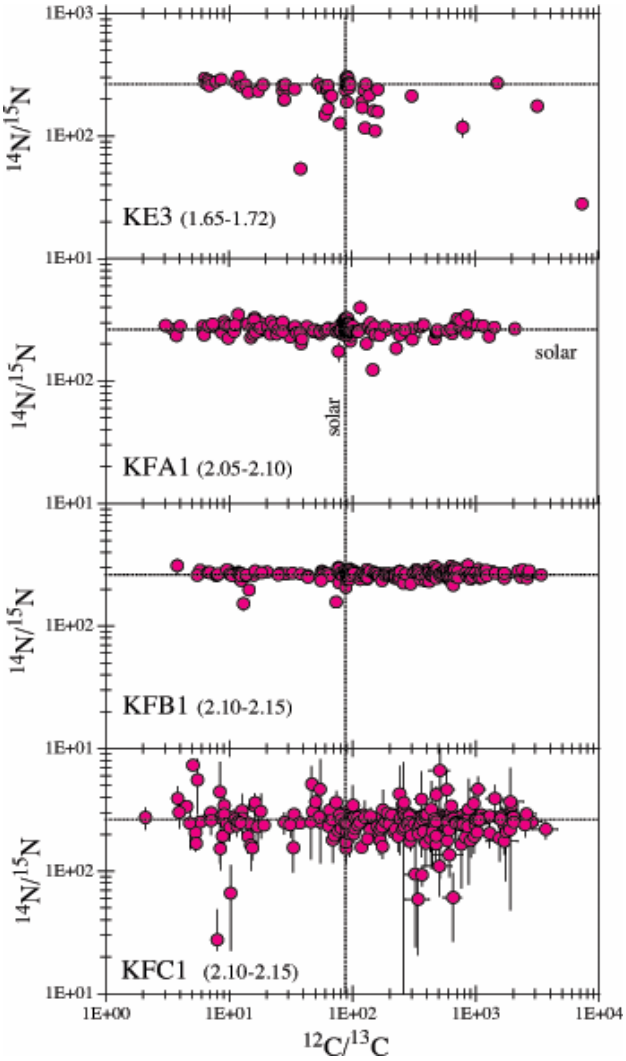

Figure 1.7 C and N ratios of Murchison graphite grains from the different density fractions. (data from Amari et al., 2005)

origin. Grains with large ^{12}C excesses become more abundant in higher-density fractions (KFB1 and KFC1). Low-density grains exhibit ^{15}N excesses, but nearly all of the other presolar graphite grains in Murchison have terrestrial ^{14}N/^{15}N ratios (Figure 1.7). A possible explanation for this effect is that the nitrogen equilibrated either on the parent body or in the laboratory (Hoppe et al., 1995). The puzzling aspect of this normal nitrogen isotopic signature is the presence of almost pure ^{22}Ne. It is expected that if nitrogen equilibrated in these grains then so should have the noble gases, especially since Ne has adsorption properties very similar to those of N. The

abundances of the trace elements H, N, O, and Si are higher in low-density grains. Numerous low-density grains (KE3 and KFA1 fractions) exhibit ^{18}O excesses (Figure 1.8). These O anomalies correlate with the carbon anomalies and have been extensively studied because these signatures point to a SN origin for these grains (Amari et al., 1995; Travaglio et al., 1999). The Si isotopic properties of these grains are similar those of SiC grains (Figure 1.9). The low-density KE3 and KFA1 fractions have ^{28}Si-rich grains, whereas some of the KFB1 and KFC1 grains (high density) exhibit ^{29}Si and ^{30}Si excesses. The ^{28}Si excesses correlate with the ^{18}O excesses and indicate a SN origin for these low-density graphite grains (similar to SiC-X grains). Additional proof of SN origin comes from the initial presence of ^{44}Ti (Nittler et al., 1996) and ^{41}Ca in some of these grains (Amari et al., 1996). Stadermann et al. (2005) measured C, N, O and Ti isotopic ratios in TiC subgrains in a KE3 graphite grain from Murchison that had SN isotopic signatures. The subgrains were found to be significantly more anomalous in O isotopes than the original graphite, indicating that the subgrains could have formed in a different region of the SN ejecta compared to the parent grain or retained the O isotopic composition of the parent star more efficiently than the parent grain. The presence of ^{44}Ca, from the decay of ^{44}Ti, was also detected in one subgrain, confirming the SN origin of the graphite grain. The high-density grains probably originated from AGB stars of low metallicity as indicated by Kr data (Amari et al. 1995) and large ^{30}Si excesses correlated with high ^{12}C/^{13}C ratios (Amari et al. 2003; 2004; 2005). TEM studies indicate that TiC subgrains from high density graphites have high concentrations of s-process elements like Zr, Mo, and Ru (Bernatowicz et al. 1996; Croat et al. 2005). These elements are produced in copious amounts in the He intershell region of thermally pulsing AGB stars and transported to the envelope by repeated third dredge-up events. Some graphite grains show nova signatures: low ^{20}Ne/^{22}Ne ratios (not compatible with any known He-burning stellar source) (Nichols et al. 1995), ^{12}C/^{13}C ratios in the 4 – 10 range,

and a $^{14}N/^{15}N$ ratio of 8.5 along with large ^{30}Si excesses (Amari et al. 2001).

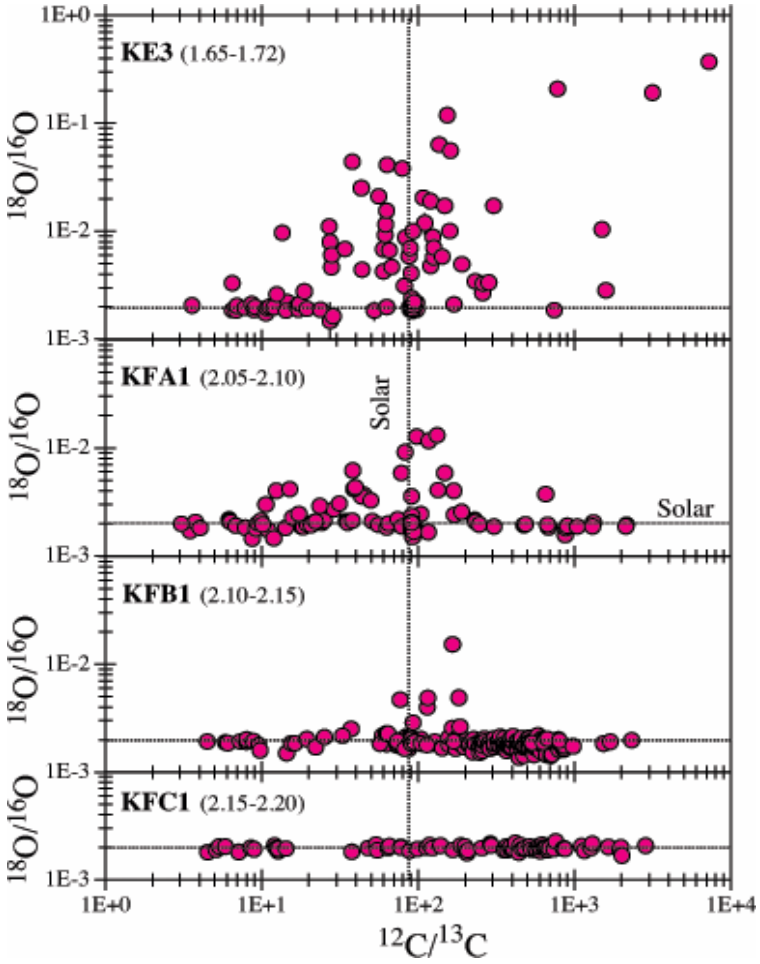

Figure 1.8 Oxygen isotopic ratios of Murchison graphite grains from different density fractions. Numbers in parentheses denote the density range in a given fraction in g cm^{-3}. (data from Hoppe et al., 1995; Travaglio et al., 1999; Amari et al., 2005)

Clearly, presolar graphite in a single meteorite can have multiple sources. Previous studies seem to indicate that most graphite grains from Murchison have a SN origin, which is strange, since stars that can produce SiC grains are also, theoretically, able to produce graphite. A large fraction of the SiC grain population originate from AGB stars but a much smaller population of graphite grains from AGB stars has been positively identified. A proper understanding of condensation of carbon phases from stellar atmospheres (e.g. Bernatowicz et al. 1996; 2005) and their survival in the ISM is needed.

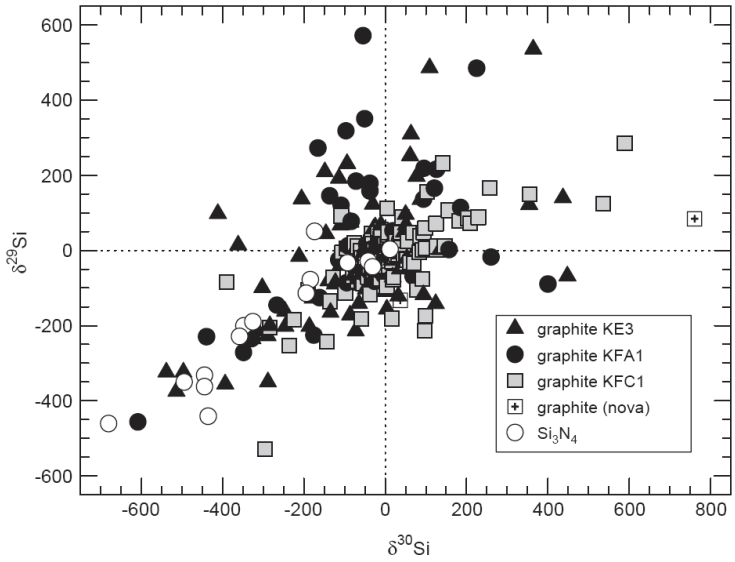

Figure 1.9 Si isotopic ratios of Murchison graphite grains from the various density fractions. The ratios are plotted as δ-values or deviations from the terrestrial ratios, in permil (‰). The dotted lines represent solar ratios. (Source: Lodders and Amari, 2005)

Based on noble gas analyses, Huss and Lewis (1995) estimated the abundance of presolar graphite in the carbonaceous chondrite (CI) Orgueil to be an order of magnitude higher than that in Murchison. Pravdivtseva et al. (2004) made an effort to isolate this presolar graphite in Orgueil, using the separation procedure previously applied to Murchison. They obtained a fraction with a density of ~ 1.8 g cm^{-3} and grain size > 1 μm. Observations in a scanning electron microscope (SEM) showed that grains from this Orgueil fraction closely resemble those of Murchison graphite, exhibiting onion-type morphology. However, NanoSIMS isotopic analyses of C and N of 162 grains yielded only normal ratios, indicating that the grains had a solar system origin (Pravdivtseva et al., 2004). In addition, Ne isotopic analysis of 14 individual grains, by high-transmission ion-counting noble gas mass spectrometry (Hohenberg, 1980), did not detect any excesses in ^{22}Ne above the blank.

The work of this dissertation was motivated by the need to identify and further study similar, and maybe, additional presolar graphite grain populations from other meteorites and to constrain their stellar sources better.

1.5 Overview of the presented research and dissertation

The main objective of this research was to study the isotopic properties of presolar graphite from Orgueil, which, despite its inferred high abundance in this meteorite, had been elusive up until now. This dissertation presents the results and implications of multi-element isotopic analyses of presolar graphite grains from the carbonaceous chondrite, Orgueil. It includes a report on the successful isolation and preliminary isotopic study of presolar graphite grains from different density fractions of Orgueil (Chapter 2). Chapter 3 presents C, Ca, and Ti isotopic data on unique ^{13}C-enriched grains and discusses their possible stellar sources. Chapter 4 contains a detailed, comprehensive study of all 345 presolar graphite grains analyzed for this dissertation. Conclusions and scope for future studies are presented in the concluding chapter.

1.6 Statement of Labor

The following three chapters in this dissertation are based upon two published papers and one paper that is in preparation for publication.

- Chapter 2 is published as "Isotopic analyses of presolar graphite grains from Orgueil" in *New Astronomy Reviews* (Jadhav et al. 2006).
- Chapter 3 appears in the *Astrophysical Journal* as "New stellar sources for high-density, presolar graphite grains" (Jadhav et al. 2008).
- Chapter 4 titled "Multi-element isotopic analyses of presolar graphite grains from Orgueil" is being prepared for publication in *Geochimica et Cosmochimica Acta*.

The new separation of carbonaceous and refractory presolar grains from Orgueil was undertaken by Dr. Teruyuki Maruoka. The subsequent sample preparations and isotopic studies presented in this dissertation, and the preparation of the above

referenced publications are primarily my work under the expert guidance and help of my advisors, Professors Ernst Zinner and Sachiko Amari.

References

Amari S., Anders A., Virag A., and Zinner E. (1990) Interstellar graphite in meteorites. Nature 345, 238-240.

Amari S., Gao X., Nittler L., Zinner E., José J., Hernanz M., and Lewis R. S. (2001a) Presolar grains from novae. Astrophys. J. 551, 1065-1072.

Amari S., Hoppe P., Zinner E., and Lewis R. S. (1992) Interstellar SiC with unusual isotopic compositions: grains from a supernova? Astrophys. J. 394, L43-L46.

Amari S., Lewis R. S., and Anders E. (1994) Interstellar grains in meteorites. I. Isolation of SiC, graphite, and diamond: size distributions of SiC and graphite. Geochim. Cosmochim. Acta 58, 459-470.

Amari S., Nittler L. R., Zinner E., Gallino R., Lugaro M., and Lewis R. S. (2001b) Presolar SiC grains of type Y: origin from low-metallicity AGB stars. Astrophys. J. 546, 248-266.

Amari S., Nittler L. R., Zinner E., Lodders K., and Lewis R. S. (2001c) Presolar SiC grains of type A and B: their isotopic compositions and stellar origins. Astrophys. J. 559, 463-483.

Amari S., Zinner E., and Lewis R. S. (1996) ^{41}Ca in presolar graphite of supernova origin. Astrophys. J. 470, L101-L104.

Amari S., Stadermann F. J., Zinner E., and Lewis R. S. (2003) Continued study of presolar graphite from Murchison separate KFA1. Lunar Planetary Science XXXIV, Abstract #1864.

Amari S., Zinner E., and Lewis R. S. (2004) Comparison study of presolar graphite separates KE3 and KFA1 from the Murchison meteorite. Lunar Planetary Science XXXV, Abstract #2103.

Amari S., Zinner E., and Lewis R. S. (2005) Presolar graphite and its noble gases. Lunar Planet. Sci. XXXVI, Abstract #1867.

Bernatowicz T. J., Amari S., Zinner E., and Lewis R. S. (1991) Interstellar grains within interstellar grains. Astrophys. J. 373, L73-L76.

Bernatowicz, T. J., Bradley J., Amari S., Messenger S., and Lewis R. (1999) New kinds of massive star condensates in a presolar graphite from Murchison. Lunar Planet. Sci. XXX. Abstract #1392.

Bernatowicz T. J., Cowsik R., Gibbons P. C., Lodders K., Fegley B., Jr., Amari S., and Lewis R. S. (1996) Constraints on stellar grain formation from presolar graphite in the Murchison meteorite. Astrophys. J. 472, 760-782.

Bernatowicz T. J., Fraundorf G., Tang M., Anders E., Wopenka B., Zinner E., and Fraundorf P. (1987) Evidence for interstellar SiC in the Murray carbonaceous meteorite. Nature 330, 728-730.

Bernatowicz T. J., Akande O. W., Croat T. K., and Cowsik R. (2005) Constraints on grain formation around carbon stars from laboratory studies of presolar graphite. Astrophys. J. 631, 988-1000.

Black D. C. (1972) On the origins of trapped helium, neon and argon isotopic variations in meteorites. Geochim. Cosmochim. Acta 36, 377-394.

Black D. C. and Pepin R. O. (1969) Trapped neon in meteorites II. Earth and Planet. Sci. Lett. 6, 395-405.

Cameron A. G. W. (1962) The formation of the sun and planets. Icarus 1, 13-69.

Choi B.G., Huss G.R., Wasserburg G.J., and Gallino R. (1998) Presolar corundum and spinel in ordinary chondrites: origins from AGB stars and a supernova. Science 282, 1284-1289.

Clayton D. D. (1975) Na-22, Ne-E, extinct radioactive anomalies and unsupported Ar-40. Nature 257, 36-37.

Clayton R. N., Grossman L., and Mayeda T. K. (1973) A component of primitive nuclear composition in carbonaceous meteorites. Science 182, 485-488.

Croat T. K., Bernatowicz T. J., Amari S., Messenger S., and Stadermann F. J. (2003) Structural, chemical, and isotopic microanalytical investigations of graphite from supernovae. Geochim. Cosmochim. Acta 67, 4705-4725.

Croat T. K., Stadermann F. J., and Bernatowicz T. J. (2005) Presolar graphite from AGB stars: Microstructure and s-process enrichment. Astrophysical Journal 631, 976-987.

Eberhardt P., Jungck M. H. A., Meier F. O. and Niederer F. (1979) Presolar grains in Orgueil: evidence from neon-E. Astrophys. J. 234, L169-L171.

Eberhardt P., Jungck M. H. A., Meier F. O., and Niederer F. R. (1981) A neon-E rich phase in Orgueil: results obtained on density separates. Geochim. Cosmochim. Acta 45, 1515-1528.

Halbout J., Mayeda T. K., and Clayton R. N. (1986) Carbon isotopes and light element abundances in carbonaceous chondrites. Earth Planet. Sci. Lett. 80, 1-18.

Heck Ph. R., Marhas K. K., Baur H., Hoppe P., and Wieler R. (2005) Presolar He and Ne in Single Circumstellar SiC Grains Extracted from the Murchison and Murray Meteorites. Lunar Planet. Sci. XXXVI, Abstract #1938.

Hohenberg C.M. (1980) High sensitivity pulse-counting mass spectrometer system for noble gas analysis. Rev. Sci. Instr. 51, 1075-1082.

Hoppe P., Amari S., Zinner E., Ireland T., and Lewis R. S. (1994) Carbon, nitrogen, magnesium, silicon, titanium isotopic compositions of single interstellar silicon carbide grains from the Murchison carbonaceous chondrite. Astrophys. J. 430, 870-890.

Hoppe P., Amari S., Zinner E., and Lewis R. S. (1995) Isotopic compositions of C, N, O, Mg and Si, trace element abundances, and morphologies of single circumstellar graphite grains in four density fractions from the Murchison meteorite. Geochim. Cosmochim. Acta 59, 4029-4056.

Hoppe P., Strebel R., Eberhardt P., Gallino R., Lugaro M., Amari S., and Lewis R. S. (1997) Meteoritic silicon carbide grains with unusual Si-isotopic compositions: evidence for an origin in low-mass metallicity asymptotic giant branch stars. Astrophys. J. 487, L101-L104.

Huss G. R. and Lewis R. S. (1995) Presolar diamond, SiC and graphite in primitive chondrites: abundances as a function of meteorite class and petrologic type. Geochim. Cosmochim. Acta 59, 115-160.

Jadhav M., Amari S., Zinner E., and Maruoka T. (2006) Isotopic analysis of presolar graphite grains from Orgueil. New Astronomy Reviews 50, 591-595.

Jadhav M., Amari S., Marhas K. K., Zinner E., Maruoka T., and Gallino R. (2008) New stellar sources for high-density, presolar graphite grains. Astrophysical Journal 682, 1479-1485.

José J., Hernanz M., Amari S., Lodders, K., Zinner E. (2004) The imprint of nova nucleosynthesis in presolar grains. Astrophys. J. 612, 414-428.

Jungck M. H. A. (1982) Pure ^{22}Ne in the meteorite Orgueil. E. Reinhardt, München, 80 pp.

Lambert D. L., Gustafsson B., Eriksson K., and Hinkle K. H. (1986) The chemical composition of carbon stars: I. Carbon, nitrogen, and oxygen in 30 cool carbon stars in the galactic disk. Astrophys. J. Suppl. 62, 373-425.

Lewis R. S., Alaerts L., Matsuda J. I., and Anders E. (1979) Stellar condensates in meteorites: Isotopic evidence from noble gases. Astrophys. J. 234, L165-L168.

Lewis R. S., Anders E., Wright I. P., Norris S. J., and Pillinger C. T. (1983) Isotopically anomalous nitrogen in primitive meteorites. Nature 305, 767-771.

Lewis R. S., Tang M., Wacker J. F., Anders E., and Steel E. (1987) Interstellar diamonds in meteorites. Nature 326, 160-162.

Maas R., Loss R. D., Rosman K. J. R., DeLaeter J. R., Lewis R. S., Huss G. R., and Lugmair G. W. (2001) Isotope anomalies in tellurium and palladium from Allende nanodiamonds. Meteorit. Planet. Sci. 36, 849-858.

Messenger S., Keller L. P., Stadermann F. J., Walker R. M., and Zinner E. (2003) Samples of stars beyond the solar system: Silicate grains in interplanetary dust. Science 300, 105-108.

Nguyen A. N. (2005) Characterization of presolar silicate grains in primitive meteorites by multi-detection raster ion imaging in the NanoSIMS. Ph.D. thesis, Washington University.

Nguyen A. N. and Zinner E. (2004) Discovery of ancient silicate stardust in a meteorite. Science 303, 1496-1499.

Nichols R. H., Jr., Kehm K., and Hohenberg C. M. (1995) Microanalytical laser

extraction of noble gases: Techniques and applications. In Advances in Analytical Geochemistry, Vol. 2, pp. 119-140. JAI Press Inc.

Nittler L. R., Alexander C. M. O'D, Gao X., Walker R. M., and Zinner E. (1994) Interstellar oxide grains from the Tieschitz ordinary chondrite. Nature 370, 443-446.

Nittler L. R., Amari S., Zinner E., Woosley S. E., and Lewis R. S. (1996) Extinct ^{44}Ti in presolar graphite and SiC: proof of a supernova origin. Astrophys. J. 462, L31-L34.

Nittler L. R. and Hoppe P. (2004a) New presolar silicon carbide grains with nova isotope signatures. Lunar Planet. Sci. XXXV, Abstract #1598.

Nittler L. R. and Hoppe P. (2004b) High initial ^{26}Al/^{27}Al ratios in presolar SiC grains from novae. Meteor. Planet. Sci. 39, A78.

Nittler L. R., Hoppe P., Alexander C. M. O'D., Amari S., Eberhardt P., Gao X., Lewis R. S., Strebel R., Walker R. M., and Zinner E. (1995) Silicon nitride from supernovae. Astrophys. J. 453, L25-L28.

Owen T., Mahaffy P. R., Niemann H. B., Atreya S., and Wong M. (2001) Protosolar nitrogen. Astrophys. J. 553, L77-L79.

Pravdivtseva O., Zinner E., Meshik A. P., Hohenberg C. M., and Walker R. M. (2004) Lunar Planet. Sci. XXXV, Abstract #2096.

Reynolds J. H., and Turner G. (1964) Rare gases in the chondrite Renazzo. J. Geophys. Res. 69, 3263-3281.

Richter S., Ott U., and Begemann F. (1998) Tellurium in presolar diamonds as an indicator for rapid separation of supernova ejecta. Nature 391, 261-263.

Savina M. R., Pellin M. J., Tripa C. E., Veryovkin I. V., Calaway W. F., and Davis A. M. (2003) Analyzing individual presolar grains with CHARISMA. Geochim. Cosmochim. Acta 67, 3215-3225.

Srinivasan B., and Anders E. (1978) Noble gases in the Murchison meteorite: possible relics of s-process nucleosynthesis. Science 201, 51-56.

Stadermann F. J., Croat T. K., Bernatowicz T. J., Amari S., Messenger S., Walker R. M., and Zinner E. (2005) Supernova graphite in the NanoSIMS: Carbon, oxygen and titanium isotopic compositions of a spherule and its TiC sub-components. Geochimica et Cosmochimica Acta 69, 177-188.

Tang M. and Anders E. (1988) Isotopic anomalies of Ne, Xe, and C in meteorites: II. Interstellar diamond and SiC: carriers of exotic noble gases. Geochim. Cosmochim. Acta 52, 1235-1244.

Tang M., Lewis R. S., Anders E., Grady M. M., Wright I. P., and Pillinger C. T. (1988) Isotopic anomalies of Ne, Xe, and C in meteorites. I. Separation of carriers by density and chemical resistance. Geochim. Cosmochim. Acta 52, 1221-1234.

Travaglio C., Gallino R., Amari S., Zinner E., Woosley S., and Lewis R. S. (1999) Low-density graphite grains and mixing in type II supernovae. Astrophys. J. 510, 325-354.

Wasserburg G. J., Boothroyd A. I., and Sackmann I. J. (1995) Deep circulation in red giant stars: a solution to the carbon and oxygen isotope puzzle? Astrophys. J. 447, L37-L40.

Zinner E., Amari S., Wopenka B., and Lewis R. S. (1995) Interstellar graphite in meteorites: isotopic compositions and structural properties of single graphite grains from Murchison. Meteoritics 30, 209-226.

Chapter 2

ISOTOPIC ANALYSIS OF PRESOLAR GRAPHITE GRAINS FROM ORGUEIL

Jadhav, M., Amari, S., Zinner, E., & Maruoka, T. 2006, New Astronomy Reviews, 50, 591-595.

Abstract

We report the successful isolation and isotopic analysis of presolar graphite grains from the Orgueil CI chondrite. Isotopic measurements were made on seven density fractions, with grain sizes > 1 μm: ORG1b (1.59 – 1.67 g cm^{-3}), 1c (1.67 – 1.75 g cm^{-3}), 1d (1.75 – 1.92 g cm^{-3}), 1f (2.02 – 2.04 g cm^{-3}), 1g (2.04 – 2.12 g cm^{-3}), 1h (2.12 – 2.16 g cm^{-3}) and 1i (2.16 – 2.30 g cm^{-3}). We measured C, N, O, and Si isotopes with the NanoSIMS. All the fractions, except ORG1b and ORG1h, contain presolar graphite as demonstrated by the large range of ^{12}C/^{13}C ratios (4 – 1746) measured in individual grains. The abundance of grains with isotopically light carbon increases with increasing density. Some of the low-density grains are enriched in ^{18}O, ^{15}N and ^{28}Si. As the density increases, the grains mostly exhibit solar oxygen and nitrogen isotopic ratios. However, the high density grains are enriched in ^{29}Si and ^{30}Si. The ^{18}O and ^{28}Si excesses indicate that the low-density grains originated from supernovae, while the high-density grains (with ^{30}Si and ^{12}C excesses) probably originated from

AGB stars with low metallicities.

2.1 Introduction

Presolar graphite was first isolated from the Murchison CM2 meteorite as the carrier of Ne-E(L) (almost pure ^{22}Ne) by Amari et al. (1990). Since then these grains from Murchison have been extensively studied, and almost everything we know about presolar graphite is based on these studies (Amari et al. 1990; 1995; Hoppe et al. 1995; Zinner et al. 1995; Travaglio et al. 1999). The lack of studies on graphite grains from other meteorites rests on the fact that, although graphite can be found in the most primitive meteorites (Huss and Lewis 1995), it has a low abundance compared to SiC (Huss and Lewis 1995), and the separation procedure for graphite is far more complicated than that for SiC (Amari et al. 1994). Complications during the separation arise because graphite is chemically not as resistant as SiC or oxide minerals, and because it needs to be isolated from other carbonaceous material in the meteorite that has similar chemical properties. Carbonaceous phases, in particular presolar graphite grains, are believed to condense from gases with C/O $>$ 1. The envelopes of carbon stars, Wolf-Rayet (WR) stars, novae, and supernova (SN) zones all satisfy this condition at some time in their lifecycles. In order to gain a proper understanding of condensation of carbon phases from stellar atmospheres and their survival in the interstellar medium (ISM) as well as to obtain information on stellar nucleosynthesis, presolar graphite populations from other meteorites need to be identified and studied for their isotopic compositions.

Based on noble gas analyses, Huss and Lewis (1995) estimated the abundance of presolar graphite in the carbonaceous chondrite (CI) Orgueil to be an order of magnitude higher than that in Murchison. Thus, an effort was made by Pravdivtseva et al. (2004) to isolate presolar graphite in Orgueil, using the separation procedure previously applied to Murchison. They obtained a fraction with a density of 1.8 g

cm^{-3} and grain size $> 1\mu$m. Although these grains closely resembled the onion-type grains of Murchison (Hoppe et al. 1995), NanoSIMS isotopic analyses of C and N of 162 grains yielded only normal ratios, indicating that the grains had a solar system origin (Pravdivtseva et al. 2004). Additional Ne isotopic analysis of 14 individual grains did not detect any excesses in ^{22}Ne above the blank.

We undertook a new separation of carbonaceous and refractory presolar grains from Orgueil (Jadhav et al. 2005). The main objective was to isolate presolar graphite from Orgueil, which, despite its inferred high abundance in this meteorite, has been elusive until now. We present C, N, O and Si isotopic analyses of graphite grains from seven density fractions of Orgueil. We also discuss the possible stellar sources for the anomalous graphite grains found.

2.2 Experimental procedure and methods

Our sample of Orgueil was obtained from the National Museum of Natural History in Paris. We subjected 24.16 g to essentially the same separation procedure carried out for Murchison graphite by Amari et al. (1994) to obtain ten final density fractions. The lightest density fraction, ORG1a (< 1.59 g cm^{-3}) contains organic matter and the heaviest fraction, ORG1j (> 2.3 g cm^{-3}) is expected to contain SiC and oxides. At least a few of the remaining eight density fractions were expected to contain presolar graphite grains. These fractions were then separated according to size with a cutoff of 1 μm.

Carbonaceous grains were located in a JEOL-840A SEM and identified by energy dispersive X-ray (EDX) analysis. Candidate grains were selected on the basis of high C content and morphological features characteristic of Murchison graphite (spherules with a platy onion or knobby cauliflower appearance (Hoppe et al. 1995)).

This initial characterization in the SEM was followed by isotopic analyses of the candidate grains in the NanoSIMS. $^{12}C^-$, $^{13}C^-$, $^{16}O^-$ and $^{18}O^-$ (analysis phase 1)

Table 2.1 Number of carbonaceous grains identified in each density fraction, the type of isotopic ratios measured for them and the number of presolar grains identified in each fraction

Fraction Name	Density	# of carbonaceous grains				# of presolar grains found
		C	N	O	Si	
ORG1b	1.59 – 1.67	22	–	22	–	0
ORG1c	1.67 – 1.75	7	7	7	7	2
ORG1d	1.75 – 1.92	32	32	32	32	19
ORG1e	1.93 – 2.02	–	–	–	–	–
ORG1f	2.02 – 2.04	72	72	72	72	65
ORG1g	2.04 – 2.12	52	51	52	51	38
ORG1h	2.12 – 2.16	18	–	18	–	0
ORG1i	2.16 – 2.30	9	9	9	9	6

and, $^{12}C^{14}N^-$, $^{12}C^{15}N^-$, $^{28}Si^-$, $^{29}Si^-$ and $^{30}Si^-$ (phase 2) secondary ions produced by bombarding the sample with a Cs^+ primary beam were counted in multidetection mode.

2.3 Results

Table 2.1 lists the number of carbonaceous grains identified in the different fractions, the kind of isotopic data obtained on them and the number of grains that were found to contain isotopic anomalies.

Some of our density fractions of Orgueil contain large concentrations (much higher than in graphite separates from Murchison) of macromolecular carbonaceous material, in which graphite grains are often found embedded. This material made identification of graphite grains in Orgueil difficult. Most of the grains from the density separates are spherules and look very similar to Murchison presolar graphite grains; they have smooth surfaces and a platy, onion-like morphology (Hoppe et al. 1995). Some potato-shaped presolar graphite grains were also found. We did not find any grains with cauliflower-type morphology, which had been seen in the low density fractions

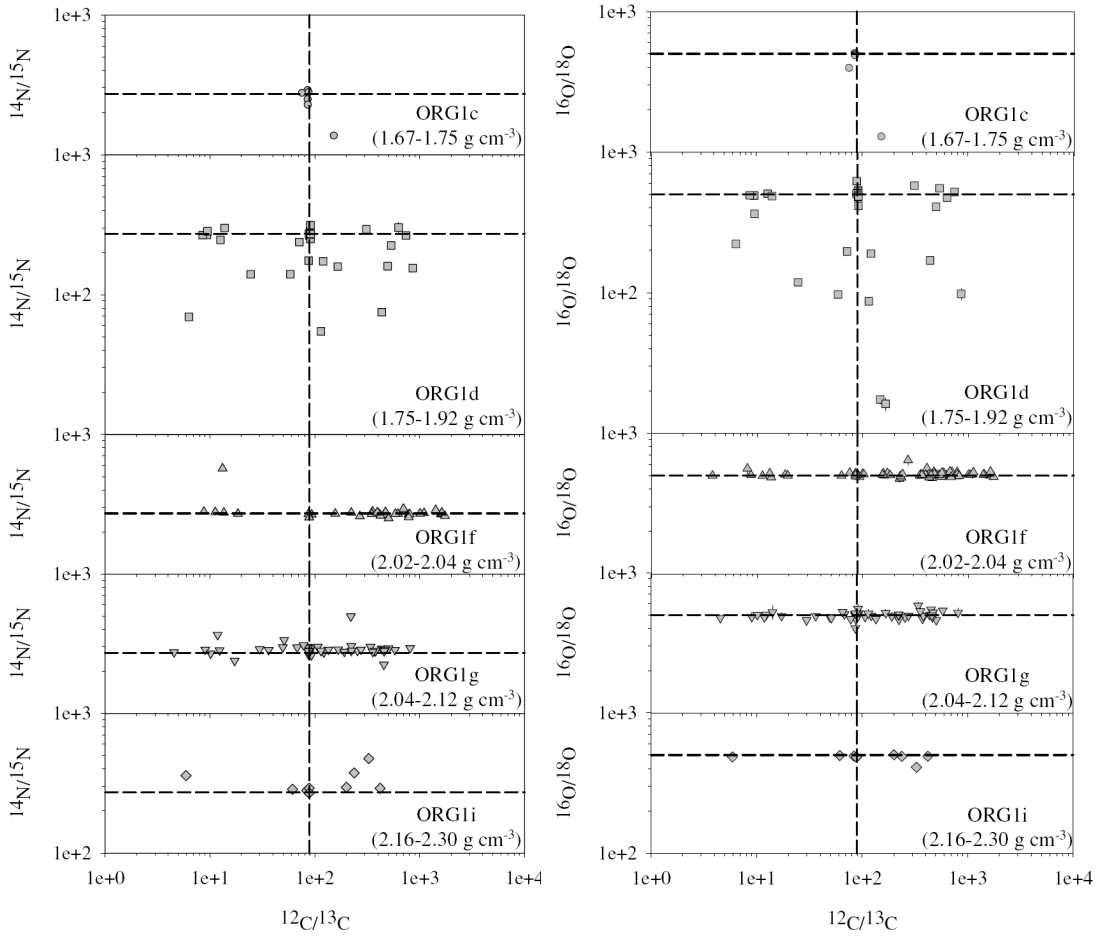

Figure 2.1 *Left Panel*: $^{14}N/^{15}N$ and $^{12}C/^{13}C$ measured in individual graphite grains from different density fractions of the Orgueil meteorite. Solar values of $^{14}N/^{15}N$ = 272 and $^{12}C/^{13}C$ = 89 are indicated by the dashed lines in the plots.
Right Panel: Oxygen and carbon isotopic ratios of graphite grains from different density fractions. The dashed lines in each plot indicate the solar ratios of $^{16}O/^{18}O$ = 499 and $^{12}C/^{13}C$ = 89.

of Murchison (Hoppe et al. 1995). The sizes of the grains range from 2 to 30 μm. Unlike for Murchison, in Orgueil the average grain size increases with density.

Five of the seven density fractions studied have isotopically anomalous graphite (Table 2.1). The $^{12}C/^{13}C$ ratios of the grains range from 4 to 1746 (Figure 2.1). The C ratios of the ORG1b and 1h grains are close to solar and do not show the large variations that are expected in presolar graphite (Hoppe et al. 1995). However, 29% of all grains in ORG1c, 59% in ORG1d, 90% in ORG1f, 73% in ORG1g, and 67% of the grains in ORG1i have C isotopic anomalies. The grains from ORG1h

are morphologically different from the grains of the other fractions, in that they are smooth spherules with very little surface morphology. Grains of such morphology have been found to be isotopically normal in Murchison studies as well (Zinner et al. 1995). In general, grains with isotopically light carbon are more abundant in the higher density fractions (ORG1f, 1g and 1i; Figure 2.1). A minor population of grains with $^{12}C/^{13}C \sim 10$ is observed in all fractions heavier than ORG1c (Figure 2.1). Similar C isotopic distributions, a higher abundance of grains with $^{12}C/^{13}C >$ solar in grains with higher density, and the presence of a population around $^{12}C/^{13}C \sim 10$, have also been observed in Murchison graphite (Hoppe et al., 1995).

Figure 2.1 show the C, N, and O isotopic compositions measured in the grains of the various density fractions. The low-density fractions, ORG1c and 1d, contain some grains that have ^{15}N and ^{18}O excesses. Most of the grains that contain isotopically heavy nitrogen also have ^{18}O excesses. Since ^{18}O excesses are a signature of a SN origin (Travaglio et al. 1999), they indicate that ORG1c and 1d contain SN graphite. At higher densities (ORG1f, 1g and 1i), the $^{14}N/^{15}N$ and $^{16}O/^{18}O$ ratios become surprisingly normal. This is especially puzzling in view of the large range of $^{12}C/^{13}C$ ratios seen in these grains. A possible explanation for this fact is that initially anomalous N and O isotopically equilibrated by exchange with normal N and O, either on the parent body or in the laboratory (Zinner et al. 1995), and the normal N and O ratios of high density grains cannot be considered to represent the isotopic signatures of their stellar sources. The silicon isotopic compositions of the grains also depend on density (Figure 2.2). The low-density fractions ORG1c and 1d contain grains with ^{28}Si excesses. Some of these excesses correlate with ^{18}O and ^{15}N excesses. Excesses in ^{28}Si and ^{18}O are indicative of a SN origin. The high-density grains from ORG1f, 1g and 1i, however, are enriched in ^{29}Si and ^{30}Si. Most ^{30}Si-rich grains contain isotopically light carbon (Figure 2.3). These signatures are expected for low-metallicity AGB stars where during the thermally pulsing phase ^{12}C and $^{29,30}Si$ are mixed by the

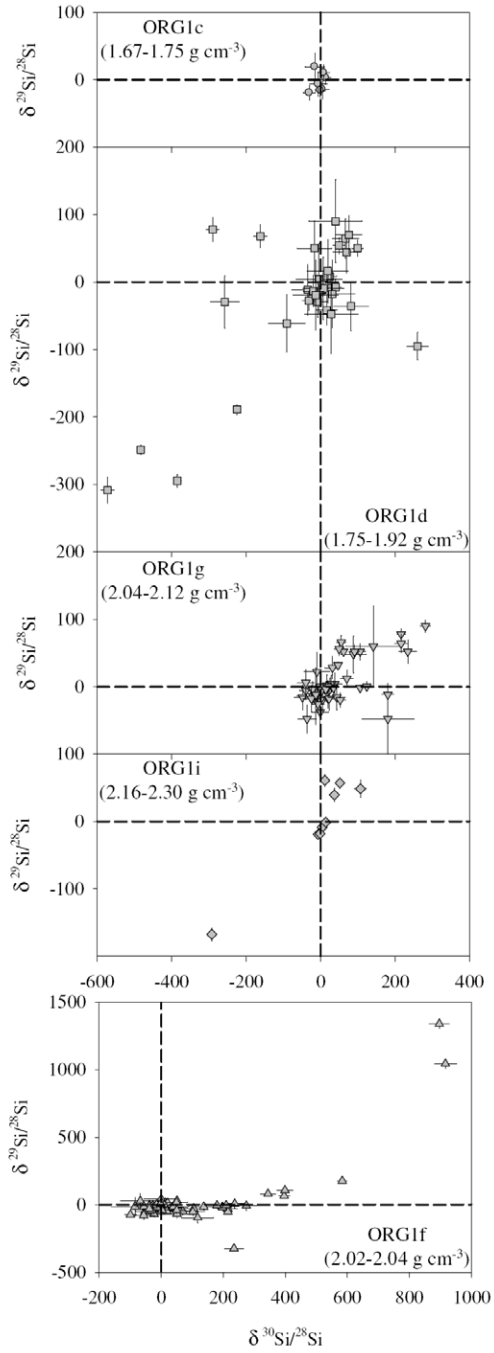

Figure 2.2 Delta-value three-isotope plots of the Si ratios measured in graphite grains from different density fractions. The ratios are plotted as δ-values, deviations from the terrestrial ratios $^{29}Si/^{28}Si = 0.050633$ and $^{30}Si/^{28}Si = 0.033621$, in permil (‰). Error bars are 1 σ. Dashed lines indicate the solar ratios ($\delta\ ^{29}Si/^{28}Si = \delta\ ^{30}Si/^{28}Si = 0$).

third dredge-up (TDU) from the He shell into their envelopes (Hoppe et al. 1997; Busso et al. 1999).

In general, Orgueil graphite grains appear to be rather similar to Murchison graphite, both morphologically and in their isotopic properties, an exception being the lack of cauliflower-type grain in Orgueil.

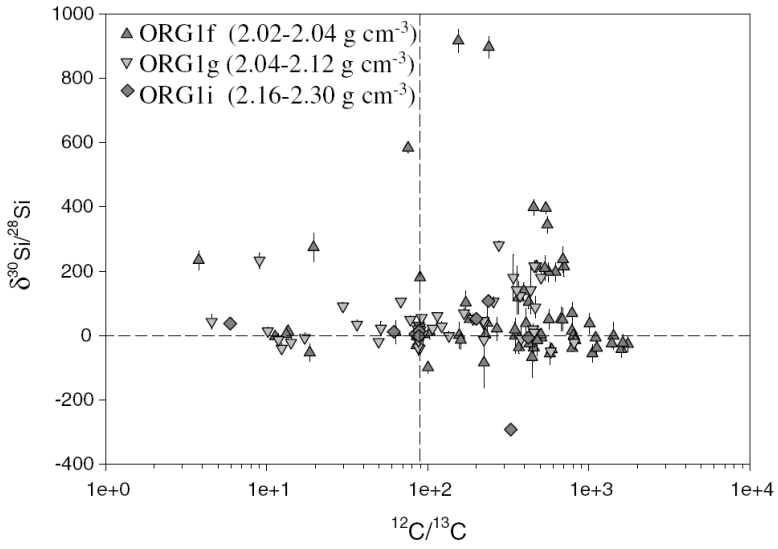

Figure 2.3 The δ ^{30}Si/^{28}Si values of graphite grains from the high-density fractions, ORG1f, 1g and 1i, are plotted against their ^{12}C/^{13}C ratios. The dashed lines indicate solar values and error bars are 1 σ.

2.4 Discussion

While there still remains a multitude of unanswered questions about presolar graphite grains and their stellar sources, one issue seems to have cleared up. There exists a large population of SiC grains from AGB stars. However, in spite of the fact that Kr isotopic measurements of bulk samples indicated the presence of AGB graphite grains in the highest density fraction from Murchison (Amari et al. 1995), before this study and a recent study by Amari et al. (2005) only few such grains have been identified from single-grain isotopic analysis. This was a puzzle because both graphite and SiC grains are expected to condense around similar C-rich stars. High-density graphite grains from the Murchison fractions KFB1 and KFC1 have been analyzed with the IMS-3f in the past (Hoppe et al. 1995), but due to the low sensitivity of the instrument it was

difficult to obtain Si isotopic data for these grains with sufficiently high precision. The NanoSIMS, however, with its high sensitivity, allows us to measure the Si isotopes of high-density graphite grains with much higher precision and hence, finally, allows us to investigate graphite grains from low-metallicity AGB stars. A recent NanoSIMS study by Amari et al. (2005) of the Murchison KFB1 and KFC1 fractions, has also found graphite grains that originated from low-metallicity AGB stars.

While high-density graphite grains have high $^{12}C/^{13}C$ ratios and large ^{30}Si excesses, no SiC grains with similar C and Si isotopic signatures have been found (Hoppe et al. 1997; Nittler and Alexander 2003). The relatively low $^{12}C/^{13}C$ ratios in type Z SiC grains, which have large ^{30}Si excesses, have been explained by invoking extra mixing, cool bottom processing (CBP) (Hoppe et al. 1997; Nollett et al. 2003). This process leads to proton capture on ^{12}C mixed into the envelope by the third dredge-up, lowering the $^{12}C/^{13}C$ ratio. A possible explanation for the high $^{12}C/^{13}C$ ratios in high-density graphite grains could be that these grains formed around low-metallicity AGB stars that did not experience any CBP. Such stars are predicted to have not only high $^{12}C/^{13}C$ ratios but also very high C/O ratios. Because of the large relative excess of C over Si in the envelope of such stars, graphite, but not SiC grains are expected to condense (Bernatowicz et al. 2006). Thus it appears that the presence or absence of CBP in low-metallicity stars is a criterion whether SiC or graphite grains form in the envelope of such stars, both with large ^{30}Si excesses, but SiC with low and graphite with high $^{12}C/^{13}C$ ratios.

2.5 Conclusions

Presolar graphite has been successfully isolated from Orgueil. Five of the seven density fractions analyzed contain presolar graphite as indicated by isotopically anomalous carbon. The morphologic and isotopic characteristics of Orgueil graphite are similar to those of Murchison. We have found evidence of SN graphite in the low-density

fractions and grains from low-metallicity AGB stars in the high-density fractions.

References

Amari, S., Anders, E., Virag, A., Zinner, E., 1990. Nature 345, 238.

Amari, S., Lewis, R. S., Anders, E., 1994. Geochim. Cosmochim. Acta 58, 459.

Amari, S., Lewis, R. S., Anders, E., 1995. Geochim. Cosmochim. Acta 59, 1411.

Amari, S., Zinner, E., Lewis, R. S., 2005. Meteorit. Planet. Sci. 40, A15.

Bernatowicz, T. J., Croat, T. K., Daulton, T. L., 2006, in Meteorites and the Early Solar System II, ed. D. S. Lauretta & H. Y. McSween, Jr. Univ. of Arizona, Tucson.

Busso, M., Gallino, R., Wasserburg, G. J., 1999. Ann. Rev. Astron. Astrophys. 37, 239.

Hoppe, P., Amari, S., Zinner, E., Lewis, R. S., 1995. Geochim. Cosmochim. Acta 59, 4029.

Hoppe, P., Annen, P., Strebel, R., Eberhardt, P., Gallino, R., Lugaro, M., Amari, S., Lewis, R. S., 1997. Astrophys. J. 487, L101.

Huss, G. R., Lewis, R. S., 1995. Geochim. Cosmochim. Acta 59, 115.

Jadhav, M., Maruoka, T., Amari, S., Zinner, E., 2005. Lunar & Planet. Sci. XXXVI, Abstract #1976.

Nittler, L. R., Alexander, C. M. O. D., 2003. Geochim. Cosmochim. Acta 67, 4961.

Nollett, K. M., Busso, M., Wasserburg, G. J., 2003. Astrophys. J. 582, 1036.

Pravdivtseva, O., Zinner, E., Meshik, A. P., Hohenberg, C. M., Walker, R. M., 2004. Lunar Planet. Sci. XXXV, Abstract #2096.

Travaglio, C., Gallino, R., Amari, S., Zinner, E., Woosley, S., Lewis, R. S., 1999. Astrophys. J. 510, 325.

Zinner, E., Amari, S., Wopenka, B., Lewis, R. S., 1995. Meteoritics 30, 209.

Chapter 3

NEW STELLAR SOURCES FOR HIGH-DENSITY, PRESOLAR GRAPHITE GRAINS

Jadhav M., Amari S., Marhas K. K., Zinner E., Maruoka T., and Gallino R. (2008) New stellar sources for high-density, presolar graphite grains. Astrophysical Journal 682, 1479-1485.

Abstract

We present C, N, O, Si, Al-Mg, K, Ca and Ti isotopic analyses of seven high-density (ORG1f, $\rho \sim 2.02 - 2.04$ g cm^{-3}) graphite grains from Orgueil with ^{12}C/^{13}C ratios smaller than 20. The presence of ^{44}Ti in three of these grains indicates an origin in Type II supernovae (SNe). The ^{13}C excesses in these SNe grains, however, remain enigmatic. The remaining grains have extremely large Ca and Ti isotopic anomalies, some of which are much larger than those predicted for envelopes of asymptotic giant branch (AGB) stars. These anomalies in conjunction with low ^{12}C/^{13}C ratios can only be explained by pure nucleosynthetic He-shell components of AGB stars. Born-again AGB stars that experience a late He flash are able to explain the low ^{12}C/^{13}C ratios of some of the grains along with the presence of extreme enrichments in the Ca and Ti isotopes. This study indicates that high-density graphite grains have multiple stellar sources: SNe and born-again AGB stars, in addition to the previously established

low-metallicity AGB stars.

3.1 Introduction

Presolar graphite grains were first isolated from the Murchison CM2 meteorite as the carrier of Ne-E(L) (almost pure ^{22}Ne) by Amari et al. (1990). Since then presolar graphites have also been isolated from the CI chondrite Orgueil (Jadhav et al. 2006). Extensive isotopic studies (Amari et al. 1990; Amari, Lewis & Anders 1995; Hoppe et al. 1995; Zinner et al. 1995; Travaglio et al. 1999; Jadhav et al. 2006) of graphite grains from these meteorites have shown that the isotopic properties of presolar graphites are density-dependent. Many low-density (LD) graphite grains have large excesses in ^{15}N, ^{18}O and ^{28}Si (Travaglio et al. 1999; Jadhav et al. 2006). A few of these LD grains show evidence for ^{44}Ti (Nittler et al. 1996), have large excesses in ^{41}K (due to the decay of ^{41}Ca) (Amari, Zinner & Lewis 1996) and high inferred ^{26}Al/^{27}Al ratios. These isotopic compositions, in addition to high ^{12}C/^{13}C ratios, are similar to those of SiC-X grains, which are known to have a supernova (SN) origin. Travaglio et al. (1999) were able to match these major isotopic signatures of LD grains by performing mixing calculations of different layers of Type II SNe. On the other hand, a large fraction of high-density (HD) graphite grains appears to have an origin in low-metallicity, asymptotic giant branch (AGB) stars (Zinner, Amari & Jadhav 2006a). In transmission electron microscopy (TEM) studies, Bernatowicz et al. (1996) and Croat, Stadermann & Bernatowicz (2005) found HD grains from Murchison that contain subgrains rich in the s-process elements Zr, Mo, and Ru, indicating an AGB origin. Many HD graphites have large ^{30}Si excesses that are correlated with high ^{12}C/^{13}C ratios (Amari, Zinner & Lewis 2005; Jadhav et al. 2006). Similar signatures are expected for low-metallicity AGB stars where, during the thermally pulsing phase, ^{12}C and ^{29,30}Si from the He shell are mixed into the envelope by third dredge-up (TDU) (Busso, Gallino & Wasserburg 1999; Zinner, Amari & Jadhav 2006a). These models

not only predict high $^{12}C/^{13}C$ ratios but also high C/O ratios, which produce an ideal environment for graphite condensation (Lodders & Fegley 1997). The large, relative excess of C over Si in the envelopes of such stars causes graphite and not SiC grains to condense (Bernatowicz, Croat & Daulton 2006), which could be an explanation for the absence of any SiC grains that have similar high $^{12}C/^{13}C$ ratios and large ^{30}Si excesses (Hoppe et al. 1997; Nittler & Alexander 2003).

Both LD and HD graphite grains from Murchison and Orgueil contain a minor population of grains that have $^{12}C/^{13}C$ ratios ~ 10. The nucleosynthetic source(s) of grains with such low $^{12}C/^{13}C$ ratios is still unknown. Amari et al. (2001) have suggested J stars and born-again giants like Sakurai's object as the sources of SiC grains of type A and B, which have $^{12}C/^{13}C < 10$. We present here the results of isotopic analyses of seven HD graphite grains with $^{12}C/^{13}C < 20$ from the Orgueil, ORG1f ($2.02 - 2.04$ g cm^{-3}) density fraction.

3.2 Experimental Methods

Large grains (> 2 μm) from the high-density fraction of Orgueil, ORG1f ($2.02 - 2.04$ g cm^{-3}), were selected for these measurements. This size selection was made to ensure that multi-element isotopic analyses can be made on the grains. Spherical, carbonaceous grains were first identified by X-ray analysis in the scanning electron microscope (SEM) and then transferred with a micromanipulator onto a gold-foil mount. This procedure was essential to isolate the grains from the large amounts of macromolecular carbonaceous material, in which graphite grains from Orgueil are often found embedded. Analysis of isolated grains reduces contamination from the surrounding material. The Cameca NanoSIMS 50 at Washington University was used to measure C, N, O, Si, Al-Mg, K, Ca, and Ti isotopes on forty-four grains from ORG1f. We used a Cs^+ primary beam to generate negative secondary ions of ^{12}C, ^{13}C, ^{16}O, and ^{18}O in phase 1 of the analyses, and of $^{12}C^{14}N$, $^{12}C^{15}N$, ^{28}Si, ^{29}Si, and

^{30}Si in phase 2. These ions were counted in multidetection mode. In phase 3 of the analyses, positive secondary ions of ^{12}C, ^{24}Mg, ^{25}Mg, ^{26}Mg, and ^{27}Al, produced with an O^- beam, were detected. The K, Ca, and Ti measurements were carried out with the O^- beam in a combination of peak-jumping and multidetection modes. Positive secondary ions of ^{39}K, ^{41}K, and ^{43}Ca (B field 1) and ^{12}C, ^{40}Ca, ^{42}Ca, ^{44}Ca, and ^{48}Ti (B field 2) were measured to obtain K and Ca ratios. Ti isotopes were measured using three magnetic fields: at B_1 we detected ^{46}Ti, ^{48}Ti, and ^{50}Ti; B_2 – ^{47}Ti, ^{49}Ti, and ^{51}V; and B_3 – ^{12}C, ^{40}Ca, ^{48}Ti, ^{50}Ti, and ^{52}Cr. Vanadium-51 and ^{52}Cr were used to correct the ^{50}Ti signal for isobaric interferences from V and Cr, and, ^{40}Ca was measured to correct for Ca interferences at masses 46 and 48.

The isotopic measurements were carried out at sufficiently high mass resolutions in order to avoid molecular interferences (e.g., SiO at mass 44). The unresolvable isobaric peaks were as follows: (a) ^{46}Ca and ^{46}Ti at mass 46, (b) ^{48}Ca and ^{48}Ti at mass 48, and (c) ^{50}Ti and ^{50}Cr at mass 50. The abundances of ^{46}Ca and ^{48}Ca are so low that we do not expect these interferences to produce significant anomalies. We applied corrections for these interferences by assuming normal or terrestrial ^{46}Ca/^{40}Ca and ^{48}Ca/^{40}Ca ratios. For the one grain that was found to have a large ^{46}Ti anomaly, we are able to rule out the possibility of a large contribution from the ^{46}Ca signal (see discussion on grain g-9 in Section 4). Further, a large ^{48}Ca signal will cause deficits in the Ti isotopic ratios that are normalised to ^{48}Ti. The observed excesses in such grains will, as a result, be lower limits. We also assume that all the contribution from ^{50}Cr to the ^{50}Ti signal is terrestrial. This is a reasonable assumption because the grains acquire large amounts of terrestrial Cr in the laboratory from $Na_2Cr_2O_7$, which is used as an oxidising agent during the chemical separation procedure for these grains.

Similar to previous measurements (Jadhav et al. 2006), a majority of the HD graphite grains in this study have large ^{12}C/^{13}C ratios. We present here the results

of our isotopic analyses on a subset of seven grains that have $^{12}C/^{13}C < 20$.

3.3 Results

C, N, O, Si, and Al-Mg isotopes: The $^{12}C/^{13}C$ ratios of the seven grains range from 4 – 18 (Table 3.1). The N, O, Si, Al-Mg and K isotopic ratios of these grains are listed in Table 3.1. We were able to obtain $^{14}N/^{15}N$ ratios for only four of these grains. Grain g-29 exhibits an excess in ^{14}N ($^{14}N/^{15}N = 412 \pm 6$) while grain g-o67 is enriched in ^{15}N ($^{14}N/^{15}N = 51 \pm 1$). The other two grains have solar $^{14}N/^{15}N$ ratio (~ 272) within errors. Only one grain, g-38, has an anomalous $^{16}O/^{18}O$ ratio of 602 ± 14 (solar $^{16}O/^{18}O \sim 499$), the rest have terrestrial O isotopic ratios. Solar N and O ratios have also been previously obtained on Murchison and Orgueil HD grains (Hoppe et al. 1995; Jadhav et al. 2006). This puzzling result in view of the large range of C isotopic ratios seen in these grains has been attributed to equilibration with normal N and O, either on the parent body or in the laboratory (Hoppe et al. 1995). No stellar source is known to produce anomalous C and normal N simultaneously. The Si isotopes of these seven grains show a similar behaviour. Six grains have close to normal $^{29,30}Si/^{28}Si$ ratios. The largest anomaly was seen in grain g-o67, which is depleted in ^{29}Si ($\delta^{29}Si = -325 \pm 18$) and enriched in ^{30}Si ($\delta^{30}Si = 235 \pm 30$). This grain is highly enriched in ^{13}C ($^{12}C/^{13}C \sim 4$; solar 89) and ^{15}N ($^{14}N/^{15}N = 51 \pm 1$). All the grains were found to be normal in $^{25}Mg/^{24}Mg$ within errors. Grain g-o67 has the largest ^{26}Mg excess ($\delta^{26}Mg = 1593 \pm 140$) and a large inferred $^{26}Al/^{27}Al$ ratio of 0.010 ± 0.001. Another grain, g-38, with a $\delta^{26}Mg$ value of 336 ± 49 has an inferred $^{26}Al/^{27}Al$ ratio of 0.00050 ± 0.00007. The Al/Mg ratios for the remaining grains were too low for detection of radiogenic ^{26}Mg. It is possible that the equilibration processes affecting the N and O isotopes also dilute the Si and Mg isotopes in these HD graphite grains. Thus, apart from the large ^{13}C excesses, these grains are mostly normal in the N, O, Si, and Al-Mg isotopic ratios (Table 3.1).

Table 3.1 C, N, O, Si, Al-Mg, K, Ca, Ti Isotopic Ratios of High-Density Graphite Grains from ORG1f with $^{12}C/^{12}C < 20$

Grain	$^{14}N/^{15}N$	$^{16}O/^{18}O$	$\delta^{29}Si/^{28}Si$ (‰)	$\delta^{30}Si/^{28}Si$ (‰)	$\delta^{25}Mg/^{24}Mg$ (‰)	$\delta^{26}Mg/^{24}Mg$ (‰)	$^{26}Al/^{27}Al$ ($\times10^{-3}$)	$^{41}K/^{39}K$ ($\times10^{-2}$)
g-1	267±18	520±7	-20±13	-35±18	22±25	-15±23	b	7.310±0.238
g-38	a	602±14	-68±21	-20±28	-6±42	336±49	0.472±0.069	7.938±0.771
g-o67	51±1	500±11	-325±18	235±30	1±78	1593±140	9.732±0.857	7.302±0.139
g-9	294±7	518±10	-27±24	-74±30	1±23	-23±22	b	8.031±0.184
g-29	412±6	525±9	-34±19	-65±25	-26±15	-1±15	b	7.281±0.091
g-40	a	519±9	-7±19	-38±24	-22±11	-13±11	b	7.247±0.058
g-34	a	515±11	-16±20	-47±25	5±26	6±25	b	7.249±0.073

Grain	$^{12}C/^{13}C$	$^{41}Ca/^{40}Ca$ ($x10^{-3}$)	$\delta^{42}Ca/^{40}Ca$ (‰)	$\delta^{43}Ca/^{40}Ca$ (‰)	$\delta^{44}Ca/^{40}Ca$ (‰)	$^{44}Ti/^{48}Ti$ ($x10^{-3}$)	$\delta^{46}Ti/^{48}Ti$ (‰)	$\delta^{47}Ti/^{48}Ti$ (‰)	$\delta^{49}Ti/^{48}Ti$ (‰)	$\delta^{50}Ti/^{48}Ti$ (‰)
g-1	14	0.3 ± 0.9	-152 ± 96	156 ± 239	6018 ± 203	0.179 ± 0.008	-15 ± 8	-28 ± 9	161 ± 11	44 ± 15
g-38	4	1.2 ± 1.2	-118 ± 177	-602 ± 274	51886 ± 1499	0.765 ± 0.028	-77 ± 12	-98 ± 15	125 ± 6	242 ± 6
g-o67	4	0.3 ± 0.3	63 ± 52	15 ± 107	3767 ± 77	0.595 ± 0.025	2 ± 4	14 ± 4	169 ± 5	236 ± 6
g-9	18	2.3 ± 0.4	16028 ± 316	27641 ± 805	9396 ± 151	c	35032 ± 4432	1376 ± 371	2278 ± 298	32827 ± 4594
g-29	10	0.2 ± 0.2	1451 ± 50	1628 ± 100	540 ± 24	c	d	d	d	d
g-40	11	0.2 ± 0.3	3375 ± 65	3662 ± 138	554 ± 22	c	d	d	d	d
g-34	8	0.1 ± 0.1	5064 ± 60	7410 ± 146	2179 ± 25	c	d	d	d	d

Note: Errors are 1 σ; δ values are deviations from solar ratios per mil.
[a] Not measured because a large signal from $^{13}C_2$ gives rise to an unresolvable interference at mass 26 while measuring $^{12}C^{14}N$.
[b] No $^{26}Al/^{27}Al$ ratios were derived for these grains since they do not exhibit any ^{26}Mg excesses.
[c] Did not derive $^{44}Ti/^{48}Ti$ ratio for these grains because the $\delta^{44}Ca/^{40}Ca$ values are comparable to the $\delta^{42}Ca/^{40}Ca$ and $\delta^{43}Ca/^{40}Ca$ values.
[d] Not measured because of very low Ti signal.

K, Ca, and Ti isotopes: Six of the grains have a normal $^{41}K/^{39}K$ ratio (0.072) within errors. Grain g-9 is the only one with an elevated $^{41}K/^{39}K$ ratio of 0.080 ± 0.002 (Table 3.1). Since the intrinsic concentration of K in graphite grains is expected to be very low, we attribute the ^{41}K excess in this grain to the decay of ^{41}Ca ($T_{1/2} = 1.03 \times 10^5$ a) (Amari, Zinner & Lewis 1996) and obtain an inferred $^{41}Ca/^{40}Ca$ ratio of 0.002 (Table 3.1). The Ca and Ti isotopic compositions of the seven grains are given in Table 3.1 and plotted as isotopic patterns in Figures 3.1 – 3.4. Three of the grains (g-1, g-38, and g-o67) have solar (within errors) or sub-solar $^{42}Ca/^{40}Ca$ and $^{43}Ca/^{40}Ca$ ratios but display enormous ^{44}Ca excesses. Their $^{46}Ti/^{48}Ti$ and $^{47}Ti/^{48}Ti$ ratios are normal (within errors) or sub-solar whereas the $^{49}Ti/^{48}Ti$ and $^{50}Ti/^{48}Ti$ ratios are larger than the terrestrial values. The other four grains exhibit large excesses in ^{42}Ca, ^{43}Ca, and ^{44}Ca and these excesses are especially large in grain g-9. This grain also has large excesses in ^{46}Ti and ^{50}Ti and relatively smaller excesses in ^{47}Ti and ^{49}Ti. The Ti concentrations in grains g-29, g-40, and g-34 were too low to be able to obtain Ti isotopic data.

In the following section we discuss in detail the C, Ca, and Ti isotopic ratios and the clues they provide in determining the possible stellar sources for these grains.

3.4 Discussion

Figure 3.1a shows the Ca isotopic patterns for the three grains, g-1, g-38 and g-o67, which contain large ^{44}Ca excesses. Neutron capture either in AGB stars or in interior zones of Type II SNe can produce excesses in ^{44}Ca relative to ^{40}Ca. However, in all these cases the excesses in ^{42}Ca and ^{43}Ca are expected to be larger than those in ^{44}Ca. This is clearly not the case for these three grains. Furthermore, the ^{44}Ca excesses are much greater than those predicted for the He/C and O/C zones of a type II SNe (Woosley & Weaver 1995). Thus the ^{44}Ca excesses must come from the decay of the short-lived radionuclide, ^{44}Ti ($T_{1/2} = 60$ a). During SIMS analysis we observed the

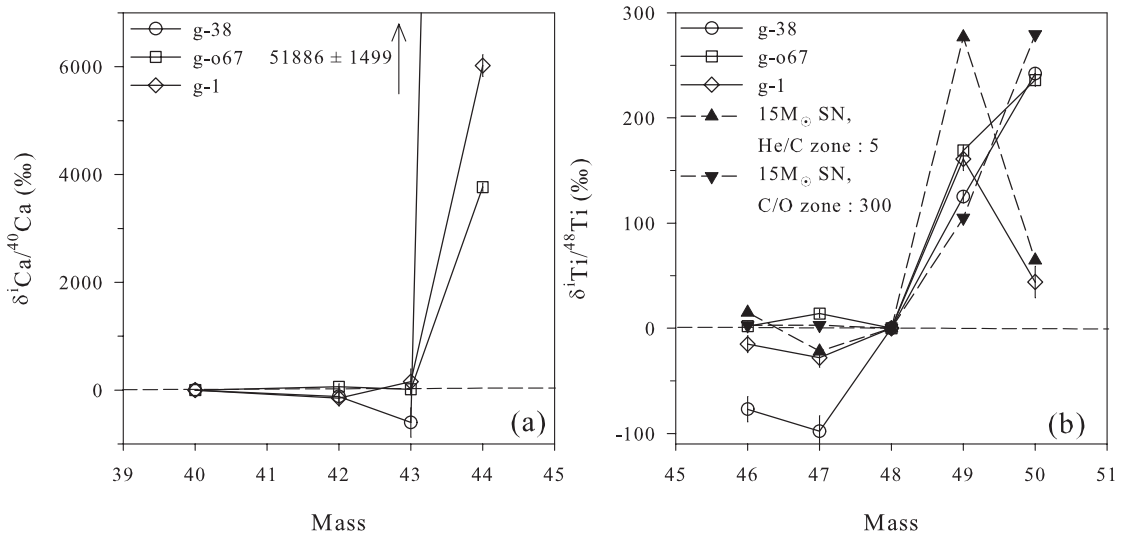

Figure 3.1 The Ca (a) and Ti (b) isotopic patterns observed in three graphite grains are plotted versus mass number and compared with theoretical models of stellar sources. The ratios are plotted as delta values, deviations from solar ratios in per mil (‰). Error bars in this and subsequent plots are 1 σ.(a) The grains, g-38, g-o67, g-1, have ^{44}Ca excesses that vastly exceed any anomalies in ^{42,43}Ca, indicating the initial presence of the short-lived radionuclide ^{44}Ti. (b) Grain g-1 has a Ti isotopic pattern similar to that seen in the He/C zone of a $15M_{\odot}$ SN while, the patterns for grains g-38 and g-o67 agree well with those predicted for the C/O zone of a $15M_{\odot}$ SN. The theoretical isotopic ratios seen in these zones are normalized to match the size of the anomalies observed in the grains.

^{44}Ca ion signals for these three grains to be perfectly correlated with the ^{48}Ti ion signals but not with those of the other Ca isotopes, providing additional evidence that the ^{44}Ca excesses must be from the decay of ^{44}Ti. Titanium-44 is produced only in SN explosions (Timmes et al. 1996; Woosley & Weaver 1995; Iyudin et al. 1994; Vink et al. 2001) and hence the initial presence of this isotope in grains g-1, g-38, and g-o67 indicates a SN origin. The derived ^{44}Ti/^{48}Ti ratios for these grains are given in Table 3.1. Titanium-44 is produced in the Ni- and Si-rich zones of type II SNe by α-rich freeze-out from quasi-statistical equilibrium (Woosley, Arnett & Clayton 1973; Woosley & Weaver 1995; Timmes et al. 1996) and can be found in graphite grains provided some ^{44}Ti from the inner zones is mixed with material from the carbon-rich, outer zones. The Ti isotopic patterns for these grains (Figure 3.1b) match those

seen in the C/O and He/C zones of a $15M_{\odot}$ SN (Woosley & Weaver 1995). Grain g-o67 exhibits an excess in ^{15}N and has a high ^{26}Al/^{27}Al ratio – signatures consistent with a SN origin. Nitrogen-15 is abundant at the bottom of the He/C zone and high ^{26}Al/^{27}Al ratios are found in the He/N zone that had undergone H burning (Forestini, Paulus & Arnould 1991; Mowlavi & Meynet 2000; Karakas & Lattanzio 2003). The only highly unusual signature in this grain is its low ^{12}C/^{13}C ratio ($\sim$ 4). Most of the SiC X grains that show evidence for ^{44}Ti have higher ^{12}C/^{13}C ratios (Nittler et al. 1996). The He/N zone has a low ^{12}C/^{13}C ratio, however, in order to achieve the low ^{14}N/^{15}N ratio and the Ti isotopic signatures of this grain, material from the underlying He/C and C/O zones has to be mixed to material from the He/N zone. These two zones have not only extremely high ^{12}C/^{13}C ratios but also C contents that are higher than that in the He/N zone by large factors. Thus, it is unclear how grain g-o67 can have such a low ^{12}C/^{13}C ratio after admixture of material from lower zones to match the Ti isotopic ratios. A similar problem is posed by the other two SN grains. Grain g-38 has a moderately high ^{26}Al/^{27}Al ratio (0.0005 ± 0.00007), lower than what is found in almost all SN zones with the exception of the lower layers of the He/C zone. Grain g-1 is normal (within errors) in N, O, Si, Al-Mg and K isotopes. Both grains have low ^{12}C/^{13}C ratios ($\sim$ 4 and 14) but have ^{49}Ti and ^{50}Ti excesses that require contributions from zones with large abundances of almost pure ^{12}C.

Grain g-9 has extreme ^{42,43,44}Ca and ^{46,47,49,50}Ti excesses (Figures 3.2a,b). These excesses and the ^{41}Ca/^{40}Ca ratio (0.0023 ± 0.0004) are incompatible with an AGB origin. The ^{41}Ca/^{40}Ca ratios expected in AGB stars are on the order of 10^{-4} to 10^{-5} (Amari, Zinner & Lewis 1996; Gallino et al. 1998; Wasserburg et al. 1995). High ratios can be obtained in the He/C, C/O and O-rich zones of Type II SNe where the ^{22}Ne$(\alpha, n)^{25}$Mg reaction provides ample neutrons for the production of ^{41}Ca (Woosley & Weaver 1995). That the observed ^{41}Ca/^{40}Ca ratio in grain g-9 is smaller can be explained by mixing with material from the He/N zone or isotopic equilibration. On

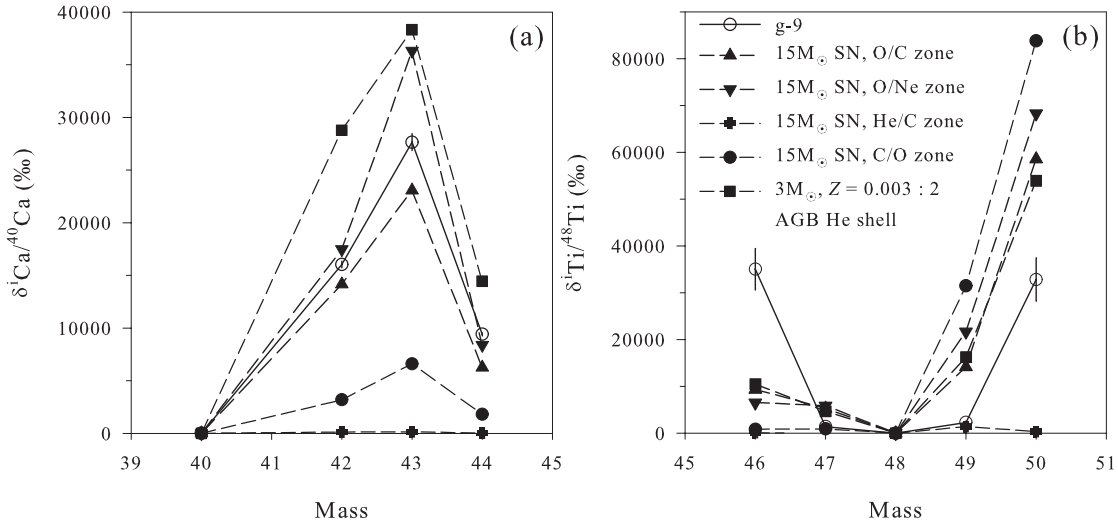

Figure 3.2 The Ca (a) and Ti (b) isotopic patterns observed in grain g-9 are plotted versus mass number and compared with theoretical predictions. The ratios are plotted as delta values. This grain has Ca and Ti isotopic patterns that are similar to those predicted for O-rich (O/C and O/Ne) zones of a $15M_{\odot}$ SN and for the He shell of a $3M_{\odot}$ AGB star with metallicity $Z = 0.003$. The predicted pattern of the He shell was diluted by a factor of 2 to fit the Ca isotopic pattern seen in the grain. However, the large ^{46}Ti excess cannot be explained. This grain has a $^{12}C/^{13}C$ ratio ~ 18.

the other hand, as seen in Figure 3.2a, the Ca isotopic excesses observed in grain g-9 are too high to permit any mixing with the He/N zones. They are higher than those found in the He/C or C/O zones of a $15M_{\odot}$ SN and one has to go to the O/C and O/Ne zones to match the excesses seen in the grain (Figure 3.2a). Figure 3.2b shows that the C/O zone could explain the large ^{49,50}Ti excesses but not the ^{46}Ti excess. The O/C and O/Ne zones are able to account for the large ^{47,49,50}Ti anomalies (but not ^{46}Ti) seen in this grain. If grain g-9 originated in a SN then it requires pure O/C or O/Ne zone materials to explain its Ca and Ti isotopic compositions. However, the C in all these zones is essentially pure ^{12}C and the carbon abundances are much higher than that in the He/N zone, the only place with a low $^{12}C/^{13}C$ ratio of ~ 3.6 (Woosley & Weaver 1995). This makes it impossible to achieve the low $^{12}C/^{13}C$ ratio of 18 in grain g-9 while maintaining the large Ca and Ti excesses by mixing of material from the He/N zone with material from the C/O, O/C, or O/Ne zones. What makes

the situation even more difficult is that the extremely high Ca isotopic ratios in the O/C and O/Ne zones are in part the result of a substantial drop in the abundance of ^{40}Ca (the reference isotope in these ratios) as one goes below the He/C zone.

The origin of the huge ^{46}Ti excess in g-9 is unknown. Two possible explanations for this large ^{46}Ti excess can be ruled out. A large contribution could have been from ^{46}Ca because in our SIMS measurement we could not resolve the ^{46}Ca and ^{46}Ti signals from one another (this requires a mass resolving power of 43,233, which is beyond the capability of the NanoSIMS). We used the measured Ca/Ti ratio of this grain (~ 35) to calculate the ^{46}Ca signal expected from the abundance pattern in a AGB He-shell (see below) or a SN zone that matches the other Ca isotopic ratios of the grain. We found that the expected contribution from ^{46}Ca is much too small to explain the large ^{46}Ti excess observed in this grain. Alternatively, an $\sim 1\%$ contribution from the Si/O zone of a $15M_{\odot}$ SN, which has a high abundance of ^{46}Ti (Woosley & Weaver 1995), could explain the ^{46}Ti excess. However, such a contribution will result in a large ^{40}Ca excess and in turn, deficits in ^{43,44}Ca, which are not observed. It is essential to point out at this stage that it is not necessary for both the Ca and Ti anomalies in a single graphite to originate from the same stellar source. This is because all the Ti is obtained from subgrains within the graphite grain while Ca is found to be uniformly distributed in the host grain. The parent grain and the subgrain could have condensed in completely different stellar environments and the Ca and Ti anomalies could represent these distinct stellar sources.

In the remainder of this discussion we will attempt to explain the Ca and Ti excesses in grains g-9, g-34, g-29, and g-40 by comparing them with predictions for the He shell of AGB nucleosynthesis models. These models have been discussed in detail by Gallino et al. (1998) and more recently, by Zinner et al. (2006b). The Gallino et al. (1998) models calculate nuclear abundances at the surface of AGB stars by mixing He shell material into the envelope by TDU. However, we use pure He shell

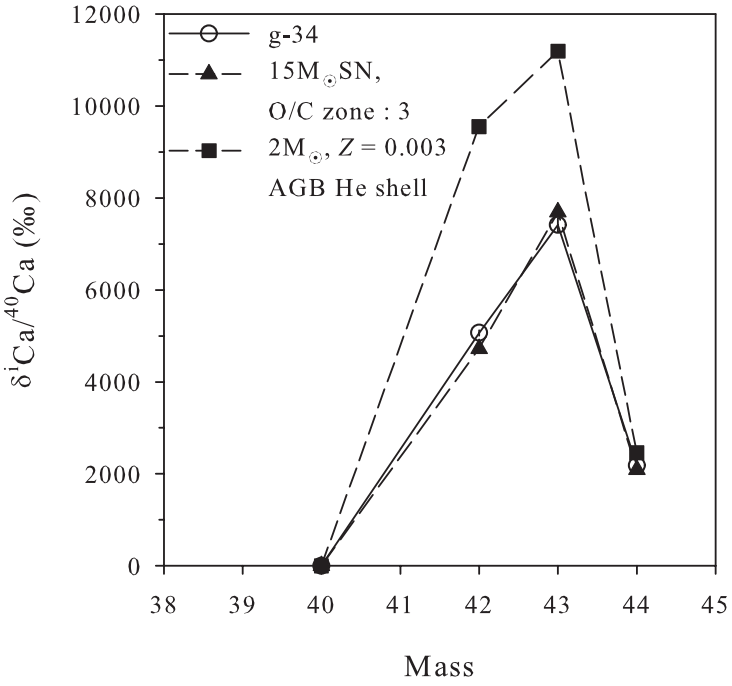

Figure 3.3 The Ca isotopic pattern observed in grain g-34, is plotted versus mass number and compared with model predictions. The ratios are plotted as delta values. This grain has a $^{12}C/^{13}C$ ratio of ~ 8 and a Ca isotopic pattern that matches the pattern predicted for the C/O zone of a $15M_{\odot}$ SN and that of the He shell of a $2M_{\odot}$ AGB star with metallicity, $Z = 0.003$ (divided by three).

predictions (without dilution with envelope material) from these models to explain the excesses seen in the aforementioned grains.

The size of the Ca and Ti excesses seen in grain g-9 is incompatible with an AGB star origin since no AGB nucleosynthetic model can account for such high $\delta^{42,43,44}$Ca and $\delta^{47,49,50}$Ti values in its envelope. These signatures can be matched by slight dilution of pure He shell material of a $3M_{\odot}$, low metallicity ($Z = 0.003$) AGB star (Figures 3.2a,b). However, the He shell of an AGB star consists of almost pure ^{12}C, making it difficult to explain the ^{13}C excess in this grain. We shall discuss a possible stellar source that can explain the signatures seen in grain g-9 in detail farther below, since the remaining grains also require a similar explanation.

Grain g-34 has a low $^{12}C/^{13}C$ ratio of ~ 8 and has a Ca isotopic pattern that matches closely that expected in the C/O zone of a $15M_{\odot}$ SN (Figure 3.3). However,

this and underlying zones contain essentially pure ^{12}C. Similar to grain g-9, mixing between the He/N zone and the O/C and O/Ne zones cannot match both the Ca isotopic ratios and the low ^{12}C/^{13}C ratio of this grain. Alternatively, the Ca excesses of this grain can be explained by the He shell of a $2M_{\odot}$, $Z = 0.003$ AGB star (Figure 3.3).

The situation is the same for the last two grains, g-29 and g-40. Although excesses in ^{42,43,44}Ca are smaller than those in the previously discussed grains, any admixture from the underlying SN zones to material from the He/N zones required to match the Ca isotopic ratios increases the ^{12}C/^{13}C ratio far beyond those (10 and 11) measured in these grains. On the other hand, the Ca anomalies are much larger than those predicted for the envelope of AGB stars. Apart from the high C and Ca isotopic anomalies in both these grains, grain g-29 also exhibits an excess in ^{14}N (^{14}N/^{15}N$\sim$ 412).

The Ca patterns of g-29 and g-40 match those of pure nucleosynthetic components theoretically predicted for the He shell of a $2M_{\odot}$ AGB star of solar metallicity (Figure 3.4). However, both grains have ^{12}C/^{13}C ratios of ~ 10 that completely disagree with the type of nucleosynthesis taking place in a He-burning shell. The basic problem is that the Ca (and Ti) isotopic compositions of our graphite grains show the signature of neutron capture, requiring He burning, which results in the production of ^{12}C. This is in disagreement with the low ^{12}C/^{13}C ratios found in the grains, which are the result of H burning in the CNO cycle. One possible stellar source that combines an s-process signature with that of H burning are born-again AGB or post-AGB stars that undergo a very late He flash. These stars, typified by Sakurai's object (V4334Sgr), undergo a very late thermal pulse (VLTP) during their descent along the white dwarf cooling track, long after they have left the AGB phase (Asplund et al. 1999). The spectroscopic observations of Sakurai's object by Duerbeck & Benetti (1996), Asplund et al. (1997, 1999), and Kipper & Klochkova (1997) have shown that it is rich in He,

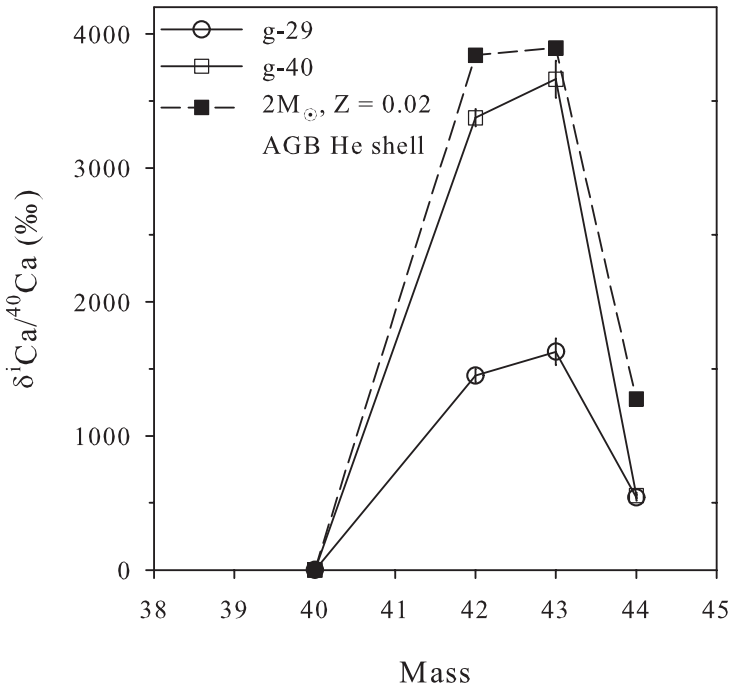

Figure 3.4 The Ca isotopic patterns obtained for grains g-29 and g-40, are plotted versus mass number and compared with that predicted for the He shell of a $2M_{\odot}$ AGB star of solar metallicity. The ratios are plotted as delta values. Both grains are highly enriched in ^{13}C (^{12}C/^{13}C ratio of g-29 is 10 and of g-40 is 11). These grains could have originated from born-again AGB stars, which have envelopes with very low ^{12}C/^{13}C ratios and enrichments in s-process elemental abundances.

C, N, O (C > O) and the s-process elements, along with being deficient in H. The object also has a ^{12}C/^{13}C ratio of 1.5 – 5.0. Complete H-burning is evidenced by H deficiency and high He abundances. The simultaneous occurrence of a low ^{12}C/^{13}C ratio along with s-process elemental enrichments indicates that H-burning occurred after the star left the AGB track. At this stage in its evolution the star has lost most of its envelope as a planetary nebula and only a thin residual H-rich layer is left. Herwig et al. (1999) and Herwig (2001) studied evolutionary models of $2M_{\odot}$ stars that undergo a VLTP. They showed that in such objects the He-flash-powered convection zone, which is rich in freshly produced ^{12}C, can mix with the residual H-rich envelope and cause convective H burning via the CN cycle. The ^{12}C/^{13}C ratio is thus drastically reduced as ^{12}C is converted to ^{13}C. The surface of the star is H-rich

before the convection zone extends into the envelope but becomes rapidly depleted in H as convective H-burning continues. The envelope continues to remain C-rich because it is thin and the residual envelope had only a limited number of protons, which prevents the CN cycle from reaching equilibrium (^{14}N is less abundant than ^{12}C) before all the H is exhausted. Iben (1984) and Renzini (1982) estimated that $10-25\%$ of stars that leave the AGB phase and are on the white dwarf track undergo a late He flash.

Thus, we propose that grains g-29 and g-40, and possibly g-34 and g-9, condensed in the atmosphere of such an object. The low ^{12}C/^{13}C ratios in the grains are explained by limited H burning of the residual envelope. The large neutron-capture effects in Ca and Ti are explained by the fact that the heavy-element compositions on the surface of a born-again AGB star are very similar to those of the He shell because there is not much envelope material to dilute them. The currently cooling Sakurai's object is known to be producing large quantities of C-rich dust (Asplund et al. 1997, 1999). Infrared observations of the atmosphere of this star indicate the presence of graphite dust in the atmosphere (Eyres et al. 1998). Born-again stars, like Sakurai's object, have also been considered to be viable candidates for the sources of SiC grains of type A and B (Amari et al. 2001). These grains are characterized by their low ^{12}C/^{13}C ratios (< 10) and a large range of ^{14}N/^{15}N ratios (40 – 10^4). Some of them were also found to be enriched in s-process elements.

In summary, we find that seven graphite grains with ^{12}C/^{13}C < 20 have puzzling origins. The three grains g-1, g-38 and g-o67 certainly come from type II SNe as indicated by the presence of ^{44}Ti. There exists no explanation for their low ^{12}C/^{13}C ratios in conjunction with their Ti isotopic compositions. Similar signatures have been seen by Nittler et al. (1996) in one LD graphite grain from Murchison (KE3c-242). This grain shows evidence for ^{44}Ti, has a ^{12}C/^{13}C ratio of 6.91 ± 0.02, an ^{26}Al/^{27}Al ratio of 0.0018 ± 0.0003 and has normal N and O. Nittler & Hoppe (2005) found one

SiC grain that has ^{28}Si, ^{49}Ti, and ^{44}Ca excesses and a high inferred ^{26}Al/^{27}Al ratio but a very low ^{12}C/^{13}C ratio. All the isotopes in this SiC grain indicate a SN origin except the C isotopic compositions.

One remaining puzzle is why grains g-9, g-29, g-34, and g-40 seem to retain almost pure nucleosynthetic components in Ca and Ti, but are essentially normal in their Mg and Si isotopic compositions. The neutron-capture reactions that affected the Ca and Ti isotopes of the grains should also have changed their Mg and Si isotopic compositions significantly. Isotopic equilibrations, as invoked for N, are a possibility but we have to better understand siting and bonding of various trace elements in graphite grains before we can arrive at a conclusion.

Material for the seven grains that have been discussed above still remains after the SIMS analyses. We intend to measure heavy element (Mo, Zr, Sr, Ba) isotopes in these grains with resonant ionization mass spectrometry (RIMS) at the Argonne National Laboratory. Such coordinated analyses might help to address some of the unanswered questions regarding these grains.

3.5 Conclusions

The measurements of Ca and Ti isotopic compositions in high-density graphite grains with ^{12}C/^{13}C < 20 lead us to consider Type II SNe and born-again AGB stars as stellar sources of high-density graphite grains, in addition to low-metallicity AGB stars. Thus, high-density graphite grains seem to have multiple stellar sources. More isotopic systems need to be measured on the grains discussed in this paper and additional grains with similar ^{13}C excesses need to be isolated and studied extensively in order to better constrain the stellar sources of this particular population of presolar graphite grains. We hope that this study will trigger theoretical efforts to create additional nucleosynthetic models that will result in a better understanding of the isotopic signatures seen in such grains. The detection and study of more objects like Sakurai's

object could strengthen the hypothesis that these objects are valid stellar sources of some presolar grains.

Acknowledgments: The authors appreciate the detailed review by the anonymous referee that helped improve this paper. We thank Tim Smolar for his assistance with the NanoSIMS. This work was supported by NASA grant NNG05GF81G and the Italian MIUR-PRINO6 grant.

References

Amari, S., Anders, A., Virag, A., & Zinner, E. 1990, Nature, 345, 238

Amari, S., Lewis, R. S., & Anders, E. 1995, Geochim. Cosmochim. Acta, 59, 1411

Amari, S., Zinner, E., & Lewis, R. S. 1996, ApJ, 470, L101

Amari, S., Nittler, L. R., Zinner, E., Lodders, K., & Lewis, R. S. 2001, ApJ, 559, 463

Amari, S., Zinner, E., & Lewis, R. S. 2005, Meteorit. Planet. Sci., 40, A15

Asplund, M., Gustafsson, B., Lambert, D. L., & Kameswara Rao, N. 1997, A&A, 321, L17

Asplund, M., Lambert, D. L., Kipper, T., Pollacco, D., & Shetrone, M. D. 1999, A&A, 343, 507

Bernatowicz, T. J., Cowsik, R., Gibbons, P. C., Lodders, K., Fegley, B., Jr., Amari, S., & Lewis, R. S. 1996, ApJ, 472, 760

Bernatowicz, T. J., Croat, T. K., & Daulton, T. L. 2006, in Meteorites and the Early Solar System II, ed. D. S. Lauretta & H. Y. McSween, Jr. (Univ. of Arizona, Tucson & LPI), 109

Busso, M., Gallino, R., & Wasserburg, G. J. 1999, ARA&A, 37, 239

Croat, T. K., Stadermann, F. J., & Bernatowicz, T. J. 2005, ApJ, 631, 976

Duerbeck, H. W., & Benetti, S. 1996, ApJ, 468, L111

Eyres, S. P. S., Evans, A., Geballe, T. R., Salama, A., & Smalley, B. 1998, MNRAS, 298, L37

Forestini, M., Paulus, G., & Arnould, M. 1991, A&A, 252, 597

Gallino, R., Arlandini, C., Busso, M., Lugaro, M., Travaglio, C., Straniero, O., Chieffi, A., & Limongi, M. 1998, ApJ, 497, 388

Herwig, F., Blöcker, T., Langer, N., & Driebe, T. 1999, A&A, 349, L5

Herwig, F. 2001, Ap&SS, 275, 15

Hoppe, P., Amari, S., Zinner, E., & Lewis, R. S. 1995, Geochim. Cosmochim. Acta, 59, 4029

Hoppe, P., Annen, P., Strebel, R., Eberhardt, P., Gallino, R., Lugaro, M., Amari, S., & Lewis, R. S. 1997, ApJ, 487, L101

Iben, I., Jr. 1984, ApJ, 277, 333

Iyudin, A. F., Diehl, R., Bloemen, H., Hermsen, W., Lichti, G. G., Morris, D., Ryan, J., Schönfelder, V., Steinle, H., Varendorff, M., de Vries, C., & Winkler, C. 1994, A&A, 284, L1

Jadhav, M., Amari, S., Zinner, E., & Maruoka, T. 2006, New Astronomy Reviews, 50, 591

Karakas, A. I., & Lattanzio, J. C. 2003, 20, 279

Kipper, T., & Klochkova, V. G. 1997, A&A, 324, L65

Lodders, K., & Fegley B., Jr. 1997, in AIP Conf. Proc. 402, Astrophysical Implications of the Laboratory Study of Presolar Materials, eds. T. J. Bernatowicz & E. Zinner. (Woodbury, New York: AIP), 391

Mowlavi, N., & Meynet, G. 2000, A&A, 361, 959

Nittler, L. R., Amari, S., Zinner, E., Woosley, S. E., & Lewis, R. S. 1996, ApJ, 462, L31

Nittler, L. R., & Alexander, C. M. O'D. 2003, Geochim. Cosmochim. Acta 67, 4961

Nittler, L. R., & Hoppe, P. 2005, ApJ, 631, L89

Renzini, A. 1982, in Wolf-Rayet Stars: Observations, Physics, Evolution, ed. C. W. H. de Loore & A. J. Willis (Dordrecht: Reidel), 413

Timmes, F. X., Woosley, S. E., Hartmann, D. H., & Hoffman, R. D. 1996, ApJ, 464, 332

Travaglio, C., Gallino, R., Amari, S., Zinner, E., Woosley, S., & Lewis, R. S. 1999, ApJ, 510, 325

Vink, J., Laming, J. M., Kaastra, J. S., Bleeker, J. A. M., Bloemen, H., & Oberlack, U. 2001, ApJ, 560, L79

Wasserburg, G. J., Gallino, R., Busso, M., Goswami, J. N., & Raiteri, C. M. 1995, ApJ, 440, L101

Woosley, S. E., Arnett, W. D., & Clayton, D. D. 1973, ApJS, 26, 231

Woosley, S. E., & Weaver, T. A. 1995, ApJS, 101, 181

Zinner, E., Amari, S., Wopenka, B., & Lewis, R. S. 1995, Meteoritics, 30, 209

Zinner, E., Amari, S., & Jadhav, M. 2006a, in ISNA Proc. - Nuclei in the Cosmos-IX, POS, 019

Zinner, E., Nittler, L. R., Gallino, R., Karakas, A. I., Lugaro. M., Straniero, O., & Lattanzio, J. C. 2006b, ApJ, 650, 350

Chapter 4

MULTI-ELEMENT ISOTOPIC ANALYSES OF PRESOLAR GRAPHITE GRAINS FROM ORGUEIL

Abstract

We report isotopic analyses of presolar graphite grains from the Orgueil CI chondrite. NanoSIMS isotopic measurements were made on 345 grains from seven density fractions, with grain sizes > 1 μm: OR1b (1.59 – 1.67 g cm^{-3}), OR1c (1.67 – 1.75 g cm^{-3}), OR1d (1.75 – 1.92 g cm^{-3}), OR1f (2.02 – 2.04 g cm^{-3}), OR1g (2.04 – 2.12 g cm^{-3}), OR1h (2.12 – 2.16 g cm^{-3}), and OR1i (2.16 – 2.30 g cm^{-3}). We measured C, N, O, Si, Al-Mg, K, Ca, and Ti isotopes in multidetection mode with the NanoSIMS. All the fractions, except OR1b and OR1h, contain presolar graphite as demonstrated by the large range of carbon isotopic ratios (4 – 2478) measured in individual grains. The occurence of isotopically light carbon in the grains increases with increasing density. Some isotopic properties are dependent on density: low-density grains contain ^{18}O, ^{15}N, and ^{28}Si, excesses while the majority of high-density grains contain normal O and N and do not exhibit any ^{28}Si excesses. However, high-density grains are generally enriched in ^{29}Si and ^{30}Si. The ^{15}N, ^{18}O, and ^{28}Si excesses in low-density grains indicate that most of them originated from supernovae, while high-density grains (with ^{30}Si and ^{12}C excesses) originated from asymptotic giant branch stars with low metallicities.

We also find evidence for the extinct radionuclides ^{26}Al, ^{41}Ca, and ^{44}Ti in grains from both density fractions. The derived ^{26}Al/^{27}Al ratios in the low-density fractions are high (up to 0.7), while the high-density grains have much smaller ratios (0.01 – 10^{-4}). The inferred ^{41}Ca/^{40}Ca ratios in all the grains range from 0.0004 to 0.01. The higher ends of the ranges in both these isotopic ratios are predicted for supernovae while the lower values are expected in asymptotic giant branch stars. The ^{44}Ti/^{48}Ti ratios inferred from ^{44}Ca excesses range from 0.0004 – 0.008 in grains from both density fractions. The initial presence of the short-lived radionuclide ^{44}Ti indicates that these grains are bona fide SN grains. Some of these grains have very low ^{12}C/^{13}C ratios. Such large ^{13}C-enrichements together with other SN signatures, like ^{18}O and ^{15}N, excesses cannot be obtained from mixing of different SN layers without lowering the C/O ratio of the mix below unity. This scenario does not allow carbonaceous grains to condense around a supernova. Other grains with low ^{12}C/^{13}C ratios (without evidence for ^{44}Ti) and large excesses in ^{42,43}Ca and ^{46,47,49,50}Ti might originate from born-again asymptotic giant branch stars, such as Sakurai's object, that can achieve low ^{12}C/^{13}C ratios and large s-process enrichments in Ca and Ti. In such stars, limited mixing of the He-burning intershell with the thin, residual hydrogen envelope leads to the production of ^{13}C and enables material with s-process enrichments and low ^{12}C/^{13}C ratios to occur on the surface simultaneously.

This study concludes that most low-density graphite grains originate from supernovae while high-density graphite grains have multiple stellar sources: low-metallicity and born-again asymptotic giant branch stars, as well as supernovae.

4.1 Introduction

Amari et al. (1990) isolated the first presolar graphite grains from the Murchison CM2 meteorite by identifying the grains to be carriers of the exotic noble gas component, Ne-E(L) (almost pure ^{22}Ne). Subsequently, extensive isotopic studies were carried out

on the Murchison density fractions: KE1 and KE3 (1.6 – 2.05 g cm^{-3}), KFA1 (2.05 – 2.10 g cm^{-3}), KFB1 (2.10 – 2.15 g cm^{-3}), and KFC1 (2.15 – 2.20 g cm^{-3}) (Amari et al. 1990, 1995; Hoppe et al. 1995; Zinner et al. 1995; Travaglio et al. 1999). All isotopically identified presolar graphite grains in Murchison seem to be spherical with diameters > 1 μm (ranging up to ~ 20 μm). Structural and isotopic properties of Murchison presolar graphite vary with density (Amari et al., 1995; Hoppe et al., 1995). Since then graphite grains have also been isolated from the CI chondrite, Orgueil (Jadhav et al. 2006). Similar spherical grains were identified and studied in different density fractions of Orgueil (Jadhav et al. 2006; 2008). In general, Orgueil graphite grains appear to be rather similar to Murchison graphite, both morphologically and in their isotopic properties. However, while there are many similarities between the graphite grains from the two meteorites, there are also some important differences, as will be seen in this study. Many low-density graphite grains from both meteorites exhibit evidence for a supernova origin. Their isotopic properties are similar to those of SiC-X grains, which are known to have a supernova origin (Amari et al. 1992). They have large excesses in ^{15}N, ^{18}O, and ^{28}Si (Amari et al. 1995; Jadhav et al. 2006). Most of the low-density grains show evidence for the short-lived radioisotope, ^{44}Ti (Nittler et al. 1996), have large excesses in ^{41}K (due to the decay of ^{41}Ca) (Amari et al. 1996), and high inferred ^{26}Al/^{27}Al ratios. Travaglio et al. (1999) were able to reproduce these major isotopic signatures of low-density grains by performing mixing calculations of the different layers of Type II SNe. On the other hand, low-metallicity, asymptotic giant branch (AGB) stars seem to be the source of a large fraction of high-density graphite grains. One of the s-process components of Kr, (Kr-SH) with a high ^{86}Kr/^{82}Kr ratio, resides in the high-density fraction of Murchison graphites and is believed to originate from AGB stars (Amari et al. 1995). Additional evidence for AGB graphites came from TEM studies by Croat et al. (2005). They found that high-density grains from Murchison contain subgrains rich in the s-process elements

Zr, Mo, and Ru, indicating an AGB origin. High-density graphites were also found to have large ^{30}Si excesses that are correlated with high ^{12}C/^{13}C ratios (Amari et al. 2005; Jadhav et al. 2006). In low-metallicity AGB stars, ^{12}C and ^{29,30}Si from the He shell are mixed into the envelope by third dredge-up (TDU) during the thermally pulsing phase (Busso et al. 1999; Zinner et al. 2006a). Such models predict high ^{12}C/^{13}C ratios as well as very high C/O ratios, which is an ideal environment for the condensation of graphite grains (Lodders and Fegley 1997). The stellar source(s) of graphite grains with very low ^{12}C/^{13}C ratios still remains a matter of debate. The low-density and high-density graphite grains from Murchison and Orgueil both contain a minor population of grains that have ^{12}C/^{13}C ratios $\sim$ 10 and lower. A recent study of high-density (OR1f - 2.02 – 2.04 g cm^{-3}) graphite grains from Orgueil (Jadhav et al. 2008) found extremely high Ca and Ti ratios in some grains with ^{12}C/^{13}C ratios $<$ 20. These anomalies can only be explained by pure nucleosynthetic He-shell components of AGB stars. Born-again AGB stars, like Sakurai's object (V4334 Sgr), have low ^{12}C/^{13}C ($\sim$ 4) and exhibit enhanced s-process elemental abundances (Asplund et al. 1997; 1999). The study concluded that born-again AGB stars could be the likely sources of the graphites with very low ^{12}C/^{13}C ratios and extreme Ca and Ti anomalies.

This paper is a comprehensive report of all 345 Orgueil graphites studied to date and a discussion of their nucleosynthetic sources. All the data presented in this paper are available in the electronic appendix (PSGWeb). The paper is an extension of previous publications, Jadhav et al. (2006; 2008), and conference abstracts. In addition to new data on presolar graphite grains from Orgueil, it also contains detailed experimental procedures that were not reported in the above-mentioned publications. We also introduce new nomenclature for the Orgueil graphite density separates and mounts that will be used in publications henceforth.

4.2 Experimental Methods

4.2.1 Chemical and physical separation of the graphite grains

The separation procedure used for this study was essentially the same as that carried out for Murchison graphite (Amari et al. 1994). The following is a brief description of the chemical and physical techniques that were used to separate graphite grains from Orgueil. The Orgueil sample was obtained from the National Museum of Natural History in Paris. We started with 24.16 g of the meteorite and treated it with a mixture of toluene and methanol to remove soluble organic matter. This treatment was repeated four times until 0.57 g ($\sim$ 2.35% of the original sample) of organic matter was removed. The silicates were then removed by alternating treatments with 10M HF-1M HCl and 6M HCl (14 times). Each dissolution cycle was carried out at 70°C for 15 hours. This preparation was concluded by washing the sample with a mixture of 6M HCl-0.6M H_3BO_3 to remove insoluble fluorides. The washing was repeated twice at room temperature and thrice at 70°C. Next, a mixture of 2N H_2SO_4-0.5N $Na_2Cr_2O_7$ was used to oxidize the remaining reactive kerogen. This treatment was carried out at 75°C for 20 hours (unfortunately, when the graphite grains were later being prepared for analysis it was discovered that, in contrast to Murchison, this oxidizing method did not remove all the insoluble organic matter). In order to extract nanodiamonds from the sample, we used the fact that diamonds are known to become colloidal when treated with solutions with pH $>$ 2 (Lewis et al., 1989). Therefore, the oxidized residue was treated with 0.1M NaOH (seven times). The supernatant was then removed, leaving a sediment of graphite, SiC, some oxides, and left-over kerogen. The sediment was further separated according to density by using sodium polytungstate [$Na_6(H_2W_{12}O_{40})$] (SPT). This solution is ideal for the separation of carbonaceous grains because its density can be adjusted from 1 to 3.1 g cm^{-3}, which encompasses the range of densities of interstellar graphite. The density

of SPT can be varied by dissolving it and hence, diluting it, in distilled or de-ionized water. Sodium polytungstate solution of a range of densities was poured into a test tube containing the sample. This mixture was then centrifuged to obtain a continuous density gradient. Ten final density fractions of carbonaceous material were obtained. The lightest density fraction, OR1a (< 1.59 g cm^{-3}), contains organic matter and the heaviest fraction, OR1j (> 2.3 g cm^{-3}), is expected to contain SiC and oxide grains. At least a few of the remaining eight density fractions were expected to contain presolar graphite. These eight fractions were then further centrifuged and separated according to size with a lower cutoff of 1 μm. Since all the presolar graphite grains that carry Ne-E(L) in Murchison have diameters > 1 μm, only those fractions were studied.

4.2.2 Grain-mount nomenclature

The different density fractions of the Orgueil graphites are tabulated in Table 4.1. We introduce a new nomenclature to name the graphite grains. Each grain label contains the name of the meteorite, the grain-size fraction, the density fraction, the analysis mount number, and finally, the grain number on that particular mount. For example, the grain label OR1d2m-4 indicates the following: OR = Orgueil, 1d = grains larger than 1 μm from the "d" density fraction (1.75 – 1.92 g cm^{-3}) (See Table 4.1), 2m = second mount of grains from this density fraction that were isotopically analysed, and 4 = the grain number on this mount.

4.2.3 Sample preparation

To prepare the initial set of grain mounts (OR1(b,c,d,e,f,g,h,i)1m) that were analyzed in the NanoSIMS, material from each density fraction was suspended in a solution of water and isopropanol (1:4). The isopropanol lowers surface tension and increases viscosity, which prevents the grains from clumping together. These suspen-

sions were then mixed well in an ultra-sonic bath, and small amounts (0.15 – 0.4 μl at a time) were deposited on high-purity gold foil mounts that are custom-made for the NanoSIMS. There is a substantially higher amount of insoluble macromolecular carbon left over in Orgueil density separates than in the Murchison separates. This material often covers up to about 500 μm^2-areas on a grain mount. It has not been determined yet why the chemical separation procedure was not able to remove this material in Orgueil. During the NanoSIMS measurements of the grains from the 1m mounts, we found that the secondary ion signal was heavily contaminated by the macromolecular carbonaceous material, in which the graphite grains are often found embedded. This does not pose much of a problem when measuring large grains with the Cs^+ primary beam as the beam can be focused onto the central portions of the grain, thus cutting off most of the contribution from the surrounding macromolecular carbon. However, this problem becomes inhibiting when the O^- primary beam is used to measure positive secondary ions and no secondary electron images are available to navigate the mount. In this case, we use the total ion count to locate grains on the mount. If the grains are surrounded by the macromolecular carbon then it becomes almost impossible to separate the total ion counts from the grains and from the macromolecular carbon surroundings. Hence, subsequent mounts (OR1d2m, 3m, 4m; OR1f2m) were prepared by picking candidate grains with a micromanipulator and transferring them to another NanoSIMS gold-foil mount. This procedure was essential to isolate the grains from the large amounts of macromolecular carbon on the mounts. It reduces contamination from the surrounding material and also makes it easier to locate the grains for future analyses. We picked larger grains (> 2 μm) for analyses because these graphites are intended to be part of an extensive correlated study to measure the isotopes of light, selected elements up to Ni with the NanoSIMS, and heavy ($>$ Ni) element isotopes with the resonant ionization mass spectrometry (RIMS) technique. This size selection allows the grains to survive extensive sputter-

ing. After mounting the grains, we coated the mount with a thin ($\sim$ 10 – 20 nm) layer of gold to prevent the grains from falling off.

Standard grains were then deposited on each mount to aid tuning of the secondary ion beam in the NanoSIMS and to correct for different detection efficiencies of the electron multipliers and for instrumental mass fractionation. Terrestrial graphite deposited from a colloidal suspension (DAG) was used as the C isotope standard for all the mounts, except OR1d4m. Instead, synthetic SiC was used as a C standard for OR1d4m. Murchison matrix grains were used as a standard for O isotopes. Synthetic SiC and SiC-Si_3N_4 grains were used as standards for terrestrial Si and N isotopic measurements, respectively. We used Burma spinel ($MgAl_2O_4$) for Al-Mg isotopes and perovskite ($CaTiO_3$) grains as standards for Ca, K, and Ti isotopes.

4.2.4 EDX analyses and grain mount documentation

Mounted grains from each density fraction were analyzed in a scanning electron microscope (SEM). Carbonaceous grains were located and identified by conducting energy dispersive X-ray (EDX) analysis with a JEOL-840A SEM. Candidate grains were selected on the basis of high C content (as determined by the EDX analysis) and morphological features characteristic of Murchison graphite (spherical with a platy 'onion' or knobby 'cauliflower' appearance (Hoppe et al. 1995)). Every grain was then "documented". This involved recording the (x,y) coordinates of each grain on the mount, taking pictures of the grids on which the grains were found, and making a map with relative grain locations of the entire mount. Secondary electron pictures of some grains were taken with the SEM or the Auger Nanoprobe (Figure 4.1). In addition, mean grain sizes were also determined in the SEM. For irregularly shaped grains we used the formula for ellipsoids to determine the diameter, $D = (A \times B^2)^{1/3}$, where A and B are the major and minor axes, respectively. A coordinate transformation program (written by Larry Nittler) was used to determine the corresponding

coordinates in the NanoSIMS and to locate the grains.

4.2.5 NanoSIMS analyses

The initial characterization of the grains in the SEM was followed by SIMS isotopic analyses. These were carried out with the Washington University Cameca NanoSIMS 50. Isotopic measurements were carried out in five stages on each mount. The NanoSIMS has five electron multipliers that are capable of detecting five ionic species simultaneously. It can be used in multidetection and peak-jumping modes or in a combination of the two modes. Table 4.2 gives a list of the measurement stages, the secondary ions detected in parallel (Phases 1 – 3) and combined mode (Phases 4 and 5) and the mounts on which these measurements were carried out.

C, N, O, Si isotopes:

The first stage involved measuring C isotopes in combination with either N or O or Si isotopes simultaneously (Table 4.2). The remaining two elements were measured in stage two. The first two stages used a Cs^+ primary beam to produce secondary ions of $^{12}C^-$, $^{13}C^-$, $^{12}C^{14}N^-$, $^{12}C^{15}N^-$, $^{16}O^-$, $^{18}O^-$, $^{28}Si^-$, $^{29}Si^-$, and $^{30}Si^-$. Nitrogen-14 and ^{15}N measurements had to be done with the help of ^{12}C, because nitrogen does not form a stable negative ion. However, in the presence of carbon, an intense CN^- signal can be obtained. Measurements were carried out at high mass resolution, and special care was taken to resolve the $^{13}C^-$ peak from the $^{12}CH^-$ interference at mass 13, $^{18}O^-$ from $^{16}OH_2^-$ at mass 18, $^{12}C^{14}N^-$ from $^{13}C_2^-$ and $^{12}C^{13}CH^-$ at mass 26, and $^{12}C^{15}N^-$ from $^{13}C^{14}N^-$ at mass 27 (mass resolving powers of $m/\Delta m \geq 6000$ were used). Grain measurements were sandwiched by standard measurements at regular intervals (every 5 – 10 grains). In addition, the positions of the mass peaks were checked and centered before every grain and standard measurement. Sometimes the primary ion beam current had a tendency to vary over an entire run of measurements,

which resulted in a slight change in secondary ion counts. Since all the isotopes are measured simultaneously, this effect does not lead to any isotopic artifacts. The C, N, and O isotopic data were reduced by simply normalizing the measured ratios of $^{12}C/^{13}C$, $^{14}N/^{15}N$, and $^{16}O/^{18}O$ by the average ratios of the standard grains. If R_s is the average ratio measured on the standard grains and R_t is the true terrestrial (solar) ratio, then the correction factor is f, where $f = R_s/R_t$. Every grain measurement, R_m, was divided by f to give the true measured ratio. The terrestrial values (R_t) of $^{12}C/^{13}C$, $^{14}N/^{15}N$, and $^{16}O/^{18}O$ ratios used in this study are 91.2 for DAG and 92.6 for SiC, 272, and 499, respectively. Si isotopic data were reduced using: ^{29,30}Si (per mil, ‰) = $[(^{29,30}Si/^{28}Si)_{meas}/(^{29,30}Si/^{28}Si)_{std}$ - 1] × 1000, where subscripts 'meas' and 'std' stand for isotopic ratios of unknown grains and standard grains, respectively. Terrestrial values of $^{29}Si/^{28}Si = 0.0506331$ and $^{30}Si/^{28}Si = 0.0334744$ are used as 'normal ratios' in this study. Poisson errors of the isotopic ratios of standard and unknown grains were propagated appropriately, and 1 σ error bars were calculated for each measurement.

Al-Mg isotopes:

In phase 3 of the analyses, positive secondary ions of ^{12}C, ^{24}Mg, ^{25}Mg, ^{26}Mg, and ^{27}Al, produced with an O^- primary beam, were detected simultaneously. Positive ions of ^{12}C were detected in order to locate the graphite grains, because secondary electrons, so helpful during analysis of negative secondaries, cannot be used. The Burma spinel grains were measured to obtain "solar" or "normal" Mg isotopic ratios ($^{25}Mg/^{24}Mg$, $^{26}Mg/^{24}Mg$, and $^{27}Al/^{24}Mg$) and then used to calculate the relative Al^+/Mg^+ sensitivity factor (Γ), representing the different Al and Mg secondary ion yields. We assumed atomic Al/Mg = 2 for solar system spinel grains. In grains with almost normal (within uncertainties) $^{25}Mg/^{24}Mg$ ratios, the large ^{26}Mg excesses can be assumed to be from the decay of ^{26}Al ($\tau_{1/2} = 7.2 \times 10^5$ a). Addition of

isotopically normal Mg can reduce the ^{26}Mg excess relative to ^{24}Mg but it also reduces the ^{27}Al/^{24}Mg ratio by the same factor. Thus, contamination by terrestrial Mg does not affect the inferred ^{26}Al/^{27}Al ratio. In contrast, ^{27}Al contamination can decrease the calculated ^{26}Al/^{27}Al ratio and hence, special care was taken to sputter away terrestrial Al contamination and to avoid Al hotspots on the sample mount. The ^{26}Mg excesses (^{26}Mg$_{\rm excess}$) were calculated directly from the ion counts: ^{26}Mg$^+_{\rm excess}$ = ^{26}Mg$^+$ - (^{26}Mg$^+$/^{24}Mg$^+$)$_{\rm std}$ × ^{24}Mg$^+$, where (^{26}Mg$^+$/^{24}Mg$^+$)$_{\rm std}$ is the ratio measured on the standard spinel grains. The inferred ^{26}Al/^{27}Al ratios were then calculated by: ^{26}Al/^{27}Al = Γ × ^{26}Mg$^+_{\rm excess}$/^{27}Al$^+$.

K and Ca isotopes:

The K, Ca, and Ti measurements were carried out with the O^- primary beam in a combination of peak-jumping and multidetection modes. Positive secondary ions of ^{39}K, ^{41}K, and ^{43}Ca (B field 1) and ^{12}C, ^{40}Ca, ^{42}Ca, ^{44}Ca, and ^{48}Ti (B field 2) were measured to obtain K and Ca ratios. A mass resolving power > 6000 was used to resolve the ^{41}K peak from the ^{40}CaH peak. Since the intrinsic concentration of K in graphite grains is expected to be very low, and all the terrestrial K is probably from contamination, we attribute the ^{41}K excesses seen in the graphite grains to be due to the decay of ^{41}Ca ($\tau_{1/2}$ = 1.03 × 10^5 a) (Amari et al. 1996). We calculated the initial ^{41}Ca/^{40}Ca ratios in the grains similarly to the inferred ^{26}Al/^{27}Al ratios: ^{41}Ca/^{40}Ca = Γ × ^{41}K$^+_{\rm excess}$/^{40}Ca$^+$, where the sensitivity factor, Γ was assumed to be 0.333 (Hinton 1990). The ^{42,43,44}Ca values were calculated using: δ^iCa (‰) = [(^{i}Ca/^{40}Ca)$_{\rm meas}$/(^{i}Ca/^{40}Ca)$_{\rm std}$ - 1] × 1000. In grains with ^{44}Ca excesses that do not match the ^{42,43}Ca excesses, we attributed the excesses to be from the decay of the short-lived radionuclide ^{44}Ti ($\tau_{1/2}$ = 60 a). The inferred ^{44}Ti/^{48}Ti ratios were calculated similarly to the ^{26}Al/^{27}Al and ^{41}Ca/^{40}Ca ratios: ^{44}Ti/^{48}Ti = Γ × ^{44}Ca$^+_{\rm excess}$/^{48}Ti$^+$, where the relative sensitivity factor, Γ = (Ti$^+$/Ca$^+$)/(Ti/Ca)

= 0.353 (Yangting et al. 2009) was used. This factor was recently calculated by measuring the NIST standard silicate glass SRM 610 with the Washington University NanoSIMS 50. The $^{48}Ti^{+}$ signal was corrected for a contribution from $^{48}Ca^{+}$ ($^{40}Ca/^{44}Ca$ = 47.153 from Niederer and Papanastassiou, 1984).

Ti isotopes:

Three magnetic fields were used to measure Ti isotopes: B_1: $^{46}Ti^{+}$, $^{48}Ti^{+}$, and $^{50}Ti^{+}$; B_2: $^{47}Ti^{+}$, $^{49}Ti^{+}$, and $^{51}V^{+}$; and B_3: $^{12}C^{+}$, $^{40}Ca^{+}$, $^{48}Ti^{+}$, $^{50}Ti^{+}$, and $^{52}Cr^{+}$. Vanadium-51 and ^{52}Cr were used to correct the ^{50}Ti signal for isobaric interferences from ^{50}V and ^{50}Cr, and, ^{40}Ca was measured to correct for Ca interferences at masses 46 and 48. High mass resolution was used to avoid isobaric interferences (e.g. SiO at mass 44). The unresolvable ion peaks were as follows: (1) ^{46}Ca and ^{46}Ti at mass 46, (2) ^{48}Ca and ^{48}Ti at mass 48, and (3) ^{50}Ti, ^{50}V and ^{50}Cr at mass 50. Abundances of ^{46}Ca and ^{48}Ca are sufficiently low that we do not expect these interferences to produce significant anomalies. Corrections were applied for these interferences by assuming normal or terrestrial $^{46}Ca/^{40}Ca$ and $^{48}Ca/^{40}Ca$ ratios. A large ^{48}Ca interference will result in a deficit in the Ti isotopic ratios that are normalized to ^{48}Ti. In such cases, the observed excesses in these Ti isotopes will be lower limits. We also assume that the ^{50}Cr interference to the ^{50}Ti signal is entirely from terrestrial Cr because the grains inherit large quantities of terrestrial Cr from the oxidizer, $Na_2Cr_2O_7$, which is used during the chemical separation procedure for graphite grains. The following terrestrial values of $^{40}Ca/^{44}Ca$ = 47.153, $^{48}Ca/^{44}Ca$ = 0.088727, $^{46}Ca/^{44}Ca$ = 0.00152 (Niederer and Papanastassiou, 1984), $^{50}Cr/^{52}Cr$ = 0.051859 (Shields 1966) and $^{50}V/^{51}V$ = 0.002503 (Flesch et al. 1966) were used to compute the corrections mentioned above. The $\delta^{46,47,49,50}Ti$ values were calculated using: $\delta^{i}Ti$ (‰) = $[(^{i}Ti/^{48}Ti)_{meas}/(^{i}Ti/^{48}Ti)_{std}$ - 1] × 1000.

4.3 Results

The density ranges of the various density fractions of graphite grains from Orgueil are the following: The low-density (LD) graphites are OR1b, OR1c, and OR1d (1.59 – 1.92 g cm^{-3}), while OR1f, OR1g, OR1h, and OR1i (2.02 – 2.30 g cm^{-3}) are the high-density (HD) graphites (See Table 4.1).

Most of the graphite grains from the Orgueil density fractions resemble Murchison presolar graphites (Hoppe et al., 1995) (Figure 4.1). They are spherules with smooth surfaces and a platy, onion-like morphology. The diameters of the grains range from 1 to 35 μm. In contrast to Murchison graphites, the grains tend to be larger in the higher-density fractions. Very few grains with the cauliflower-type morphology were found. Cauliflower grains were the dominant morphology in the LD fractions of Murchison (Hoppe et al., 1995). Some potato-shaped presolar graphite grains with smooth surfaces were found in the Orgueil fractions.

4.3.1 Isotopic compositions of the grains

Distribution of $^{12}C/^{13}C$

Grains from five (OR1c, d, f, g, i) of the seven density fractions analyzed have isotopically anomalous carbon. Figure 4.2 displays histograms of the distribution of the $^{12}C/^{13}C$ ratio in each density fraction and C stars in the galaxy (Lambert et al. 1986). The $^{12}C/^{13}C$ ratios of the grains in these fractions vary over a large range, from $\sim$ 4 to 2478. The C isotopic ratios of grains from OR1b and OR1h are close to solar (within errors) and do not show the large variations that are expected in presolar graphite (Hoppe et al., 1995). We use the four "groups" described by Hoppe et al. (1995) to divide the grains: (1) Grains that are highly enriched in ^{13}C, with $^{12}C/^{13}C$ ratios between 0 and 20, (2) Grains moderately ^{13}C-enriched, whose $^{12}C/^{13}C$ ratios are between 20 and 80, (3) Normal or close-to-solar $^{12}C/^{13}C$ ratios between 80 and

100, and (4) Grains containing isotopically light carbon with $^{12}C/^{13}C$ ratios greater than 100.

Out of the seven grains analysed in the lowest density fraction, OR1c, five grains are normal and one grain each with moderately heavy and light C compared to the solar $^{12}C/^{13}C$ ratio of 89. Twenty-three percent of the grains analyzed in OR1d have light carbon. The highest $^{12}C/^{13}C$ ratio of 2478 is observed in one grain (OR1d3m-5) from this fraction. Thirty-two percent of the grains have equal number of grains that have extremely low $^{12}C/^{13}C$ ratios (group 1 grains) and those that belong to group 2 with moderate ^{13}C-enrichments. Forty-five percent of OR1d grains have normal C isotopic ratios within errors. The grains analyzed from the OR1f fraction have a population of 14 isotopically heavy grains with $^{12}C/^{13}C < 20$ and 4 grains that are moderately ^{13}C-enriched (group 2), while, 73% of the analyzed grains contain light carbon (group 4). Twenty-nine percent of the grains in OR1g have solar carbon ratios. Two small populations of 7 grains with heavy carbon ($^{12}C/^{13}C < 20$) and 6 grains with moderately heavy C (group 2) were measured in this fraction, but a majority (46%) of the grains has $^{12}C/^{13}C$ ratios larger than the solar value (group 4). Among the grains measured from the heaviest fraction, OR1i, are 6 grains (out of 9) that are anomalous in carbon: One grain has $^{12}C/^{13}C < 20$, one belongs to group 2, and four grains have isotopically light carbon and are group 4 grains.

Thus, we found that 1) All the grains analyzed from the OR1b and OR1h density fractions were normal; 2) grains with isotopically light C are more abundant in the HD fractions while grains with heavy C are more abundant in the LD fractions, and 3) a minor population of grains with $^{12}C/^{13}C < 20$ is observed in all the fractions heavier than OR1c. A similar density dependence of C isotopic ratios is seen in the Murchison graphites (Hoppe et al. 1995).

Nitrogen isotopes:

Compared to carbon isotope ratios, the $^{14}N/^{15}N$ ratios in the LD density fractions (Figure 4.3a) do not exhibit a very large range and are normal or of terrestrial value in most of the HD grains (Figure 4.3b). Nevertheless, anomalous grains were found in the low-density fractions. Both, OR1c and 1d contain grains with ^{15}N excesses (terrestrial $^{14}N/^{15}N \sim 272$) (Figure 4.3a). One OR1c grain (OR1c1m-6) has $^{14}N/^{15}N \sim 135$, and while OR1d has numerous grains that are slightly ^{15}N-enriched ($^{14}N/^{15}N$ ratios between 272 and 200), only 17 grains have $^{14}N/^{15}N$ ratios between 200 and 100 and 5 have $^{14}N/^{15}N$ ratios less than 100. The largest ^{15}N excess was observed in grain OR1d1m-17 ($^{14}N/^{15}N \sim 55$). The grains with large ^{15}N excesses are listed in Table 4.3 along with their other isotopic ratios.

The vast majority of grains from the HD fractions, OR1f, 1g, and 1i have normal terrestrial N ratios (Figure 4.3b). The fraction, OR1f, has three grains with ^{14}N excesses. OR1g has grain OR1g1m-33 with the highest $^{14}N/^{15}N$ ratio (= 1437) of any grain in this study. Three grains from OR1i are enriched in ^{14}N. Apart from these grains with enrichments in ^{14}N, three OR1f grains have ^{15}N enrichments. This lack of a large range of anomalies in nitrogen (Figure 4.3a and b) was observed in Murchison graphite as well (Hoppe et al., 1995) and was attributed to isotopic exchange or dilution of the original nitrogen, either on the parent body or during chemical processing in the laboratory. This seems to be a common trend in the graphite from both the meteorites. Stadermann et al. (2005) found isotopic gradients in $^{12}C/^{13}C$ and $^{16}O/^{18}O$ ratios in ultramicrotomed sections of a Murchison KE3 graphite grain. The grain was found to be most isotopically anomalous at the center. No such gradients were found in the $^{14}N/^{15}N$ ratios. These gradients were attributed to isotopic exchange with isotopically normal material in the laboratory or on the parent body.

Oxygen isotopes:

Figure 4.4 shows the $^{16}O/^{18}O$ ratios as a function of $^{12}C/^{13}C$ ratios for all the LD (Figure 4.4a) and HD fractions (Figure 4.4b). One out of 7 grains in OR1c has a substantial ^{18}O excess ($^{18}O/^{16}O$ ratio is $\sim$ 4 times the solar value). It also exhibits a ^{15}N excess. Twenty-nine percent of the OR1d grains exhibit $^{18}O/^{16}O$ ratios of up to 30 times the solar value of 0.002. More than 80% of the grains from this density fraction with ^{18}O excesses are also simultaneously enriched in ^{15}N (See Table 4.3). The contaminated OR1d3m mount was the exception where only 2 out of 8 grains with isotopically heavy O also have ^{15}N excesses. Thus, the majority of the grains with heavy O also contain isotopically heavy N (Table 4.3). These ^{18}O-enriched grains show both depletion and enrichment in ^{13}C with respect to the solar value (Figure 4.4a; Table 4.3). Thus, there does not seem to be any obvious correlation between the $^{12}C/^{13}C$ and $^{16}O/^{18}O$ ratios. A large number of grains that are ^{18}O-enriched have close-to-solar $^{12}C/^{13}C$ ratios.

Like N anomalies, O anomalies seem to disappear with increasing density. All the grains in the HD fractions, OR1f, 1g, and 1i, have $^{16}O/^{18}O$ ratios close to the solar value of 499 (Figure 4.4b).

Silicon isotopes:

The silicon isotopes, ^{28}Si, ^{29}Si, and ^{30}Si, were measured in grains from all the fractions. Figures 4.5a and b show the results of these measurements as three-isotope plots. In general, grains in the LD fractions (OR1d) are dominated by ^{28}Si excesses, while the heavier densities (OR1f, 1g, and 1i) have grains with ^{29}Si and ^{30}Si excesses.

The graphite grains in the density fraction, OR1c, were found to contain mostly normal Si isotopes (within errors) (Figure 4.5a). Among the analyzed grains from the other LD fraction, OR1d, approximately twenty grains have large ^{28}Si excesses (Figure 4.5a). Almost all the grains with ^{28}Si excesses are enriched in ^{18}O and a large

number also have ^{15}N excesses (Table 4.3). Grain OR1d4m-1 has δ^{29}Si = – 451±5 ‰and δ^{30}Si = – 660 ± 5‰, the largest ^{28}Si enrichment seen in any Orgueil graphite grain. Some grains from the LD OR1d fraction are enriched in ^{29}Si or ^{30}Si. Grain OR1d4m-3 is normal in ^{29}Si but has a large ^{30}Si depletion (δ^{30}Si = – 261 ± 20 ‰) while OR1d4m-18 is slightly depleted in ^{29}Si (^{29}Si = – 80 ± 14 ‰) and enriched in ^{30}Si (^{30}Si = 84 ± 20 ‰). Grain OR1d1m-26 is depleted in ^{30}Si, with normal ^{29}Si/^{28}Si. It is also slightly enriched in ^{18}O (^{16}C/^{18}O $\sim$ 409) and ^{15}N (^{14}N/^{15}N $\sim$ 160). Two grains, OR1d1m-17 and OR1d1m-31, are both enriched in ^{29}Si and depleted in ^{30}Si. They are highly enriched in ^{18}O and ^{15}N. Grain OR1d1m-11 has ^{30}Si and ^{28}Si excesses. It is also enriched in ^{18}O and ^{15}N and contains isotopically heavy carbon (^{12}C/^{13}C $\sim$ 6).

The anomalies observed in grains from mount OR1d3m were not as large as those observed in the previous mounts of the same density fraction. These isotopic anomalies were diluted due to contamination from the gold that was deposited on the mount prior to measurements. We only found four grains (OR1d3m-14, OR1d3m-16, OR1d3m-17, OR1d3m-18) on mount OR1d3m that contain ^{28}Si excesses. Table 4.3 shows that not all of them contain ^{15}N or ^{18}O excesses; only one grain (OR1d3m-18) contains both. These isotopic ratios of the grains on this mount were definitely diluted by the contamination mentioned above. One grain (OR1d3m-5) is ^{30}Si-enriched (δ^{30}Si = 136 ± 28 ‰) while OR1d3m-24 is slightly enriched in ^{29}Si and depleted in ^{30}Si (δ^{30}Si = – 172±19 ‰) (Figure 4.5a; Table 4.3).

Figure 4.5b shows the ^{29}Si/^{28}Si and ^{30}Si/^{28}Si ratios measured in the heavy fractions OR1f, 1g and 1i. The density fraction OR1f has 1 grain (OR1f(1,2)m-o67) that is enriched in ^{28}Si and ^{30}Si. This grain was also found to be highly enriched in ^{15}N. Two grains have extremely large ^{29}Si and ^{30}Si excesses. The largest anomalies were seen in grains: OR1f(1,2)m-o68 (δ^{29}Si = 1341 ± 35 ‰and δ^{30}Si = 896 ± 33 ‰) and OR1f(1,2)m-o70 (δ^{29}Si = 1043 ± 34 ‰and δ^{30}Si = 916 ± 36 ‰). Grains, OR1f1m-

16, OR1f1m-36, OR1f1m-34 and OR1f(1,2)m-o32 have moderately large ^{30}Si and ^{29}Si values (Figure 4.5b). Otherwise, in general, the three HD fractions OR1f, 1g, and 1i have a majority of the grains that are enriched in ^{30}Si and ^{29}Si. The heaviest fraction OR1i has one grain (OR1i1m-4) with a large depletion in ^{30}Si and a ^{28}Si excess. This grain is enriched in ^{14}N (^{14}N/^{15}N $\sim$ 475) and slightly enriched in ^{18}O (^{16}O/^{18}O $\sim$ 409).

Most of the grains on the OR1f2m high-density mount have small anomalies or have normal $\delta^{29,30}$Si/^{28}Si values. It is possible that the equilibration factors that cause the dilution of the N and O isotopic ratios also influence the Si isotopes.

Thus, the silicon isotopic data indicate distinctive trends that depend on the density of the grains, similar to the C, N and O isotopes. While the LD fractions have mostly ^{28}Si-rich grains, the HD fractions have grains that are enriched in ^{30}Si and ^{29}Si. In general, most ^{30}Si-rich grains from the HD fractions contain isotopically light carbon (Figure 4.6).

Al-Mg isotopes:

On the initial mounts, OR1(d,f)1m, on which we measured Al-Mg isotopes, the graphite grains were found embedded in macromolecular carbon. This carbonaceous material made it very difficult to find the graphite grains with the help of a total ion signal while using an O^- primary beam (See Section 4.2.3). No secondary electron image is available in this mode of measurement. Thus, the Al-Mg measurements on the OR1(d,f)1m mounts are contaminated by ion signals from the surrounding macromolecular carbon. All the graphite grains on subsequent mounts (OR1d(2,3,4m); OR1f2m) were picked out of the macromolecular surroundings, remounted and then measured for Al-Mg isotopes with relatively lower levels of contamination from the surroundings. Some interesting grains from the OR1f1m mount that had already been measured for C, N, O, and Si isotopes were picked and transferred to the OR1f2m

mount. These grains are labeled as OR1f(1,2)m-o(grain number). Additional isotopes were measured on these grains, free from stray ionic contributions from the surrounding macromolecular carbon.

Mg isotope results for the LD fraction, OR1d, are plotted as δ-values of $^{25}Mg/^{24}Mg$ and $^{26}Mg/^{24}Mg$ in permil (‰) in Figures 4.7a, b, c, and d with different ranges of the plot axes to accommodate all the data. Figure 4.8 shows Mg isotopic ratios for the grains from the HD fractions. Figure 4.9a and b display the inferred $^{26}Al/^{27}Al$ ratios as a function of $^{12}C/^{13}C$ ratios for the LD and HD fractions. Table 4.4 lists the $\delta^{25}Mg$, $\delta^{26}Mg$ values and inferred $^{26}Al/^{27}Al$ ratios for LD and HD grains with substantial ^{26}Mg excesses from the decay of short-lived ^{26}Al ($\tau_{1/2} = 7.2 \times 10^5$ a).

Figure 4.7a shows grains with the largest $\delta^{25}Mg$ and $\delta^{26}Mg$ values. Grain OR1d4m-20 has the largest inferred $^{26}Al/^{27}Al$ ratio (0.6928 ± 0.0061) seen in any presolar graphite grain so far. Such high $^{26}Al/^{27}Al$ ratios are found in SiC-X grains (Nittler et al. 1995). The largest inferred $^{26}Al/^{27}Al$ ratio previously obtained in Murchison KE3 graphites is ~ 0.146 (Travaglio et al. 1999). The grains labeled in Figure 4.7a have large $^{26}Al/^{27}Al$ ratios (Table 4.4; Figure 4.9a) and are enriched in ^{18}O and ^{28}Si. Except grain OR1d2m-32, all of these grains have ^{15}N excesses. Interestingly, 3 grains (OR1d4m-19, OR1d4m-32, OR1d4m-20) have very low $^{12}C/^{13}C$ ratios and the remaining 3 are moderately ^{13}C-enriched or have roughly solar $^{12}C/^{13}C$ ratios. In general, grains from the OR1d2m and 4m mounts have the largest ^{26}Mg excesses (Figure 4.7a, b and c). The inferred $^{26}Al/^{27}Al$ ratios range from 2×10^{-4} to 0.7 in these grains (Table 4.4; Figure 4.9a). The high $^{26}Al/^{27}Al$ ratios we found in these grains were not seen in the previous study of grains from the OR1d1m and 3m mounts, most likely because of contamination present on those mounts. The range of $^{26}Al/^{27}Al$ ratios in grains on mount OR1d1m is 2.5×10^{-4} to 0.04 and OR1d3m is 10^{-3} to 0.04. Only upper limits could be obtained for the inferred $^{26}Al/^{27}Al$ ratios of some of the grains because of the large errors associated with the measurements (Figure 4.9a).

In the HD fraction, OR1f, we found only a few grains with ^{26}Mg excesses. Grain OR1f(1,2)m-o67 has the largest ^{26}Mg excess (δ^{26}Mg = 1593 ‰) (Figure 4.8). This grain consequently has a relatively high, inferred ^{26}Al/^{27}Al ratio of 0.01 (Figure 4.9b; Table 4.4). Three other grains (OR1f2m-25, OR1f2m-38, OR1f(1,2)m-o8) have inferred ^{26}Al/^{27}Al ratios on the order of 10^{-4}. The grains with the highest ^{26}Al/^{27}Al ratios are highly enriched in ^{13}C (Figure 4.9b) while the other grains are ^{12}C-enriched.

The Al/Mg ratios in the grains of this fraction were very low and if the grains did contain ^{26}Mg excesses from the decay of radiogenic ^{26}Al then they were too small to detect. There is a possibility that the equilibration processes affecting the N and O in HD graphite grains also dilute the Mg isotopes in these grains. It is also interesting to note that grains OR1f(1,2)m-o67 and OR1f(1,2)m-o8 were measured for Mg isotopes when they were on mount OR1f1m and the surrounding material made it impossible to detect the large ^{26}Mg excesses in these grains.

In general, HD graphites exhibit very low Al/Mg ratios making the detection of ^{26}Mg excesses from radiogenic ^{26}Al very difficult.

K isotopes:

Most grains from the LD fractions, OR1d, were found to have normal ^{41}K/^{39}K ratios (solar value $\sim$ 0.072). A few grains were found to have high ^{41}K/^{39}K ratios. Five grains have ^{41}K/^{39}K ratios ranging from 0.074 – 0.106. These ^{41}K excesses can be attributed to the decay of ^{41}Ca ($\tau_{1/2} = 1.03 \times 10^5$ a) because the intrinsic concentration of K in graphite grains is expected to be very low (Amari et al. 1996). The inferred ^{41}Ca/^{40}Ca ratios for these grains range from 0.0004 to 0.01 (Figure 4.10a; Table 4.5). All grains with high ^{41}Ca/^{40}Ca ratios have ^{18}O excesses and high ^{26}Al/^{27}Al ratios. Four of them are also enriched in ^{28}Si.

The LD mount, OR1d3m, was found to be contaminated by large amounts of terrestrial K and Ca, making the detection of radiogenic ^{41}Ca nearly impossible.

Only two grains, OR1d3m-1 and OR1d3m-20, were found to have slightly elevated $^{41}K/^{39}K$ ratios and, because Ca/K ratios are fairly low, high inferred $^{41}Ca/^{40}Ca$ ratios (See Figure 4.10a; Table 4.5).

Most of the grains from the high-density fraction, OR1f, have normal $^{41}K/^{39}K$ ratios (0.072). Grains OR1f2m-9, OR1f2m-18, OR1f2m-25, OR1f2m-38, OR1f(1,2)m-o38 and OR1f(1,2)m-o68, have elevated $^{41}K/^{39}K$ ratios ranging from 0.075 – 1.000. The inferred $^{41}Ca/^{40}Ca$ ratios range up to 0.01 (Figure 4.10b; Table 4.5).

Ca isotopes:

The $^{42,43,44}Ca$ data of grains on the LD mount (Figure 4.11a and b), OR1d3m, were also affected by large amounts of Ca contamination. All the grains are normal in $^{42}Ca/^{40}Ca$ (within errors), and only one grain (OR1d3m-5) has a high $^{44}Ca/^{40}Ca$ value of 222 ± 22 ‰and a comparable excess in ^{43}Ca (δ $^{43}Ca/^{40}Ca$ = 154 ± 43 ‰). Since the ^{43}Ca and ^{44}Ca excesses are of approximately the same magnitude, they can be explained by neutron capture and the ^{44}Ca excess does not constitute evidence for the presence of ^{44}Ti. The rest of the grains have normal $^{43,44}Ca/^{40}Ca$ ratios.

Four graphite grains (OR1d4m-16, OR1d4m-20, OR1d4m-3 and OR1d4m-10) from the other LD mount, OR1d4m, were found to have high $\delta^{42,43,44}Ca/^{40}Ca$ values that appear to be correlated (Figure 4.11a and b; Table 4.6). Additionally, two grains (OR1d4m-8 and OR1d4m-9) that have solar $^{42}Ca/^{40}Ca$ values and close-to-solar $^{43}Ca/^{40}Ca$ values, contain large ^{44}Ca excesses. Slow neutron capture that gives rise to ^{44}Ca excesses are expected to produce even larger $^{42,43}Ca$ excesses and hence, we conclude that the ^{44}Ca excesses are most likely due to the decay of ^{44}Ti ($\tau_{1/2}$ = 60 a). The inferred initial $^{44}Ti/^{48}Ti$ ratios in grains OR1d4m-8 and OR1d4m-9 are listed in Table 4.7. Much higher values have been observed in SiC-X grains (Amari et al. 1992; Hoppe et al. 1996b; 2000; Nittler et al. 1996; Besmehn and Hoppe 2003) and KE3 graphites from Murchison (Travaglio et al. 1999).

Table 4.8 lists the C, Ca and Ti isotopic ratios of interesting grains from the HD fraction, OR1f. Figures 4.12a and b show that several grains from this fraction have unusually large ^{42,43,44}Ca values. Grains OR1f2m-9, OR1f2m-34, OR1f2m-18, OR1f(1,2)m-o68, OR1f2m-40 and OR1f2m-29 exhibit extremely large ^{42,43}Ca excesses. Calcium-44 excesses that are comparable to the ^{42,43}Ca excesses can be explained by neutron capture, but in grains OR1f2m-1, OR1f2m-25, OR1f2m-38, and OR1f(1,2)m-o67 the large ^{44}Ca excesses must be the result of the decay of ^{44}Ti ($\tau_{1/2}$ = 60 a). Table 4.7 lists the inferred ^{44}Ti values for these grains. Figure 4.13 clearly shows the correlation of the ^{44}Ca ion signal with that of the ^{48}Ti ion signal for grains OR1f2m-25 and OR1f(1,2)m-o67. The fact that the ^{44}Ca signal does not correlate with any other Ca ion signals is additional evidence that ^{44}Ca excesses must be from the decay of radiogenic ^{44}Ti. Three of the four grains from OR1f with ^{44}Ti excesses have ^{12}C/^{13}C ratios less than 20 (Table 4.8). OR1f2m-25 is the only grain with both ^{44}Ti and ^{12}C excesses (^{12}C/^{13}C $\sim$ 743). Approximately half the grains listed in Table 4.8, with large Ca excesses, are enriched in ^{13}C while the others are enriched in ^{12}C.

Ti isotopes:

Figures 4.14a, b and c display the Ti isotopic ratios of the grains from the LD fraction OR1d (Table 4.6). Grain OR1d4m-13 has a large excess in ^{47}Ti without any accompanying ^{46}Ti excess, and grains OR1d4m-19, OR1d4m-9 and OR1d4m-14 are significantly depleted in ^{46,47}Ti. This fraction contained several grains that have correlated excesses in ^{46,47}Ti (within errors). Eight grains are highly enriched (δ^{49}Ti > 500 ‰) in ^{49}Ti (as high as 1597 ± 85 ‰in grain OR1d3m-2; Table 4.6) while seven grains have moderate excesses (δ^{49}Ti < 500 ‰, Figure 4.14b). Due to a very high ^{50}Cr signal that interfered with ^{50}Ti, we were unable to obtain good ^{50}Ti data on a majority of these grains. The grains acquire Cr during chemical separation in the laboratory from $Na_2Cr_2O_7$, which is used as an oxidizing agent to remove macro-

molecular carbon. Three grains that have less than a 60% ^{50}Cr contribution to their ^{50}Ti ion signal have elevated δ^{50}Ti/^{48}Ti values of 259 ± 97 ‰(OR1d3m-6), 185 ± 22 ‰(OR1d3m-14) and 144±38 ‰(OR1d3m-18) 186 ± 12 ‰(OR1d4m-3) (Figure 4.14c). The remaining grains are highly contaminated with Cr, making it impossible to obtain good ^{50}Ti data. Most of the grains in this LD fraction that have Ti anomalies have ^{18}O, ^{15}N, ^{28}Si excesses, and high ^{26}Al/^{27}Al ratios.

The grains from the HD fraction, OR1f, have extremely large ^{46,47,49,50}Ti excesses similar to the ^{42,43,44}Ca excesses (Figures 4.15a, b and c; Table 4.8). Extreme Ti anomalies (greater than $\sim$ 1000 ‰) are seen in some grains. The largest of these are seen in OR1f2m-9 (δ^{46}Ti = 35032 ± 4432 ‰; δ ^{47}Ti = 1376 ± 371 ‰; δ^{49}Ti = 2278 ± 298 ‰; δ^{50}Ti = 32827 ± 4594 ‰). The other grains, some with similar large anomalies, are listed in Table 4.8 in addition to the other interesting grains from the HD fraction.

In summary, we find that the presolar graphites from Orgueil tend to have C, N, O, Al-Mg, and Si isotopic properties that are density dependent. Among LD grains, we find that many have ^{15}N, ^{18}O, ^{28}Si excesses, and high ^{26}Al/^{27}Al ratios. Most HD grains have terrestrial values of N and solar O; contain ^{29}Si and ^{30}Si excesses that correlate with ^{12}C excesses, and smaller ^{26}Al/^{27}Al ratios. The original N and O isotopic ratios in the HD fractions are assumed to be diluted by normal N and O. It is possible that the equilibration processes affecting the N and O ratios also dilute the Si and Mg isotopes in the HD grains. Curiously, though, these processes appear to have spared the Ca and Ti isotopic ratios in these grains. Some of the HD grains have extreme anomalies in Ca and Ti while their Si and Al-Mg anomalies are negligible in comparison. The s-process neutron capture reactions that cause excesses in Ca and Ti isotopes should have caused significant Mg and Si anomalies as well. The LD grains do not exhibit similar extreme anomalies in Ca and Ti.

4.4 Discussion

Presolar dust grains condense in cooling atmospheres of dying stars. This condensation could take place either in the ejecta of stellar explosions or in the outflows from late-type stars. There is an additional constraint for the condensation of C-rich dust grains: the carbon content in the gas should be greater than the oxygen content, i.e., C/O $>$ 1 (Lattimer et al., 1978; Lodders and Fegley, 1992; Sharp and Wasserburg, 1993, 1995). This condition can be satisfied in various stellar sites. The envelopes or the interior layers of carbon stars or AGB stars, Wolf-Rayet stars, novae, and SNe all satisfy this condition at some time in their lifecycles. Thus, presolar graphite grains can have several stellar sources, which are revealed by their complex isotopic compositions.

Clayton et al. (1999) and Deneault et al. (2003; 2006) theorize that carbonaceous grains can condense in O-rich (C $<$ O) regions of the ejecta of type II SNe. The C $>$ O restriction is derived from the assumption that all the available carbon is locked up in CO molecules when C $<$ O. These authors suggest that CO molecules are photo-dissociated by gamma rays from the decay of ^{56}Ni and ^{56}Co. This makes carbon available to condense C-rich grains in an O-rich environment. Such a scenario certainly circumvents the problem of explaining the presence of ^{44}Ti and ^{28}Si excesses in SiC and graphite grains without having to mix the inner, O-rich SN zones with the outer, C-rich He/C zone. However, Ebel and Grossman (2001) argue that although graphite might condense at higher temperatures in an O-rich environment, SiC is not stable under such conditions. Also, the presence of iron-metal phases and TiC sub-grains in graphite grains that exhibit SN isotopic signatures argues against the condensation of graphite in a C $<$ O environment (Croat et al. 2003). We do not consider such a scenario in this paper.

4.4.1 Nucleosynthetic Sources for Orgueil graphite

The following is a discussion of the possible stellar sources for the graphite grains whose isotopic ratios are presented in the previous section.

Bona fide supernova grains among the LD and HD density fractions:

Definite evidence of a SN origin is obtained from the presence of ^{44}Ti and ^{28}Si excesses in graphite (or any presolar) grains. Large excesses of ^{44}Ca in grains indicate the initial presence of radiogenic ^{44}Ti. Figure 4.16 shows extremely large ^{44}Ca excesses in six grains, (OR1d4m-8, OR1d4m-9, OR1f2m-1, OR1f2m-25, OR1f2m-38, and OR1f(1,2)m-o67) in comparison to the other Ca isotopes. Two of these grains belong to the LD fraction while the other four are from the HD fraction. Since neutron capture reactions are expected to produce larger excesses of ^{42,43}Ca than of ^{44}Ca, the massive excesses in ^{44}Ca seen in the grains in Figure 4.16 are attributed to the decay of ^{44}Ti ($\tau_{1/2} = 60$ a). Figure 4.17a is a schematic diagram of the interior "onion shell" structure of a massive star ($> 8 - 9\ M_{\odot}$) before its explosion as a type II SN. The different zones are labeled according to the nomenclature introduced by Meyer et al. (1995) wherein the different layers are labeled by the most abundant elements present in the zones. Figure 4.17b shows the internal isotopic structure of such a 15 $M_{\odot}$ SN model given by Rauscher et al. (2002). Titanium-44 is only produced by α-rich freezeout in the Ni and Si/S zones of Type II SNe (Woosley et al. 1973; Woosley and Weaver 1995; Timmes et al. 1996). In the Si/S zone, Si exists as almost pure ^{28}Si, which is the principal product of O-burning. Thus, the initial presence of ^{44}Ti and/or large ^{28}Si excesses in grains are a clear signature of a SN origin. The presence of these isotopic signatures in presolar grains along with others that originate from the outer layers suggests deep and inhomogeneous mixing of the various SN layers (Woosley and Weaver 1995; Rauscher et al. 2002) into the SN ejecta where the grains condense. The ^{44}Ti and ^{28}Si signatures require that material from pre-SN

zones that experienced Si-, Ne-, and O-burning and are rich in Ni, O/Si, and Si/S, respectively should be mixed in limitedly with the H- and He-burning zones that are C rich. A rather large contribution must come from the latter zones to provide C to the condensation environment and maintain the graphite condensation condition of C/O $>$ 1. X-ray observations of SN remnants (SNRs) of Cassiopeia A (Hughes et al. 2000) and SN 1978A (Ebisuzaki and Shibazaki, 1988) have indicated extensive mixing of SN ejecta. Additionally, hydrodynamic models of SN explosions by Herant et al. (1994) have predicted that mixing of various SN layers can be initiated by perturbations between the layers called Rayleigh-Taylor instabilities. Its mechanics and whether such mixing occurs on a microscopic level are still unclear.

Almost all SiC-X grains and LD graphite grains from Murchison that show evidence of ^{44}Ti have large correlated ^{28}Si excesses (Amari et al. 1992; Hoppe et al. 1994; 1996b; 2000; Nittler et al. 1996; Besmehn and Hoppe 2003). In this study, however, 3 out of 4 HD graphites that contain ^{44}Ti do not contain large ^{28}Si excesses (Figure 4.18). The Si isotopic ratios of these grains are believed to be equilibrated similar to their N and O isotopic ratios. Grain OR1f(1,2)m-o67 is depleted in ^{29}Si and enriched in ^{30}Si, and hence does not have a ^{28}Si excess. The two LD grains, OR1d4m-8 and OR1d4m-9, contain both ^{44}Ti and large ^{28}Si excesses. In addition to these 2 LD grains there are approximately 20 more LD grains that have large ^{28}Si excesses but show no evidence for the initial presence of ^{44}Ti (Figure 4.5a). In later sections, we will discuss other nucleosynthetic indicators that may or may not provide additional evidence of a SN origin for these grains. The presence of ^{44}Ti and/or ^{28}Si excesses however, indicates beyond any doubt that these grains originated in type II SNe. It is now clear that grains from different stellar sources are found in the low- and high-density types of graphites, and SN grains are present in both the density fractions of Orgueil graphites. A similar conclusion was reached from the analysis of Zr and Mo isotopes in HD graphites from Murchison by Nicolussi et al. (1998b). Several grains

showed s-process isotopic patterns for Zr and Mo, similar to mainstream SiC grains that come from AGB stars. These authors also found two grains with extreme ^{96}Zr excesses that indicate a SN origin for the HD grains.

Sources of the low-density graphites from OR1c ($\rho \sim$ 1.67 – 1.75 g cm^{-3}) and OR1d ($\rho \sim$ 1.75 – 1.92 g cm^{-3}):

Graphites from the LD fraction (KE3) of Murchison were studied extensively by Travaglio et al. (1999). Based on C, N, O, Mg, Si, K, Ca and Ti isotopic measurements and theoretical mixing models of SN layers, their work established that most of the LD graphites from Murchison originate from Type II SNe. A preliminary study of LD Orgueil graphites based on C, N, O, and Si isotopes also indicated that a large majority of grains from the LD fractions of Orgueil OR1(c,d) have a Type II SNe origin (Jadhav et al. 2006). This study presents additional data on LD grains from Orgueil and the results indicate the same stellar source based on the measured N, O, and Si isotopic ratios (See section 4.3.1). Most grains from the LD fractions are enriched in ^{15}N, ^{18}O, and ^{28}Si. As mentioned in the previous section, ^{28}Si is produced in the O/Si and Si/S zones by the O-burning reaction, ^{16}O(^{16}O,α)^{28}Si. Partial He-burning in the He/C zone produces ^{18}O via the reaction, ^{14}N(α,γ)^{18}F(e^{+},ν)^{18}O and, ^{15}N is synthesized at the bottom of the He/C zone during explosive nucleosynthesis by neutrino reactions on O. This zone also contains almost pure ^{12}C that is produced in vast quantities by the triple-α reaction. Thus, the He/C zone is characterized by extremely high ^{12}C/^{13}C ratios and low ^{14}N/^{15}N and ^{16}O/^{18}O ratios. The He/C zone is one of the three zones in a pre-SN star, along with the He/N and C/O[1] zones, that satisfies the C > O condition required for condensation of graphite grains.

[1]The C/O zone is prominent in the Woosley and Weaver (1995) SN models as a sub-zone of the O/C zone where the C abundance is larger than the O abundance (just below the He/C zone). This shows up as a very small region in the Rauscher et al. (2002) models. We refer to the C/O zone, even though we do not show it in Figures 4.17, 4.19, and 4.20, because it avoids having to add material from O-rich zones to account for some of the isotopic anomalies observed in a few grains.

The He/N zone produces ^{26}Al by the ^{25}Mg(p,γ)^{26}Al reaction. The presence of this short-lived radionuclide ($\tau_{1/2} \sim 7.2 \times 10^5$ a) is inferred from large ^{26}Mg excesses measured in presolar grains. The largest ^{26}Al/^{27}Al ratios are predicted for this zone. Obviously, these three zones need to be the major contributors to the material from which SN graphites condense. Although ^{29,30}Si excesses are produced in the He/C zone and O-rich zones by neutron-capture reactions, in most SN grains these excesses are apparently overwhelmed by the ^{28}Si from the Si/S zones. We have observed very few LD grains with large ^{29,30}Si excesses. In the He/C zone of a 15 $M_\odot$ SN, the predicted ^{29,30}Si values are $\sim$ 300‰, while those expected from the inner O-rich zones are 5,000‰ and 10,000 ‰ for ^{29}Si and ^{30}Si, respectively (Woosley and Weaver, 1995). AGB stars produce much smaller excesses of ^{29,30}Si by n-capture during He shell-burning. The large excesses in ^{41}K observed in presolar graphite grains are interpreted to be due to the initial presence of the radioisotope, ^{41}Ca ($\tau_{1/2} \sim 10^5$ a) (Amari et al. 1996). Calcium-41 is synthesized in the He/C, C/O^1 and O-rich zones of a SN by n-capture on ^{40}Ca, resulting in ^{41}Ca/^{40}Ca ratios on the order of 10^{-3} – 10^{-2} (Wasserburg et al. 1994; Zinner et al. 2006a). In the O/Si (O-burning) zone, ^{41}Ca is created by explosive nucleosynthesis. Figure 4.19 shows model abundances of the ^{40,41}Ca isotopes and ^{41}Ca/^{40}Ca ratios in the interior of a 15 $M_\odot$ pre-SN star (Rauscher et al. 2002). It is clear that the values at the higher end of the range of ^{41}Ca/^{40}Ca ratios obtained in the LD grains discussed in Section 4.3.1 can be obtained from the He/C, C/O^1 and O-rich zones of a Type II SN where the ^{13}C(α,n)^{16}O and ^{22}Ne(α,n)^{25}Mg reactions provide ample neutrons for the production of ^{41}Ca (Woosley and Weaver, 1995). The other Ca isotopes, ^{42,43}Ca, are also made by n-capture reactions in the He/C and C/O^1 zones of a type II SN. Typically, ^{43}Ca has the largest excess in the Ca isotopic pattern of a SN grain that shows no evidence for ^{44}Ti. Some of the grains on the LD mount, OR1d4m, were found to have high $\delta^{42,43,44}$Ca/^{40}Ca values that appear to be correlated (Figures 4.11a and b). This trend is consistent

with the increase in abundance of ^{42,43}Ca at the bottom of the He/C zone of a type II SN. This region also has a large abundance of ^{15}N, which is consistent with the low ^{14}N/^{15}N ratios observed in two of the grains (OR1d4m-20 and OR1d4m-16) that have large $\delta^{42,43,44}$Ca values.

The Ti isotopes, ^{46,47,49,50}Ti, are also synthesized by n-capture in the He/C zone where the isotopic pattern shows large excesses in ^{49}Ti and smaller ones in ^{50}Ti (Figure 4.20). Note that these excesses are relative to ^{48}Ti, whose abundance decreases in the He/C zone and is partly responsible for the excesses in this zone. However, extremely large Ti excesses are predicted for the O-rich zones of a type II SN. The magnitude of the ^{46,49,50}Ti excesses seen in the LD grains can be explained by admixture from the O-rich and He/C zones of a type II SN to the outer zones, which have normal Ti isotopic ratios. In Murchison grains with low ^{12}C/^{13}C ratios (10 – 100), extremely large ^{49}Ti excesses were attributed to the decay of ^{49}V ($\tau_{1/2} \sim 330$ days) (Travaglio et al. 1999).

Thus, presolar graphite grains that formed in SN ejecta are expected to contain large excesses in ^{12}C, ^{15}N, ^{18}O, ^{26}Mg (due to the decay of ^{26}Al), ^{28}Si, ^{41}K (due to the decay ^{41}Ca), ^{44}Ca (due to the decay of ^{44}Ti), ^{49}Ti and ^{50}Ti. Amongst these signatures of a SN origin, only a few (^{28}Si, ^{44}Ti and ^{49}V) are uniquely produced in a SN. Aluminium-26, ^{41}Ca, and s-process isotopes can also be produced in AGB stars. However, the expected ratios of these short-lived radionuclides relative to the the stable nuclides ^{27}Al and ^{40}Ca in AGB stars are much smaller. Calcium-41 excesses from Wolf-Rayet stars are also expected to be small. On the other hand, ^{26}Al/^{27}Al ratios can be high in Wolf-Rayet stars. Some of the highest ^{26}Al/^{27}Al ratios observed in Murchison KE3 graphites can be accounted for by the expected abundances from Wolf-Rayet stars (Arnould et al. 1997).

We find the largest ^{18}O excesses in grains with close-to-solar or solar ^{12}C/^{13}C ratios (within errors). Since ^{18}O is synthesized by partial He-burning of ^{14}N in the

He/C zone of a SN, the grains with ^{18}O excesses should be accompanied by very high ^{12}C/^{13}C ratios, because this zone contains essentially pure ^{12}C. It is unclear why these grains are not ^{12}C-enriched.

A majority of the presolar graphite grains from the LD fraction whose isotopic ratios are discussed in Section 4.3.1 contain some, if not all, the isotopic signatures that lead us to conclude that most of the LD Orgueil graphites originate from type II SNe. In general, among LD grains, there exists a correlation between the ^{15}N, ^{18}O, ^{28}Si excesses and high ^{26}Al/^{27}Al ratios, indicating that material from the different layers of a pre-SN star are mixed together during a SN explosion. The mixing has to be such that the innermost layers must mix to a minor extent with the He/C, He/N and C/O[1] layers to supply them with isotopes like, ^{28}Si and ^{44}Ti. In order for graphite (and other carbonaceous grains) to condense, the C/O ratio of the resultant mixture of layers has to be greater than 1. This requires selective mixing of the layers. Figure 4.21 shows the results of such a mixing calculation between the different layers for the LD grain, OR1d4m-3, which strongly indicates a SN origin for this grain. A majority of the isotopic ratios (C, Si, Ca, and Ti isotopes) measured in grain OR1d4m-3 can be matched by this mixing giving a resultant mix that is C-rich (C/O = 14.0): a conducive environment for the condensation of SN graphite grains. Table **??** lists the mixing percentages from the different zones required to match the anomalies seen in this grain. Most of the material comes from the He/C zone ($\sim$ 80%) with a 15% contribution from the He/N zone, about 3% from the hydrogen-rich envelope and $<$ 1% from the Si/S zone. In contrast, the ^{14}N/^{15}N, ^{16}O/^{18}O and ^{26}Al/^{27}Al isotopic ratios of the grain and the ratios from the mixing calculations do not match very well. This is because there has to be trade-off while matching the ^{12}C/^{13}C and ^{16}O/^{18}O ratios from the He/C zone and the ^{14}N/^{15}N and ^{26}Al/^{27}Al ratios from the He/N zones. If we choose to match the very high ^{12}C/^{13}C ratio of the grain, then we get the results depicted in Figure 4.21. The mix becomes highly ^{15}N and ^{18}O enriched

– both signatures not seen in this grain. It also does not acquire the high $^{26}Al/^{27}Al$ ratio that is observed in this grain. This is because ^{14}N and high $^{26}Al/^{27}Al$ ratios originate in the He/N zone of which we can mix only 15%. If we choose to match the $^{14}N/^{15}N$ ratio then the $^{12}C/^{13}C$ ratio drops a whole order of magnitude, and the $^{16}O/^{18}O$ ratio does not increase much and the mix still remains highly ^{18}O-enriched. The $^{26}Al/^{27}Al$ ratio increases enough to match that of the grain. For this to happen we need almost 70% material from the He/N zone and the remaining comes from the He/C zone. The He/N zone is ^{13}C-enriched and has a high $^{26}Al/^{27}Al$ ratio while the He/C zone has high $^{12}C/^{13}C$ ratios and much lower $^{26}Al/^{27}Al$ ratios. This gives rise to a negative correlation between these two ratios when any mixing takes place between the He/C and He/N zones. The SN models cannot account for the high $^{26}Al/^{27}Al$ and $^{12}C/^{13}C$ ratios seen in some SN grains. A similar problem is encountered when trying to explain the C and Al ratios observed in SiC-X grains (Yangting et al. 2009). Further, most mixing calculations carried out to explain the ^{18}O and ^{15}N excesses in graphite grains give rise to extremely large excesses in these isotopes, as seen above. Most graphite grains do not exhibit similar extreme excesses in these isotopes. This leads us to conclude that the N and O ratios in graphite grains are equilibrated to some extent in the LD fractions and to a much higher extent in the HD fractions, where the N and O isotopes are found to be completely normal even in SN grains.

We will now discuss a few unusual grains from the OR1d density fraction.

Grain OR1d1m-11 contains large ^{15}N and ^{18}O excesses ($^{14}N/^{15}N = 69 \pm 1$; $^{16}O/^{18}O = 227 \pm 45$). It also has a high $^{26}Al/^{27}Al$ ratio of 0.038 ± 0.001. These isotopic signatures point to a SN origin for this grain except it has a very low $^{12}C/^{13}C$ ratio (6.5), an excess in ^{30}Si ($\delta^{30}Si = 260 \pm 29$ ‰) and a depletion in ^{29}Si ($\delta^{29}Si = -95 \pm 20$ ‰). The result of a SN layer mixing exercise for this grain is shown in Figure 4.22 and the mix percentages are listed in Table **??**. Figure 4.22 shows the isotopic ratios of this grain compared to a best-fit calculation using the Rauscher et al. (2002) 15

$M_{\odot}$ SN model. In this calculation, we have constrained the model to give a $^{12}C/^{13}C$ ratio that matches that of the grain. When such a constraint is put on the mixing calculation, most of the material needed to fit the isotopic anomalies comes from the He/N zone (99.41%). This gives a C/O ratio of 2.24. The only way to keep this ratio from falling below 1 was to obtain material from the C-enriched region at the base of the He/N zone (between mass 3.81 – 4.10 $M_{\odot}$). However, the dominant contribution from the He/N zone that has a high $^{14}N/^{15}N$ ratio causes the mixture to be ^{14}N-enriched and does not even come close to matching the low $^{14}N/^{15}N$ ratio seen in this grain. This opposite trend in the measured N isotopic value and the model calculation cannot be explained by equilibration. The much lower ^{18}O excess and smaller $^{26}Al/^{27}Al$ ratio measured in the grain compared to the values obtained from the model mixture can be attributed to isotopic dilution. A possible alternative stellar source for such a grain is a nova (Starrfield et al., 1985; Wiescher et al., 1986; Woosley, 1986). The $^{14}N/^{15}N$ ratio of this grain is higher than that predicted for a typical nova explosion but nevertheless the low $^{12}C/^{13}C$ and $^{16}O/^{18}O$ ratios, the large ^{30}Si excess, and the high $^{26}Al/^{27}Al$ ratio indicate a possible nova origin for this grain (José et al. 2004).

A similar problem arises with grain OR1d4m-8. The low $^{12}C/^{13}C$ ratio ($\sim$ 14) of this grain is incompatible with its other SN signatures. The grain shows evidence for extinct ^{44}Ti ($^{44}Ti/^{48}Ti = 0.0027 \pm 0.0002$), has a very high $^{26}Al/^{27}Al$ ratio (0.236 ± 0.024), and exhibits large excesses in ^{18}O ($^{16}O/^{18}O = 325 \pm 6$), ^{28}Si ($\delta^{29}Si = -232 \pm 9$ ‰; $^{30}Si = -204 \pm 12$ ‰) and ^{49}Ti ($\delta^{49}Ti = 203 \pm 10$ ‰). A mixing of the different layers of a SN is unable to reproduce the low $^{12}C/^{13}C$ and $^{16}O/^{18}O$ ratios observed in this grain. Since this grain shows evidence for the presence of ^{44}Ti, it has to have originated from a SN. The low $^{12}C/^{13}C$ ratio, however, presents a problem while also assigning this origin to grain OR1d4m-8. Grain OR1d4m-1, with the highest $^{26}Al/^{27}Al$ ratio seen in any graphite grain, also has a low $^{12}C/^{13}C$ ratio albeit not

as low as OR1d4m-8. Nittler et al. (1996) found a graphite grain from Murchison (KE3c-242) with low a $^{12}C/^{13}C$ ratio and a high $^{26}Al/^{27}Al$ ratio, but normal N and O ratios. Another ^{13}C-enriched SiC grain with a large ^{28}Si excess was found by Nittler and Hoppe (2005). Both of these Murchison grains show evidence for extinct ^{44}Ti.

Other LD grains with an inexplicable Ti isotopic pattern are OR1d3m-7, OR1d4m-13, and OR1d3m-23 (Figure 4.23) that have considerable excesses in ^{47}Ti. Titanium-47 excesses cannot be explained by n-capture reactions. If the contributions from the decay of ^{47}Ca and ^{47}Sc were added, it would give rise to an excess of a few ‰(Travaglio et al. 1999). This Ti isotope, with the largest cross-section, is underproduced by a factor of 5 according to the galactic chemical evolution models of Timmes et al. (1995). The nucleosynthetic origin of ^{47}Ti is not well understood. Current SN models are unable to explain large ^{47}Ti excesses without accompanying larger excesses in ^{49}Ti, as seen in Figure 4.23. Apart from this ^{47}Ti excess, grain OR1d4m-13 has a high $^{26}Al/^{27}Al$ ratio (0.1414 ± 0.0011), ^{18}O ($^{16}O/^{18}O = 149 \pm 2$) and ^{15}N ($^{14}N/^{15}N = 161 \pm 2$) excesses – all SN signatures. All other isotopes have close-to-solar ratios within errors. Grain OR1d3m-7 has a low $^{12}C/^{13}C$ ratio of $\sim$ 11 but all the other isotopic ratios are normal or close-to-normal. All except the Ti isotopic ratios of grain OR1d3m-23 are close-to-solar (within errors). Similar ^{47}Ti excesses have been observed in one graphite grain (KE3d-9) from Murchison (Amari and Zinner, 1997), and a SiC grain (M11-151-4), also from Murchison (Nittler and Hoppe, 2005). We also reported a HD graphite (OR1f2m-9) from Orgueil with a similar large ^{47}Ti excess (Jadhav et al. 2008).

Recently, ultramicrotomed sections of three LD graphites from this study were analyzed in a TEM (Croat et al. 2009a; b). Grain OR1d3m-7 was picked for this study because of its low $^{12}C/^{13}C$ ratio (11). It also has a considerable ^{50}Ti excess ($\delta^{50}Ti = 259 \pm 97$ ‰). An OsRu-rich metal subgrain was found within the graphite grain, suggesting that stars like Sakurai's object that emit s-process elements- and

^{13}C-enriched dust (Asplund et al. 1997, 1999), could be plausible sources for the ^{13}C-enriched graphites (Croat et al. 2009b). Similar refractory subgrains were found in 2 Murchison HD KFC1 graphites (Croat et al. 2005). In addition, two internal SiC grains were found within OR1d3m-7. We possess TEM data on two other LD grains with slight ^{15}N and ^{18}O excesses, and solar ^{12}C/^{13}C ratios. Three SiC and many Ti-rich subgrains were detected in grain OR1d3m-2. The TiC grains lack s-process element enrichments. A large number of Ti-rich subgrains that contained no enrichments in the s-process elements but had very high Al contents were found in OR1d3m-6. In comparison, SiC subgrains were not found in Murchison LD SN grains nor were such high Al contents seen in the TiC grains. As more grains are analyzed in the TEM, we expect to be able to better constrain the stellar sources of graphites, especially those that are ^{13}C-enriched.

Sources of the high-density graphites from OR1f ($\rho \sim$ 2.02 – 2.04 g cm^{-3}), OR1g ($\rho \sim$ 2.04 – 2.12 g cm^{-3}), and OR1i ($\sim$ 2.16 – 2.30 g cm^{-3}):

Previously, HD graphite grains from the Murchison fractions KFB1 and KFC1 were analyzed with the IMS-3f (e.g., Hoppe et al., 1995). Since HD graphites tend to have a very low abundance of trace elements, an instrument with a much higher sensitivity was required to measure Si. The NanoSIMS, with its high detection capabilities, allows us to measure the Si isotopes in HD graphites with a much higher precision (Amari et al. 2003, 2004, 2005; Jadhav et al. 2006). There is now increasing evidence that a large number of HD graphites from Murchison and Orgueil originated in low metallicity AGB stars. This previous lack of high-precision measurements of the Si isotopes might also explain why more graphite grains with AGB origins had not been identified before the previously mentioned NanoSIMS studies.

In general, the HD grains from the density fractions OR1f, 1g, and 1i, are enriched in ^{29}Si and ^{30}Si. Figure 4.6 is a plot of the δ^{30}Si/^{28}Si values for the individual grains

in these density fractions as a function of their $^{12}C/^{13}C$ ratios. Most of the HD, ^{30}Si-rich grains contain isotopically light carbon (Jadhav et al. 2006). Such signatures are predicted for low-metallicity AGB stars where more ^{12}C and $^{29,30}Si$ from the He shell is dredged up into the envelope during the thermally pulsing phase than in stars of solar metallicity (Zinner et al. 2006a). Thus, low-metallicity AGB stars are the most likely source for the HD graphite grains with excesses in ^{30}Si and ^{12}C. Such stars also are predicted to have high C/O ratios and thus, are expected to preferentially condense graphite grains before SiC grains in their ejecta (Lodders and Fegley, 1997; Bernatowicz et al. 2006). This is the most likely reason why no SiC grains with high $^{12}C/^{13}C$ ratios and large ^{30}Si excesses have been found (Zinner et al. 2006a; Jadhav et al. 2006).

Observations by Leisenring et al. (2008) and Sloan et al. (2009) of molecular spectral features of circumstellar dust around AGB stars strengthen this argument. They find that the abundance of SiC grains in circumstellar dust shells decreases with decreasing stellar metallicity and is explained by the increasing C/O ratio. Such a scenario favours graphite condensation over SiC. Dust model calculations of Gail et al. (2009) also predict that AGB stars with low metallicities (~ 0.3 $Z_{\odot}$) should produce a large fraction of presolar graphite grains.

In Section 4.3.1 we reported that the N and O isotopic ratios in HD graphites were normal or terrestrial (in case of N) within errors. Such ratios observed in HD grains of both Murchison and Orgueil cannot be interpreted as an isotopic signature of the stellar source. The presence of terrestrial N and O in grains with large C anomalies is puzzling and has been attributed to isotopic exchange or dilution (either in the laboratory or the solar system). The absence of large N and O anomalies indicates that in HD graphite these elements might be more easily exchanged than in LD grains and that the original anomalies might have been extreme. Furthermore, although HD grains seem to be to equilibrated to a larger extent, LD grains might also be partially

equilibrated because the anomalies seen in most grains are not as extreme as those expected from SNe (e.g. Figures 4.21 and 4.22), as discussed in the previous section.

Fifteen graphite grains on the OR1f2m mount have very interesting isotopic anomalies. The C, Ca and Ti isotopic ratios of these grains are listed in Table 4.8. The nucleosynthetic sources of the 7 grains with $^{12}C/^{13}C$ ratios less than 20 are discussed in detail in Jadhav et al. (2008). We will only summarize the results here. We discuss the possible stellar sources of the remaining 8 grains in more detail below.

Seven graphites from the OR1f2m mount (OR1f2m-1, OR1f2m-9, OR1f2m-29, OR1f2m-34, OR1f2m-38, OR1f2m-40 and OR1f2m-o67) have $^{12}C/^{13}C < 20$. Grains OR1f2m-1, OR1f2m-38 and OR1f2m-o67 contain large ^{44}Ca excesses that indicate the initial presence of ^{44}Ti. As discussed previously, these three grains definitely originated from type II SNe. There exists, however, no explanation for their low $^{12}C/^{13}C$ ratios. It is not possible to achieve such low C ratios and still maintain C/O > 1, by mixing the He/C and He/N zones. A mixing calculation result for grain OR1f2m-o67 that is ^{13}C-enriched is shown in Figure 4.24 and the corresponding mix percentages are listed in Table 4.9. The relatively low C/O ratio (1.54) calculated for the mixture while trying to achieve the low $^{12}C/^{13}C$ ratio can be obtained by mixing 99.83% of material from the C-rich region of the He/N zone (between 3.81 – 4.10 $M_{\odot}$) with 0.09% from the He/C zone (See Table 4.9). As seen in the previous section, this does not allow us to fit the N, O, and Al isotopic anomalies observed in this grain. This brings us back to the same problem we encountered in the previous section with He/C – He/N zone mixing that gives very large ^{14}N and ^{18}O excesses, and high $^{26}Al/^{27}Al$ ratios. In the Rauscher et al. (2002) models for a 25 $M_{\odot}$ SN, there is a large ^{15}N-spike in the He/N zone that might help with this issue. However, we hesitate to use this approach because the source of this spike has not been explained in the literature.

The other four ^{13}C-enriched grains OR1f2m-29, OR1f2m-40, OR1f2m-34 and

OR1f2m-9 could have condensed in the ejecta of a born-again AGB star, like Sakurai's object (Asplund et al. 1997, 1999). The large Ca and Ti anomalies observed in these grains can be matched by those seen in the undiluted He shell of a 2 or 3 $M_{\odot}$ AGB star of metallicity, Z = 0.02 – 0.003 (Figure 4.25). Hydrogen burning in sources like Sakurai's object can explain the low $^{12}C/^{13}C$ ratios, and the large Ca and Ti anomalies in such grains reflect the composition of the He-rich intershell exposed on the surface (Jadhav et al. 2008). Stellar evolution models (Herwig et al. 1999; Herwig, 2001) of such a star indicate that low mass (2 $M_{\odot}$) stars that have left the AGB experience a very late thermal pulse. This He-flash-powered convection zone (rich in freshly produced ^{12}C) extends into the thin residual H-rich envelope and causes convective H burning via the CN cycle. This produces ^{13}C and reduces the $^{12}C/^{13}C$ ratio. Since the residual envelope has a limited supply of protons, the H is exhausted before ^{14}N becomes more abundant than ^{12}C and the envelope continues to remain C-rich. The convection during the thermal pulse also brings He-shell material rich in s-process isotopes and H-burning products together and allows them to coexist at the surface of the star. If such a star were the source of the ^{13}C-enriched grains mentioned above, we should expect to see similar nucleosynthetic signatures in the grains.

Grain OR1f2m-25 is a SN grain with a large excess in ^{44}Ca that indicates the presence of radiogenic ^{44}Ti. This grain is not ^{13}C-enriched ($^{12}C/^{13}C$ = 725) like the other grains with ^{44}Ca excesses. The result of a mixing calculation for this grain is shown in Figure 4.26. Most of the isotopic anomalies seen in this grain can be matched by mixing different layers in the proportions listed in Table 4.8. The resultant C/O ratio is 6.1. Most isotopic anomalies can be matched by mixing $\sim$ 67% of the material from the He/C zone, $\sim$ 33% from the H envelope, and $\sim$ 0.1% from the Si/S zone. The large ^{44}Ca excess in Figure 4.26 is a clear sign of the presence of ^{44}Ti (See Table 4.7). Note however, we are still unable to fit the N, O, and Al isotopic ratios. The O and Al isotopic ratios could have been equilibrated but the ^{14}N excess is puzzling. Another

grain (OR1i1m-4) from the highest density fraction (OR1i) exhibits SN signatures: ^{12}C, ^{18}O, and ^{28}Si excesses. The isotopic ratios of this ^{12}C-enriched grain can be matched fairly well by mixing material from the He/C zones to that of the Si/S zone to obtain all the isotopic anomalies.

The Ti isotopic patterns for grains OR1f2m-21, OR1f2m-39 and OR1f2m-33 are shown in Figure 4.27. The Ca isotopic ratios have large errors associated with the measurements and are hence not diagnostic in determining the stellar sources of these grains. All 3 grains have ^{12}C/^{13}C ratios greater than 300, and the Ti isotopic patterns can be matched with admixtures from the O/C and O/Ne zones of a 15 $M_{\odot}$ SN (Figure 4.27). The Ti isotopic ratios of the grains are higher than those expected from AGB stars. These grains exhibit no other SN signature other than those seen in their Ti isotopic ratios. Grain OR1f2m-39 has a relatively small, inferred ^{41}Ca/^{40}Ca ratio (0.0006 $\pm$ 0.0004) which is slightly higher than that expected from AGB stars and could be obtained in SNe. The ^{41}Ca/^{40}Ca ratios expected in AGB stars are in the range of 10^{-4} – 10^{-5} (Amari et al. 1996; Gallino et al. 1998; Wasserburg et al. 1995), while the He/C zone in a 15 $M_{\odot}$ SN has an average ^{41}Ca/^{40}Ca ratio of $\sim$ 0.009 (Woosley and Weaver, 1995).

Figure 4.28 shows the Ca pattern for OR1f2m-18 and OR1f2m-o68 and the Ti isotopic pattern for grain OR1f2m-18. Grain OR1f2m-18 has a large ^{47}Ti excess (δ^{47}Ti = 2119 $\pm$ 354 ‰), much greater than the ^{46}Ti excess, which makes its Ti isotopic pattern inexplicable as discussed in the previous section. This grain also has a high ^{41}K/^{39}K ratio of 0.1261 $\pm$ 0.002 (solar value is 0.072) resulting in a high, inferred ^{41}Ca/^{40}Ca ratio of 0.0106 $\pm$ 0.0003 that can be obtained in the He/C, C/O[1] and O-rich zones of a Type II SN (Figure 4.19). The Ca isotopic patterns of grains OR1f2m-18 and OR1f2m-o68 and the ^{49,50}Ti excesses of OR1f2m-18 can be obtained by an admixture of the C/O[1] and O-rich zones to the He/C zones of a Type II SN, as is demonstrated in Figures 4.28a and b. Grain OR1f(1,2)m-o68 also has a large

^{29,30}Si excesses (δ^{29}Si = 1341 ± 35 ‰; δ^{30}Si = 896 ± 33 ‰) and a high inferred ^{41}Ca/^{40}Ca ratio of 0.0102. Material from the O/C and O/Ne zones can produce such large Ca and Ti anomalies but adding even a very small percentage of material from these zones will cause the C/O ratio to be less than 1.

We discussed the problems encountered when mixing the He/C and He/N zones to obtain the high ^{26}Al/^{27}Al ratios seen in some grains with low ^{12}C/^{13}C ratios. The ^{14}N/^{15}N ratios obtained after such a mix are way too high (e.g. Figure 4.22 and 23) and are not seen in very many graphite grains. In their mixing calculations, Travaglio et al. (1999) reduced the N contribution from this zone by a factor of 200 by assuming that N is fractionated from other elements during the SN explosion. To date, very few SN grains with ^{14}N excesses have been found. Such grains can form from a mixture of the He/C and He/N zones of a SN and also contain lower ^{12}C/^{13}C ratios and large excesses in ^{29,30}Si. We found one such grain in the HD fraction (OR1g1m-33) with a high ^{14}N/^{15}N ratio (1437 ± 30) and low ^{12}C/^{13}C ratio ($\sim$ 15) (Figure 4.3b). This grain exhibits normal Si isotopic ratios. Further measurements of Al-Mg, Ca, and Ti isotopes in this grain will help constrain its source better. There are four more grains from the HD fractions with slightly elevated ^{14}N/^{15}N ratios (See Figure 4.3b). Three of them are ^{12}C-enriched and could originate from low-metallicity AGB stars while one is ^{13}C-enriched, a signature from the He/N zone of a SN. High ^{14}N/^{15}N ratios and ^{13}C-enrichments are also seen in mainstream SiC grains that almost certainly come from low-mass AGB stars with solar metallicity. However, it is very difficult to constrain the stellar source on the basis of C and N isotopes; but if future measurements find the ^{13}C-enriched grains also enriched in s-process isotopes then they could have originated from a star like Sakurai's object that has undergone a very late thermal pulse.

Thus, HD graphites from Orgueil seem to have several stellar sources. We have seen evidence for grains from SNe, graphites from low-metallicity AGB stars, and

grains that come from a ^{13}C-enriched stellar source (like Sakurai's object) that also supplied an abundance of s-process isotopes to the grains.

4.4.2 Comparison with Murchison graphite

Orgueil graphite grains appear to be similar to Murchison graphite in their isotopic properties. Morphologically, the onion-type grains observed in Orgueil are similar to the HD Murchison graphites but unlike in Murchison, are abundant in both the LD and HD fractions. Very few cauliflower grains have been observed in any density fraction of Orgueil. Another marked and puzzling difference exhibited by Orgueil graphite is that, unlike in Murchison, the HD Orgueil grains are, on average, much larger than the HD Murchison grains. Orgueil HD grains range up to 35 μm in diameter while the largest grain found in the Murchison HD fractions has a diameter of 12 μm, but most are smaller than 2 μm (Hoppe et al., 1995).

The lack of a large range of N anomalies is a common trend in the graphites from both meteorites (Hoppe et al., 1995). In the KE3 fraction (1.65 – 1.72 g cm^{-3}) from Murchison, about a third of the grains are SN graphites. The abundance of ^{18}O-rich grains decreases with increasing density and, in fact, grains with isotopically heavy O have not been observed in the highest Murchison density fraction KFC1 (2.15 – 2.20 g cm^{-3}). A similar trend is observed in the abundance of ^{18}O enriched grains in the density fractions of Orgueil. Recent NanoSIMS analysis of HD graphite grains (KFB1) from Murchison (Amari et al. 2005) indicate that they also have ^{30}Si excesses similar to the ones seen in the HD Orgueil (OR1f, 1g, and 1i) grains and they are thus believed to have originated from low-metallicity AGB stars. There is no Ca and Ti isotopic evidence for Murchison graphite grains from born-again AGB stars, like the ones discussed by Jadhav et al. (2008). However, a population of ^{13}C-enriched grains exists in all the density fractions of Murchison as well. Additional isotopic measurements on these ^{13}C-enriched graphites from Murchison will be needed

to constrain their stellar sources better.

4.4.3 Unresolved issues

a) Supernova models produce very large ^{18}O and ^{15}N excesses, and very high ^{26}Al/^{27}Al ratios that are not observed in most grains, whereas isotopic ratios of other elements seem to fit SN models reasonably well. The relatively small excesses obtained in the grains points to the fact that the N, O, and Mg isotopes may not be completely equilibrated. This equilibration could occur in the laboratory or in the parent body. Also, for some reason this isotopic dilution is more pronounced in the HD graphites compared to those from the LD fractions. The exact mechanism for such a dilution process needs to be investigated.

b) There seems to be a clear distinction between the sources for low-density and high-density graphites from Murchison. Apart from a few exceptions, LD grains are mainly SN grains while the HD grains originate in low-metallicity AGB stars. This distinction breaks down as we analyze more and more presolar graphite grains from Orgueil. The separate stellar sources for the high- and low-density fractions could be an inherent property of presolar graphite grains in meteorites or an artifact. Every density fraction of Orgueil contains a large amount of the macromolecular carbon that was mentioned in Section 4.2.3. Most graphite grains are found embedded in this material. It is entirely possible that grains from different densities remain embedded in this carbonaceous material and were not separated completely during the density separation. Since the average density of a fraction is measured, a few grains with different densities could be mixed in with the others (Remusat L., pers. comm.), making the density separates imperfect. The presence of this macromolecular carbon in all the density fractions of Orgueil graphites also makes it difficult to carry out meaningful abundance calculations of presolar graphite grains from Orgueil because grains embedded and hidden in this IOM will not be included in the calculations.

It is essential to study the structure and composition of this macromolecular carbon to further refine the chemical separation procedure used to extract presolar graphite grains from meteorites, especially those similar to Orgueil that are very rich in organics. Of course, the IOM is unique in its own right and must be studied from different types of meteorites in order to determine and interpret the range of compositions observed (e.g. Alexander et al. 2007).

c) Isotopic studies of the subgrains found within graphites similar to the one carried out by Stadermann et al. (2005) are very important to establish the exact nature and source of the isotopic anomalies seen in these grains. For example, most Ti measured in the graphites is found in subgrains (Figure 4.13) while Ca is uniformly distributed in the host grain. The parent grain and the subgrain could have formed under completely different condensation conditions and the Ca and Ti anomalies we find in a single grain could represent distinct layers from the stellar source. Such a scenario is not considered when the stellar sources of the grains are discussed based on the isotopic ratios measured in the parent grain alone.

d) We found grains in the HD fraction (OR1f) with extremely large Ca and Ti anomalies but almost normal N, O, Mg, and Si isotopic ratios. Neutron-capture reactions that affect the Ca and Ti isotopes should have also affected the Mg and Si isotopes considerably. The nature of the equilibrating processes that affect only Mg and Si isotopes, and not Ca and Ti isotopes needs to be identified and better understood. Sources of possible contamination also need to be identified as they make identifying stellar sources of these grains very complicated (e.g. Barzyk et al. 2007).

4.5 Summary

Presolar graphite grains from Orgueil have multiple stellar sources. In this study, we presented isotopic evidence for graphite grains from supernovae, low-metallicity

AGB stars, and born-again AGB stars. Sakurai's object-type stellar sources seem to be a likely nucleosynthetic source of grains with low $^{12}C/^{13}C$ ratios. Further isotopic studies are required to determine the exact nature of this source. Extensive correlated isotopic measurements are planned for a large fraction of the grains that remain intact after the SIMS analyses presented in this paper. Resonant ionization mass spectrometry (RIMS) analyses of Mo, Zr, Sr, and Ba isotopic ratios (e.g., Nicolussi et al., 1997; 1998 a; b; c) are planned and will be essential to completely characterize these grains and constrain their stellar sources. Raman spectroscopy and TEM studies of these grains will help elucidate the chemical environments in which these grains condensed and determine the structural differences between Murchison and Orgueil graphites.

Acknowledgements: This work was supported by NASA grant NNG05GF81G and the Italian MIUR-PRINO6 grant. We thank Frank Stadermann for Auger Nanoprobe time to obtain SEM images of some of the grains in this study. Tim Smolar's assistance with the NanoSIMS is greatly appreciated.

References

Alexander C. M. O.'D., Fogel M., Yabuta H., and Cody G. D. (2007) The origin and evolution of chondrites recorded in the elemental and isotopic compositions of their macromolecular organic matter. Geochimica et Cosmochimica Acta 71, 4380-4403.

Amari S. and Zinner E. (1997) Supernova grains from meteorites. In Astrophysical Implications of the Laboratory Study of Presolar Materials (ed. T. J. Bernatowicz and E. Zinner), pp. 287-305. AIP.

Amari S., Anders E., Virag A., and Zinner E. (1990) Interstellar graphite in meteorites. Nature 345, 238-240.

Amari S., Hoppe P., Zinner E., and Lewis R. S. (1992) Interstellar SiC with unusual

isotopic compositions: Grains from a supernova? Astrophysical Journal 394, L43-L46.

Amari S., Lewis R. S., and Anders E. (1994) Interstellar grains in meteorites: I. Isolation of SiC, graphite, and diamond; size distributions of SiC and graphite. Geochimica et Cosmochimica Acta 58, 459-470.

Amari S., Lewis R. S., and Anders E. (1995) Interstellar grains in meteorites: III. Graphite and its noble gases. Geochimica et Cosmochimica Acta 59, 1411-1426.

Amari S., Zinner E., and Lewis R. S. (1996) ^{41}Ca in presolar graphite of supernova origin. Astrophysical Journal 470, L101-L104.

Amari S., Stadermann F. J., Zinner E., and Lewis R. S. (2003) Continued study of presolar graphite from Murchison separate KFA1. Lunar Planetary Science XXXIV, Abstract #1864.

Amari S., Zinner E., and Lewis R. S. (2004) Comparison study of presolar graphite separates KE3 and KFA1 from the Murchison meteorite. Lunar Planetary Science XXXV, Abstract #2103.

Amari S., Zinner E., and Lewis R. S. (2005) Isotopic analysis of presolar graphite from the KFB1 Murchison separate. Meteoritics and Planetary Science 40, A15.

Arnould M., Meynet G., and Paulus G. (1997) Wolf-Rayet stars and their nucleosynthetic signatures in meteorites. In Astrophysical Implications of the Laboratory Study of Presolar Materials (ed. T. J. Bernatowicz and E. Zinner). AIP.

Asplund M., Gustafsson B., Lambert D. L., and Rao Kameswara N. (1997) A stellar endgame – the born-again Sakurai's object. Astronomy and Astrophysics 321, L17-L20.

Asplund M., Lambert D. L., Kipper T., Pollacco D., and Shetrone M. D. (1999) The rapid evolution of the born-again giant Sakurai's object. Astronomy and Astrophysics 343, 507-518.

Bernatowicz T. J., Croat T. K., and Daulton T. L. (2006) Origin and evolution of carbonaceous presolar grains in stellar environments. In Meteorites and the Early Solar System II (ed. D. S. Lauretta and H. Y. McSween, Jr.), pp. 109-126. Univ. of Arizona, Tucson.

Besmehn A. and Hoppe P. (2003) A NanoSIMS study of Si- and Ca-Ti-isotopic compositions of presolar silicon carbide grains from supernovae. Geochimica et Cosmochimica Acta 67, 4693-4703.

Brown P. G., Hildebrand A. R., Zolensky M. E., Grady M., Clayton R. N., Mayeda T. K., Tagliaferri E., Spalding R., MacRae N. D., Hoffman E. L., Mittlefehldt D. W., Wacker J. F., Bird J. A., Campbell M. D., Carpenter R., Gingerich H., Glatiotis M., Greiner E., Mazur M. J., McCausland P. J., and Plotkin H. (2000) The fall, recovery, orbit, and composition of the Tagish Lake meteorite: a new type of carbonaceous chondrite. Science 290, 320-325.

Busso M., Gallino R., and Wasserburg G. J. (1999) Nucleosynthesis in asymptotic giant branch stars: relevance for Galactic enrichment and solar system formation. Annual Review of Astronomy and Astrophysics 37, 239-309.

Clayton D. D., Liu W., and Dalgarno A. (1999) Condensation of carbon in radioactive supernova gas. Science 283, 1290-1292.

Croat T. K., Stadermann F. J., and Bernatowicz T. J. (2005) Presolar graphite from AGB stars: Microstructure and s-process enrichment. Astrophysical Journal 631, 976-987.

Croat T. K., Jadhav M., Lebsack E., and Bernatowicz T. J. (2009a) Low-density presolar graphite spherules from the Orgueil meteorite. Lunar and Planetary Science XL, Abstract #2175.

Croat T. K., Jadhav M., Lebsack E., and Bernatowicz T. J. (2009b) Refractory metal nuggets within presolar graphite. Meteoritics and Planetary Science 44, Abstract #5299.

Deneault E. A.-N., Clayton D. D., and Heger A. (2003) Supernova reverse shocks: SiC growth and isotopic composition. Astrophysical Journal 594, 312-325.

Deneault E. A.-N., Clayton D. D., and Meyer B. S. (2006) Growth of carbon grains in supernova ejecta. Astrophysical Journal 638, 234-240.

Ebel D. S. and Grossman L. (2001) Condensation from supernova gas made of free atoms. Geochimica et Cosmochimica Acta 65, 469-477.

Ebisuzaki T. and Shibazaki N. (1988) The effects of mixing of the ejecta on the hard x-ray emissions from SN 1987A. Astrophysical Journal 327, L5-L8.

Flesch G. D., Capellan J., and J. S. H. (1966) The abundance of the vanadium isotopes from sources of geochemical interest. Advances in Mass Spectrometry III, 571-574.

Gail H.-P., Zhukovska S. V., Hoppe P., and Trieloff M. (2009) Stardust from Asymptotic Giant Branch Stars. Astrophysical Journal 698, 1136-1154.

Gallino R., Arlandini C., Busso M., Lugaro M., Travaglio C., Straniero O., Chieffi A., and Limongi M. (1998) Evolution and nucleosynthesis in low-mass asymptotic giant branch stars. II. Neutron capture and the s-process. Astrophysical Journal 497, 388-403.

Grady M. M., Verchovsky A. B., Franchi I. A., Wright I. P., and Pillinger C. T. (2002)

Light element geochemistry of the Tagish Lake CI2 chondrite: Comparison with CI1 and CM2 meteorites. Meteoritics and Planetary Science 37, 713-735.

Guglielmo F., Epchtein N., Le Berte T., Fouque P., Hron J., Kerschbaum F., and Lepine J. R. D. (1993) Identification of 106 new infrared carbon stars in the IRAS Point Source Catalog. Astronomy and Astrophysics Supplement 99, 31-69.

Herant M., Benz W., Hix W. R., Fryer C. L., and Colgate S. A. (1994) Inside the supernova: A powerful convective engine. Astrophysical Journal 435, 339-361.

Herwig F. (2001) Internal mixing and surface abundance of [WC]-CSPN. Astrophysics and Space Science 275, 15-26.

Herwig F., Blcker T., Langer N., and Driebe T. (1999) On the formation of hydrogen-deficient post-AGB stars. Astronomy and Astrophysics 349, L5-L8.

Hinton R. W. (1990) Ion microprobe trace-element analysis of silicates: Measurement of multi-element glasses. Chemical Geology 83, 11-25.

Hoppe P., Amari S., Zinner E., Ireland T., and Lewis R. S. (1994) Carbon, nitrogen, magnesium, silicon and titanium isotopic compositions of single interstellar silicon carbide grains from the Murchison carbonaceous chondrite. Astrophysical Journal 430, 870-890.

Hoppe P., Amari S., Zinner E., and Lewis R. S. (1995) Isotopic compositions of C, N, O, Mg, and Si, trace element abundances, and morphologies of single circumstellar graphite grains in four density fractions from the Murchison meteorite. Geochimica et Cosmochimica Acta 59, 4029-4056.

Hoppe P., Kocher T. A., Eberhardt P., Amari S., and Lewis R. S. (1996) Variations of ^{44}Ti in circumstellar SiC grains of type X. Meteoritics and Planetary Science 31, 64-65.

Hoppe P., Strebel R., Eberhardt P., Amari S., and Lewis R. S. (2000) Isotopic properties of silicon carbide X grains from the Murchison meteorite in the size range 0.5 – 1.5 μm. Meteoritics and Planetary Science 35, 1157-1176.

Hughes J. P., Rakowski C. E., Burrows D. N., and Slane P. O. (2000) Nucleosynthesis and mixing in Cassiopeia A. Astrophysical Journal 528, L109-L113.

Jadhav M., Amari S., Zinner E., and Maruoka T. (2006) Isotopic analysis of presolar graphite grains from Orgueil. New Astronomy Reviews 50, 591-595.

Jadhav M., Amari S., Marhas K. K., Zinner E., Maruoka T., and Gallino R. (2008) New stellar sources for high-density, presolar graphite grains. Astrophysical Journal 682, 1479-1485.

José J., Hernanz M., Amari S., Lodders K., and Zinner E. (2004) The imprint of nova nucleosynthesis in presolar grains. Astrophysical Journal 612, 414-428.

Lambert D. L., Gustafsson B., Eriksson K., and Hinkle K. H. (1986) The chemical composition of carbon stars. I. Carbon, nitrogen, and oxygen in 30 cool carbon stars in the galactic disk. Astrophysical Journal Supplement 62, 373-425.

Lattimer J. M., Schramm D. N., and Grossman L. (1978) Condensation in supernova ejecta and isotopic anomalies in meteorites. Astrophysical Journal 219, 230-249.

Leisenring J. M., Kemper F., and Sloan G. C. (2008) Effects of metallicity on the chemical composition of carbon stars. Astrophysical Journal 681, 1557-1573.

Lewis R. S., Anders E., and Draine B. T. (1989) Properties, detectability and origin of interstellar diamonds in meteorites. Nature 339, 117-121.

Lodders K. and Fegley B., Jr. (1992) Trace element condensation in circumstellar envelopes of carbon stars. Meteoritics 27, 250-251.

Lodders K. and Fegley B., Jr. (1997) Condensation chemistry of carbon stars. In Astrophysical Implications of the Laboratory Study of Presolar Materials (ed. T. J. Bernatowicz and E. Zinner), pp. 391-423. AIP.

Meyer B. S., Weaver T. A., and Woosley S. E. (1995) Isotope source table for a 25 $M_{\odot}$ supernova. Meteoritics 30, 325-334.

Nakamura T., Umeda H., Iwamoto K., Nomoto K., Hashimoto M., Hix W. R., and Thielemann F.-K. (2001) Explosive nucleosynthesis in hypernovae. Astrophysical Journal 555, 880-899.

Nicolussi G. K., Davis A. M., Pellin M. J., Lewis R. S., Clayton R. N., and Amari S. (1997) s-Process zirconium in presolar silicon carbide grains. Science 277, 1281-1283.

Nicolussi G. K., Pellin M. J., Lewis R. S., Davis A. M., Amari S., and Clayton R. N. (1998a) Molybdenum isotopic composition of individual presolar silicon carbide grains from the Murchison meteorite. Geochimica et Cosmochimica Acta 62, 1093-1104.

Nicolussi G. K., Pellin M. J., Lewis R. S., Davis A. M., Clayton R. N., and Amari S. (1998b) Zirconium and molybdenum in individual circumstellar graphite grains: New isotopic data on the nucleosynthesis of heavy elements. Astrophysical Journal 504, 492-499.

Nicolussi G. K., Pellin M. J., Lewis R. S., Davis A. M., Clayton R. N., and Amari S. (1998c) Strontium isotopic composition in individual circumstellar silicon carbide grains: A record of s-process nucleosynthesis. Physics Review Letters 81, 3583-3586.

Niederer F. R. and Papanastassiou D. A. (1984) Ca isotopes in refractory inclusions. Geochimica et Cosmochimica Acta 48, 1279-1293.

Nittler L. R. and Hoppe P. (2005) Are presolar silicon carbide grains from novae actually from supernovae? Astrophysical Journal 631, L89-L92.

Nittler L. R., Amari S., Lewis R. S., Walker R. M., and Zinner E. (1995) ^{44}Ca and ^{49}Ti excesses in circumstellar SIC grains X from the Murchison carbonaceous chondrite. Meteoritics 30, 557.

Nittler L. R., Amari S., Zinner E., Woosley S. E., and Lewis R. S. (1996) Extinct ^{44}Ti in presolar graphite and SiC: Proof of a supernova origin. Astrophysical Journal 462, L31-L34.

PSGWeb – http://epsc.wustl.edu/~mjadhav/PresolarGraphite/

Rauscher T., Heger A., Hoffman R. D., and Woosley S. E. (2002) Nucleosynthesis in massive stars with improved nuclear and stellar physics. Astrophysical Journal 576, 323-348.

Sharp C. M. and Wasserburg G. J. (1993) Molecular equilibria and condensation sequences in carbon rich gases. Lunar Planetary Science XXIV, 1281-1282.

Sharp C. M. and Wasserburg G. J. (1995) Molecular equilibria and condensation temperatures in carbon-rich gases. Geochimica et Cosmochimica Acta 59, 1633-1652.

Shields W. R. (1966) NBS Technical Note 277. U.S. Government Publishing Office, Washington D. C.

Sloan G. C., Matsuura M., Zijlstra A. A., Lagadec E., Groenewegen M. A. T., Wood P. R., Szyszka C., Bernard-Salas J., and van Loon J. T. (2009) Dust Formation in a Galaxy with Primitive Abundances. Science 323, 353-355.

Starrfield S., Sparks W. M., and Truran J. W. (1985) Recurrent novae as a consequence of the accretion of solar material onto a 1.38 $M_{\odot}$ white dwarf. Astrophysical Journal 291, 136-146.

Stadermann F. J., Croat T. K., Bernatowicz T. J., Amari S., Messenger S., Walker R. M., and Zinner E. (2005) Supernova graphite in the NanoSIMS: Carbon, oxygen and titanium isotopic compositions of a spherule and its TiC sub-components. Geochimica et Cosmochimica Acta 69, 177-188.

Timmes F. X., Woosley S. E., and Weaver T. A. (1995) Galactic chemical evolution: Hydrogen through zinc. Astrophysical Journal Supplement 98, 617-658.

Timmes F. X., Woosley S. E., Hartmann D. H., and Hoffman R. D. (1996) The production of ^{44}Ti and ^{60}Co in supernovae. Astrophysical Journal 464, 332-341.

Travaglio C., Gallino R., Amari S., Zinner E., Woosley S., and Lewis R. S. (1999) Low-density graphite grains and mixing in type II supernovae. Astrophysical Journal 510, 325-354.

Wasserburg G. J., Busso M., Gallino R., and Raiteri C. M. (1994) Asymptotic giant branch stars as a source of short-lived radioactive nuclei in the solar nebula. Astrophysical Journal 424, 412-428.

Wasserburg G. J., Gallino R., Busso M., Goswami J. N., and Raiteri C. M. (1995) Injection of freshly synthesized ^{41}Ca in the early solar nebula by an AGB star. Astrophysical Journal 440, L101-L104.

Wiescher M., Grres J., Thielemann F.-K., and Ritter H. (1986) Explosive hydrogen burning in novae. Astronomy and Astrophysics 160, 56-72.

Woosley S. E. (1986) Nucleosynthesis and stellar evolution. In Nucleosynthesis and

Chemical Evolution (ed. B. Hauck, A. Maeder, and G. Meynet), pp. 1-195. Observatoire de Genève.

Woosley S. E. and Weaver T. A. (1995) The evolution and explosion of massive stars, II. Explosive hydrodynamics and nucleosynthesis. Astrophysical Journal Supplement 101, 181-235.

Woosley S. E., Arnett W. D., and Clayton D. D. (1973) The explosive burning of oxygen and silicon. Astrophysical Journal Supplement 26, 231-312.

Yangting L., Gyngard F., and Zinner E. (2009) Aluminum-26, ^{44}Ti and ^{49}V in SiC and Si_3N_4 grains of type X from the Qingzhen (EH3) chondrite. In preparation.

Zinner E., Amari S., Wopenka B., and Lewis R. S. (1995) Interstellar graphite in meteorites: Isotopic compositions and structural properties of single graphite grains from Murchison. Meteoritics 30, 209-226.

Zinner E., Nittler L. R., Gallino R., Karakas A. I., Lugaro M., Straniero O., and Lattanzio J. C. (2006a) Silicon and carbon isotopic ratios in AGB stars: SiC grain data, models, and the Galactic evolution of the Si isotopes. Astrophysical Journal 650, 350-373.

Zinner E., Amari S., and Jadhav M. (2006b) On the stellar sources of presolar graphite. Proceedings of the International Symposium "Nuclei in the Cosmos - IX", CERN, Geneva, June 25-30, 2006. Proceedings of Science, PoS (NIC-IX) 019.

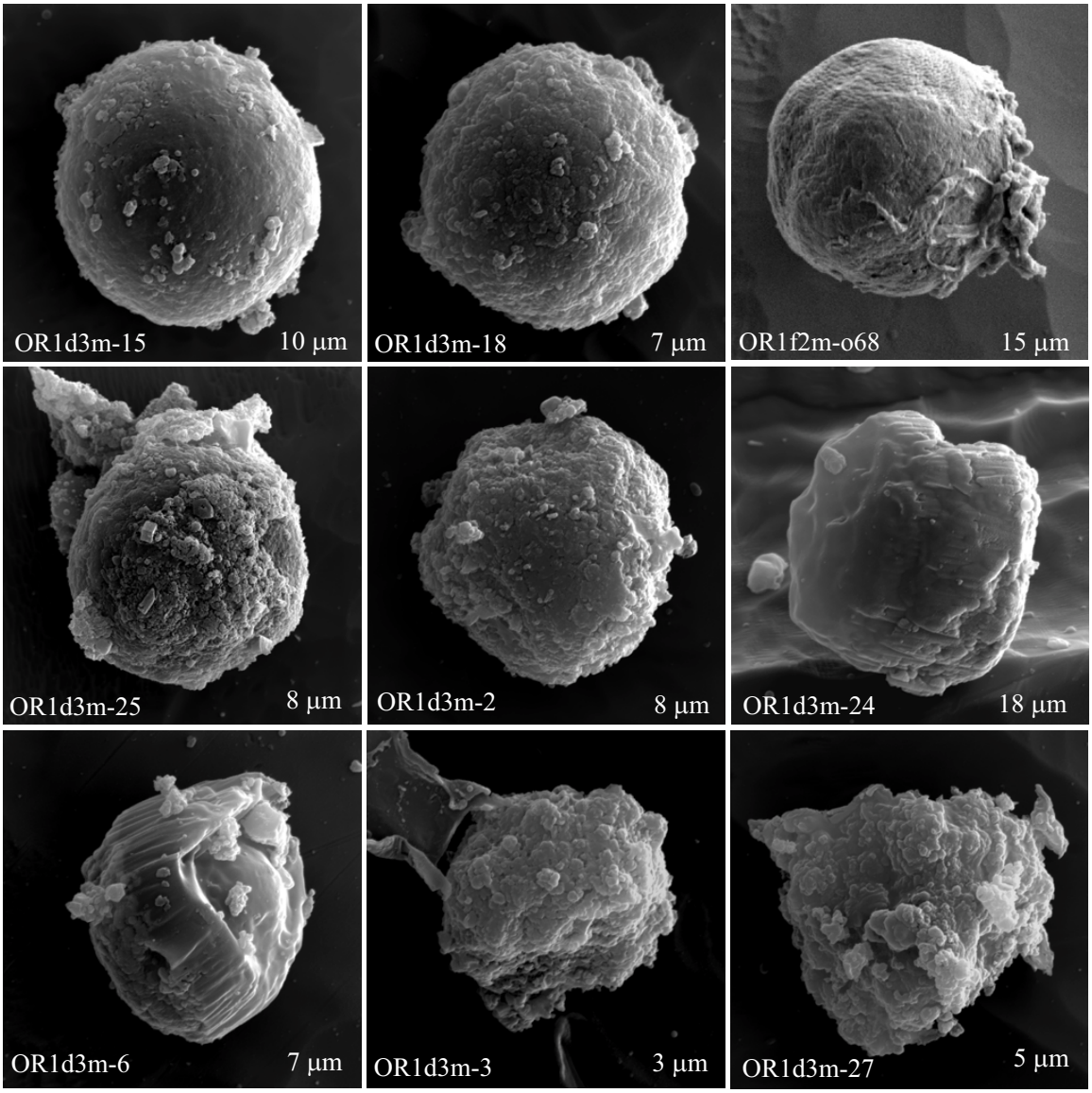

Figure 4.1 Secondary electron images of graphite grains from Orgueil taken with the Auger Nanoprobe. There is a distinct lack of cauliflower grains among the Orgueil density separates. Grain names and diameters (in μm) are indicated for the individual grains.

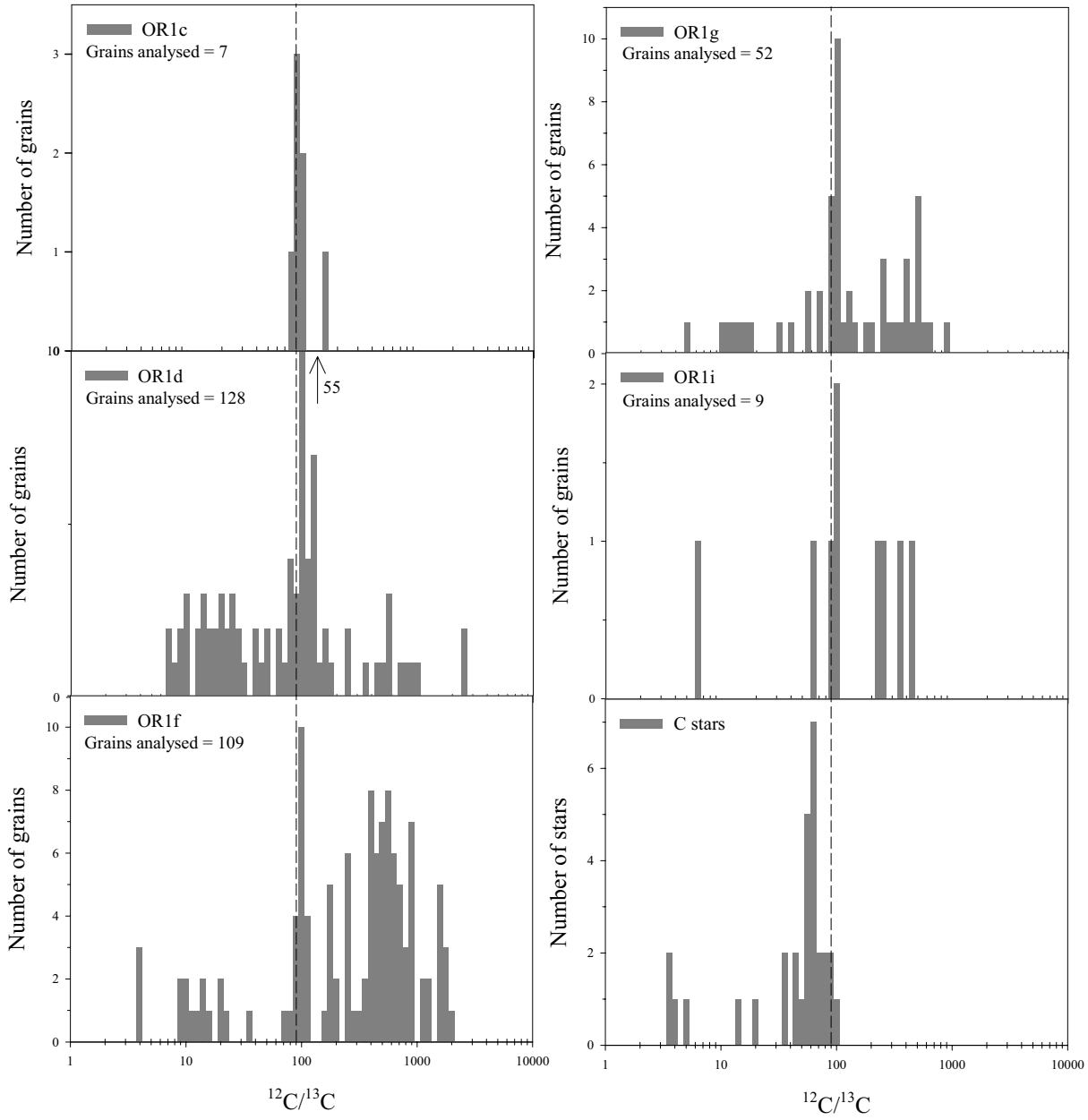

Figure 4.2 The distribution of $^{12}C/^{13}C$ ratios of the graphite grains in different density fractions from Orgueil. These ratios are compared to the C ratios measured in the atmospheres of carbon stars (Lambert et al. 1986). The solar $^{12}C/^{13}C$ ratio is ~ 89 and is indicated by the dashed lines.

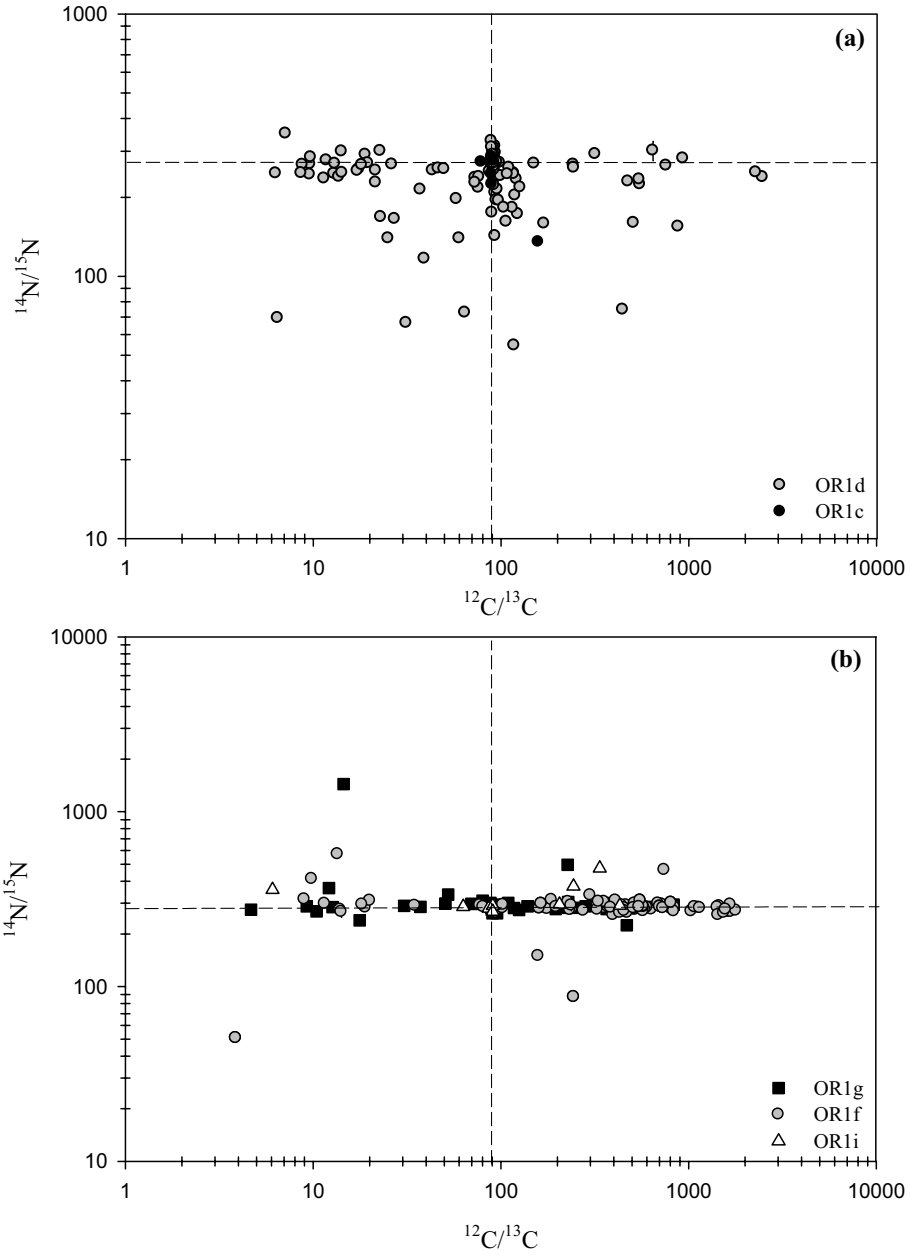

Figure 4.3 (a) Carbon and nitrogen isotopic ratios for the LD graphites from the OR1c and OR1d fractions. (b) $^{12}C/^{13}C$ and $^{14}N/^{15}N$ ratios measured for the HD graphites from the OR1f, OR1g, and OR1i fractions. Dashed lines denote solar isotopic ratios ($^{12}C/^{13}C \sim 89$; $^{14}N/^{15}N \sim 272$). Error bars are 1 σ.

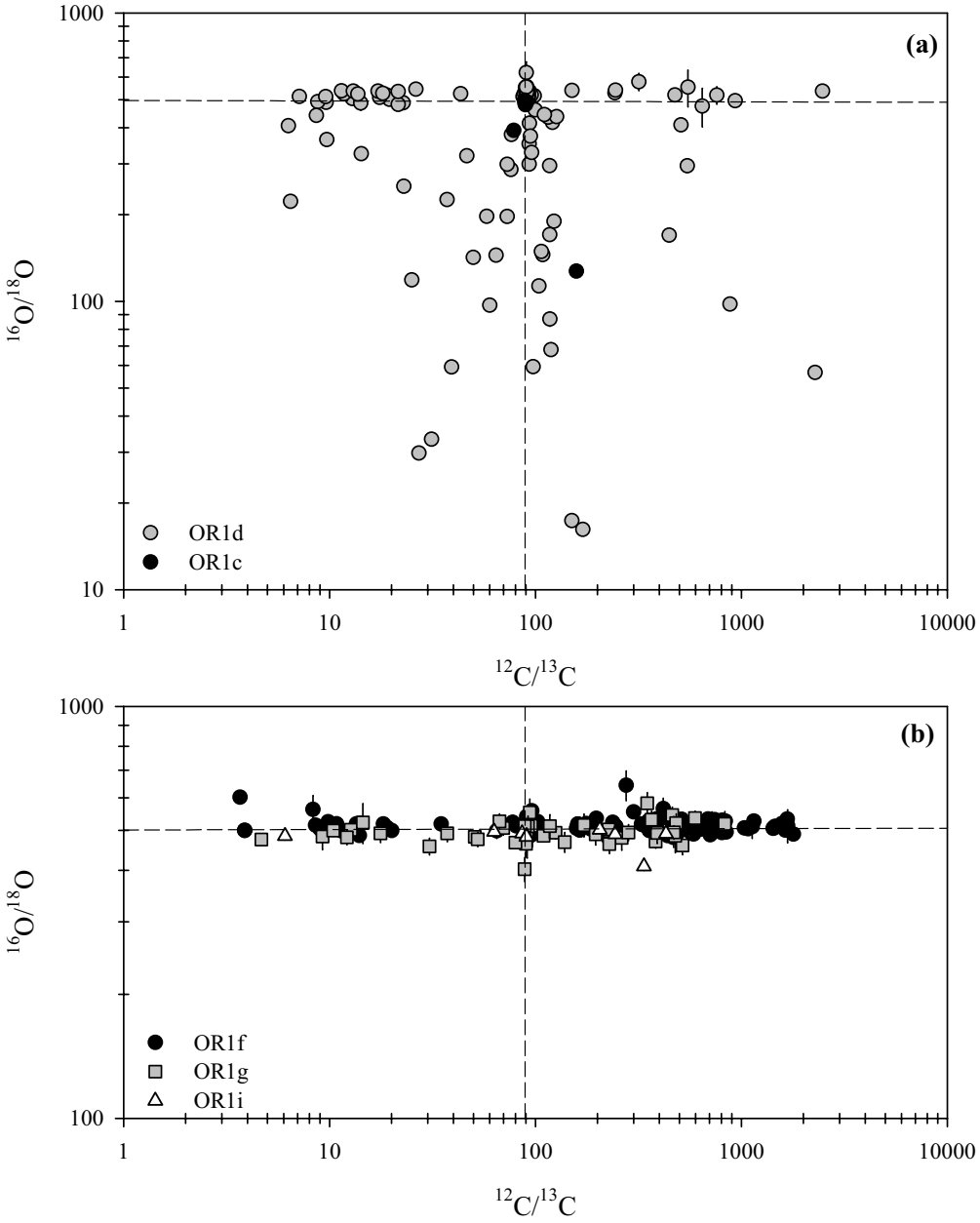

Figure 4.4 (a) Carbon and oxygen isotopic ratios for the LD graphites from the OR1c and OR1d mounts. (b) $^{12}C/^{13}C$ and $^{16}O/^{18}O$ ratios measured for the HD graphites from the OR1f, OR1g and OR1i mounts. Dashed lines denote solar isotopic ratios ($^{12}C/^{13}C \sim 89$; $^{16}O/^{18}O \sim 499$). Error bars are 1 σ.

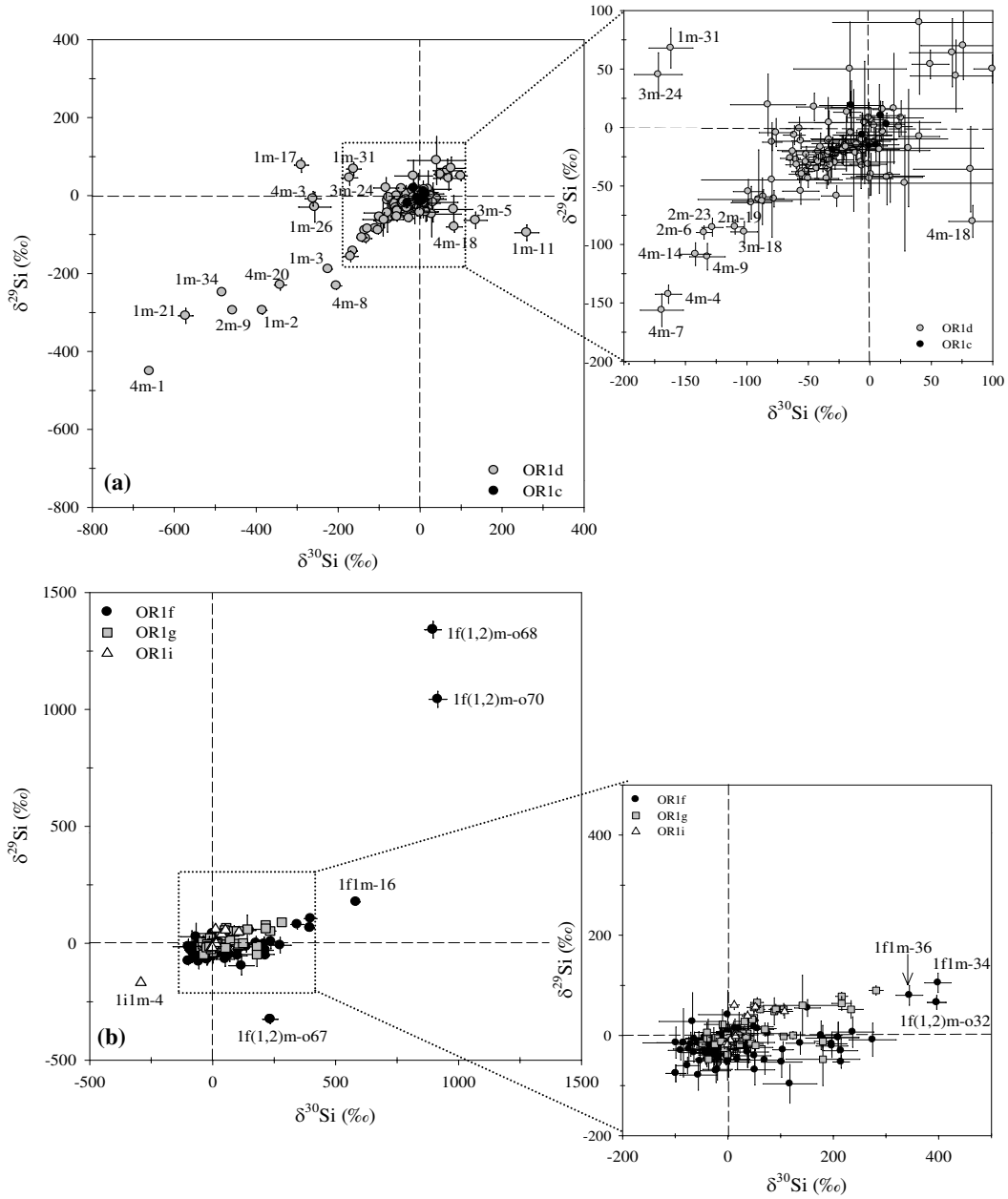

Figure 4.5 Three-isotope plots of the Si ratios measured in graphite grains from (a) LD and (b) HD fractions. The ratios are plotted as δ-values, deviations from the terrestrial ratios, in permil (‰). Error bars are 1 σ. Dashed lines indicate the solar ratios ($\delta^{29}\mathrm{Si}/^{28}\mathrm{Si} = \delta^{30}\mathrm{Si}/^{28}\mathrm{Si} = 0$).

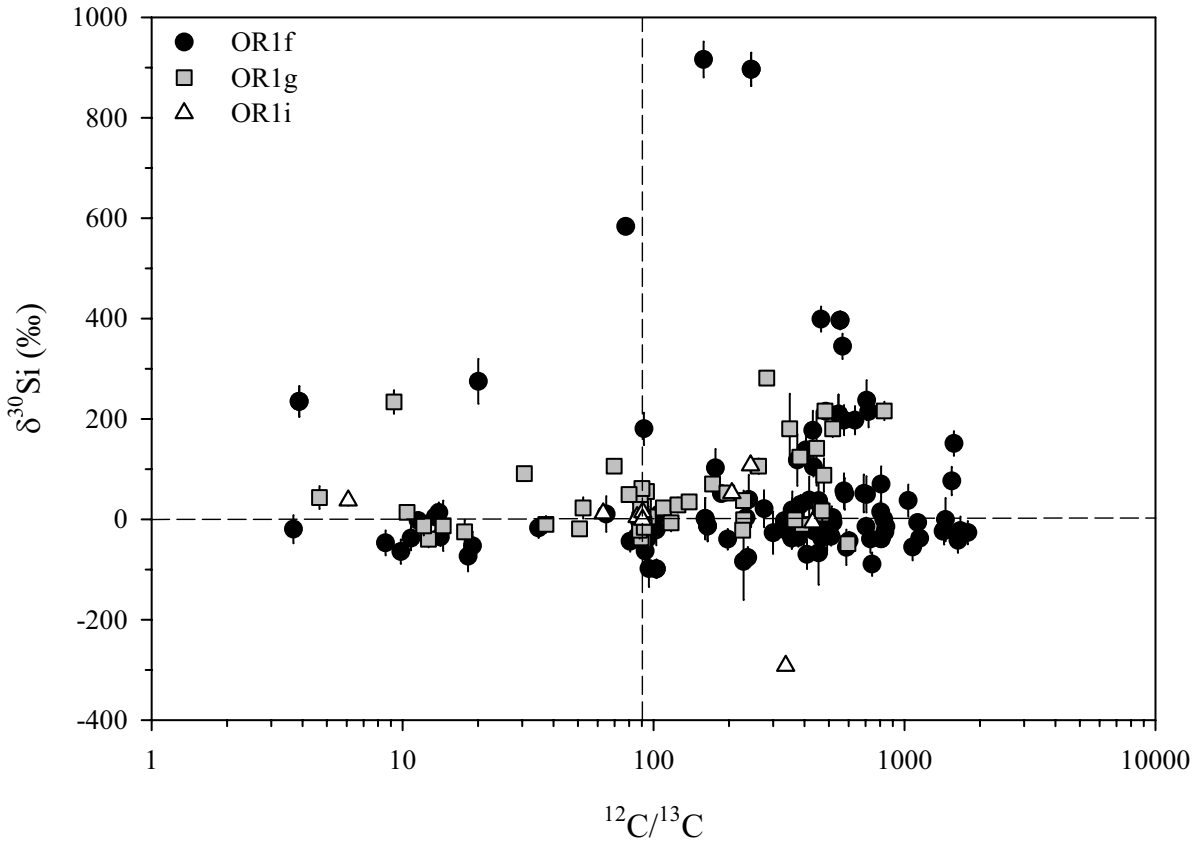

Figure 4.6 The $\delta^{30}Si/^{28}Si$ values of graphite grains from the HD fractions, OR1f, 1g and 1i, are plotted against their $^{12}C/^{13}C$ ratios. The dashed lines indicate solar values, and error bars are 1 σ.

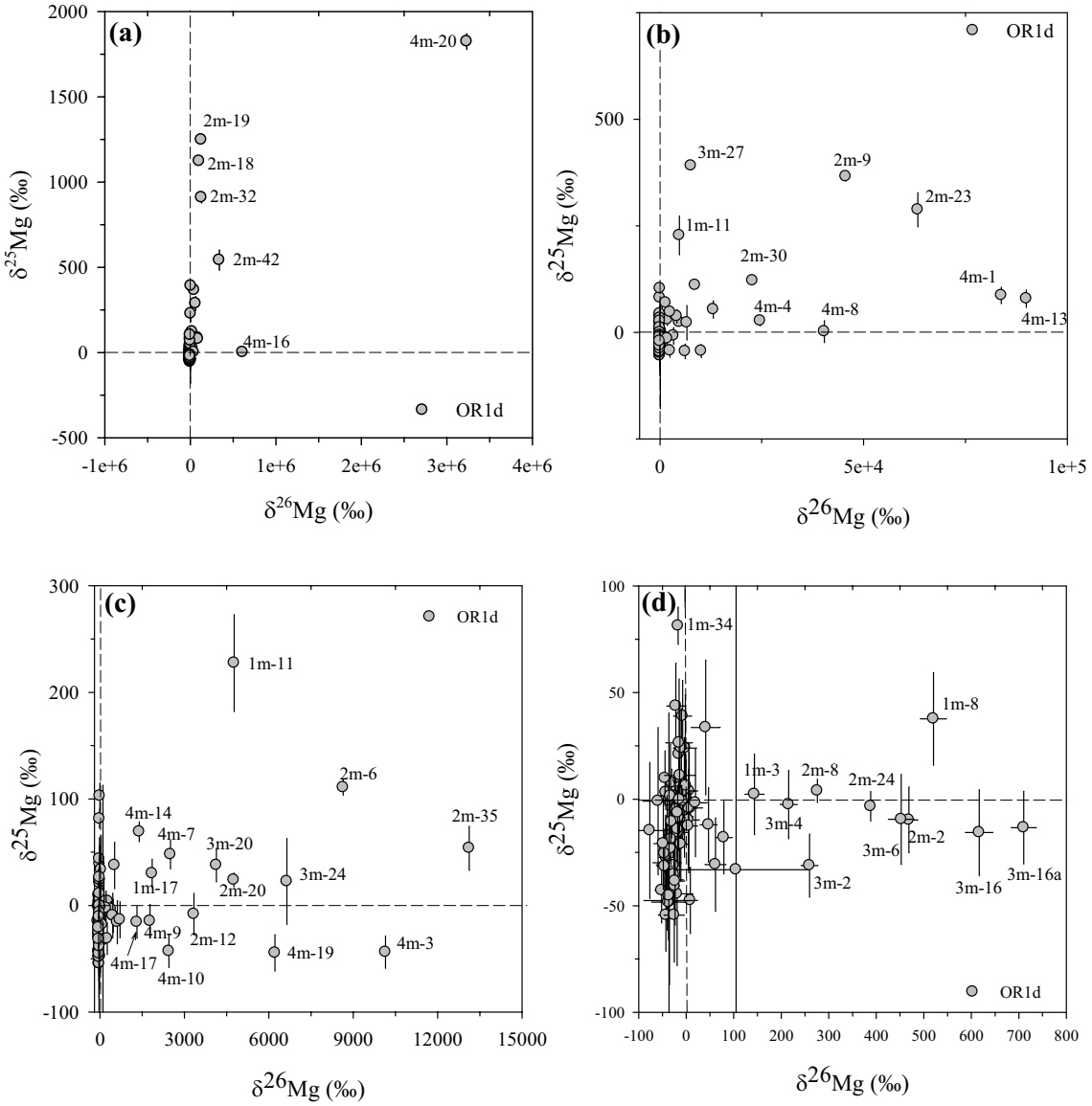

Figure 4.7 Three-isotope plots of the Mg ratios measured in graphite grains from the LD fractions. The ratios are plotted as δ-values, deviations from the terrestrial ratios in permil (‰). Error bars are 1 σ. Dashed lines indicate solar ratios (δ^{25}Mg/^{24}Mg = δ^{26}Mg/^{24}Mg = 0). Each progressive figure numbered with letters (b), (c) and (d) represents a magnified area around the origin of the previous plot.

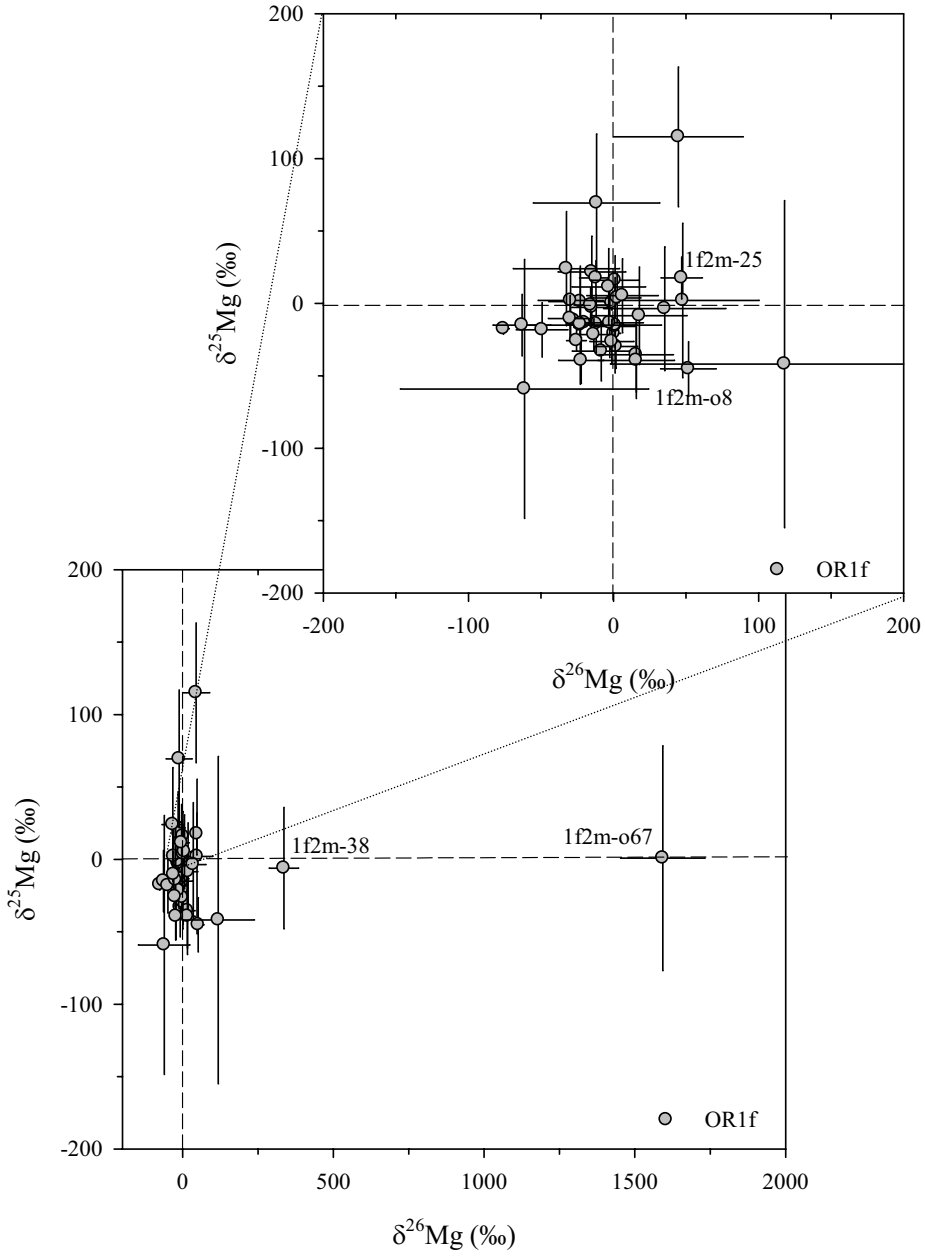

Figure 4.8 Three-isotope plots of the Mg ratios measured in graphite grains from the HD fractions. The ratios are plotted as δ-values, deviations from the terrestrial ratios in permil (‰). Error bars are 1 σ. Dashed lines indicate solar ratios ($\delta^{25}\mathrm{Mg}/^{24}\mathrm{Mg} = \delta^{26}\mathrm{Mg}/^{24}\mathrm{Mg} = 0$).

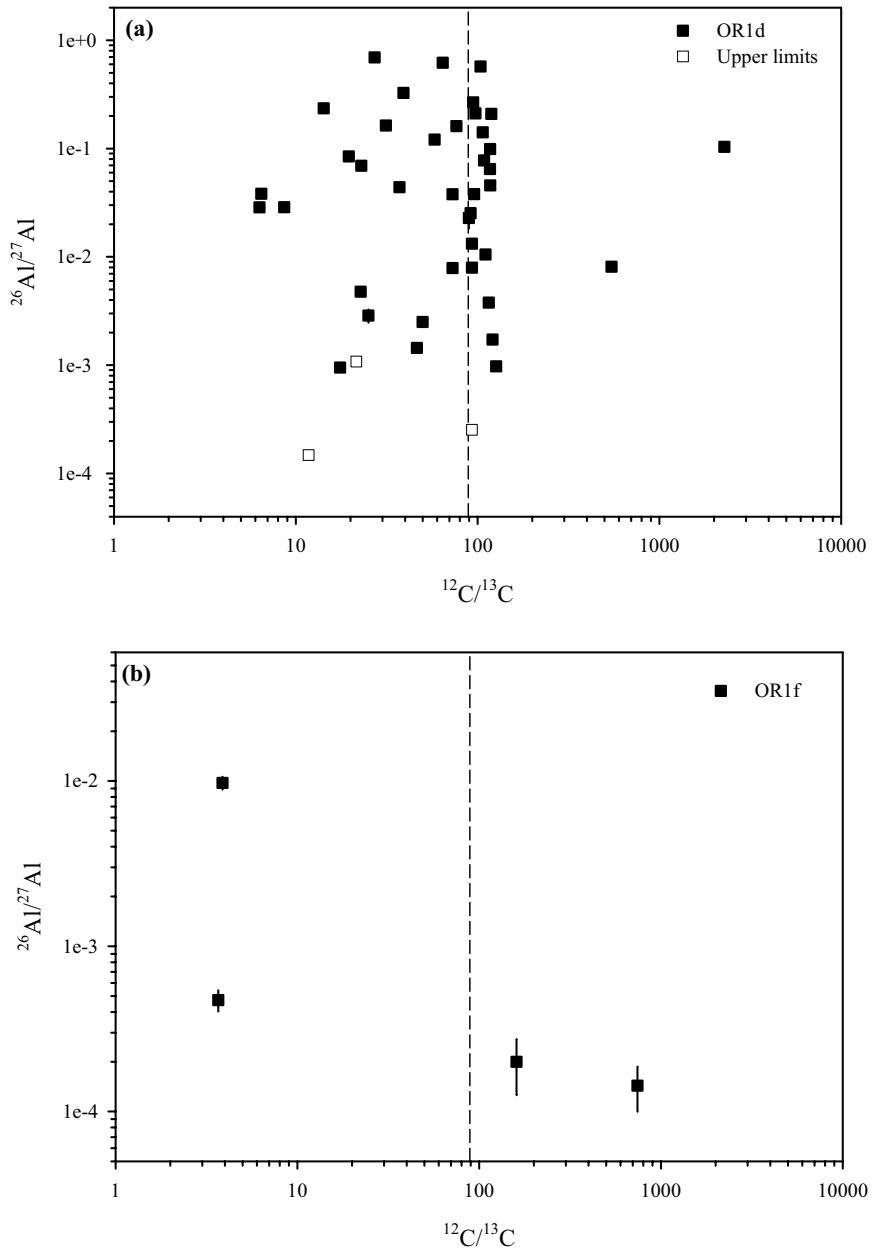

Figure 4.9 The inferred values of ^{26}Al/^{27}Al from ^{26}Mg excesses for (a) LD grains (b) HD grains. The open boxes represent upper limits for grains with large error bars. Error bars are 1 σ. The dashed lines indicate ^{12}C/^{13}C the solar ratio.

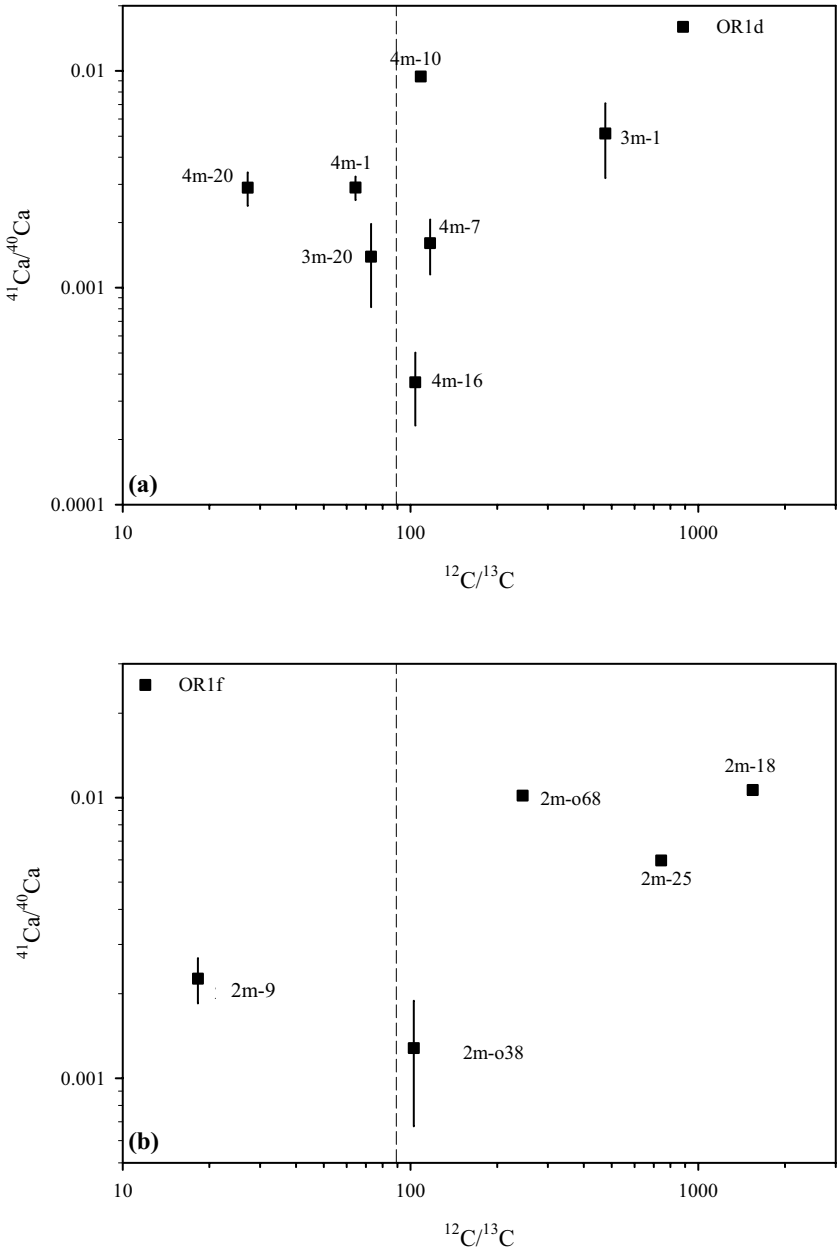

Figure 4.10 The inferred values of $^{41}Ca/^{40}Ca$ from ^{41}K excesses for (a) LD grains (b) HD grains. Error bars are 1 σ. The dashed lines indicate solar ratios.

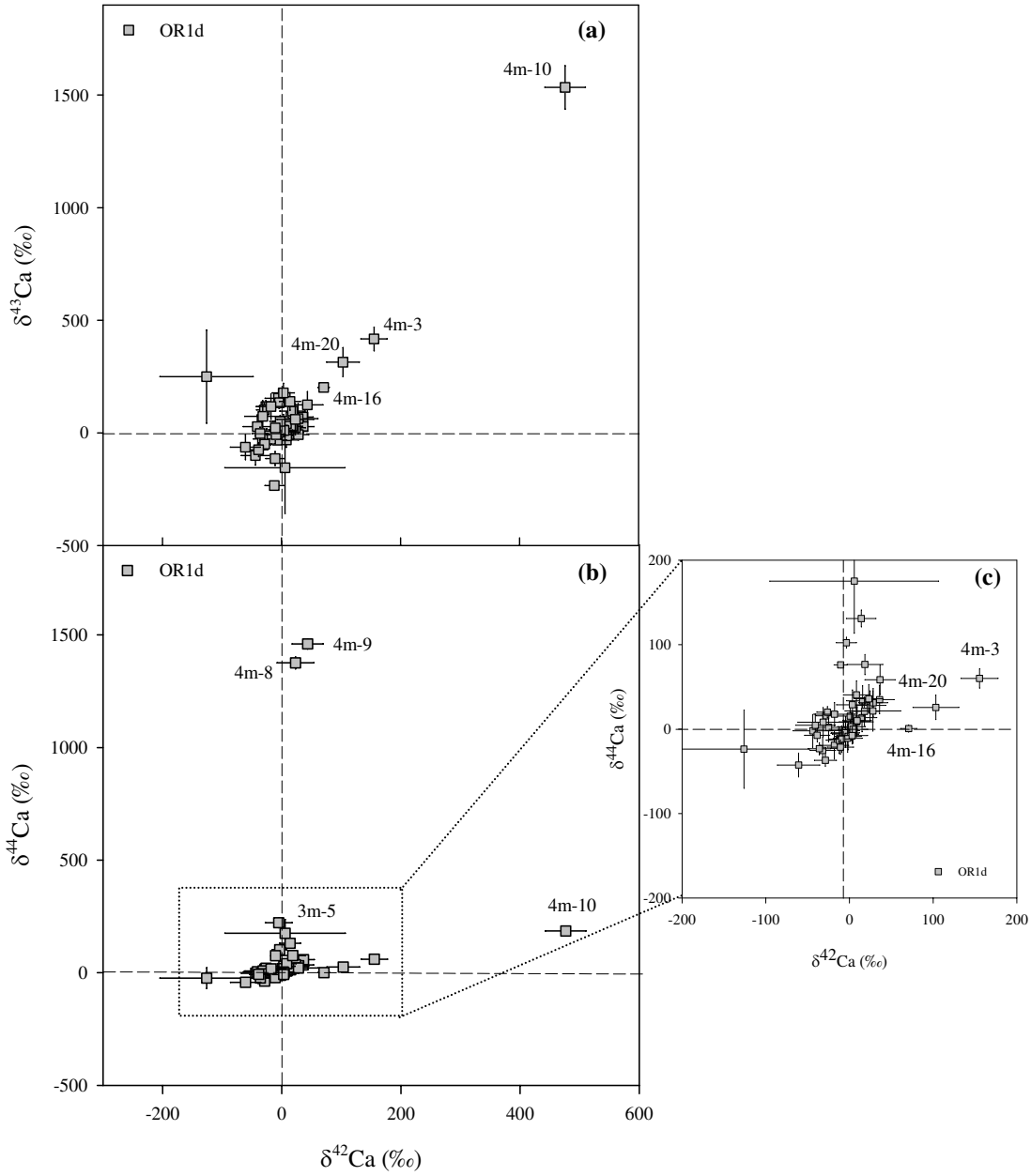

Figure 4.11 Delta-value three-isotope plots of the ^{42,43,44}Ca ratios measured in graphite grains from the LD fraction. The ratios are plotted as δ-values, deviations from the terrestrial ratios in permil (‰). Error bars are 1 σ. Dashed lines indicate solar ratios.

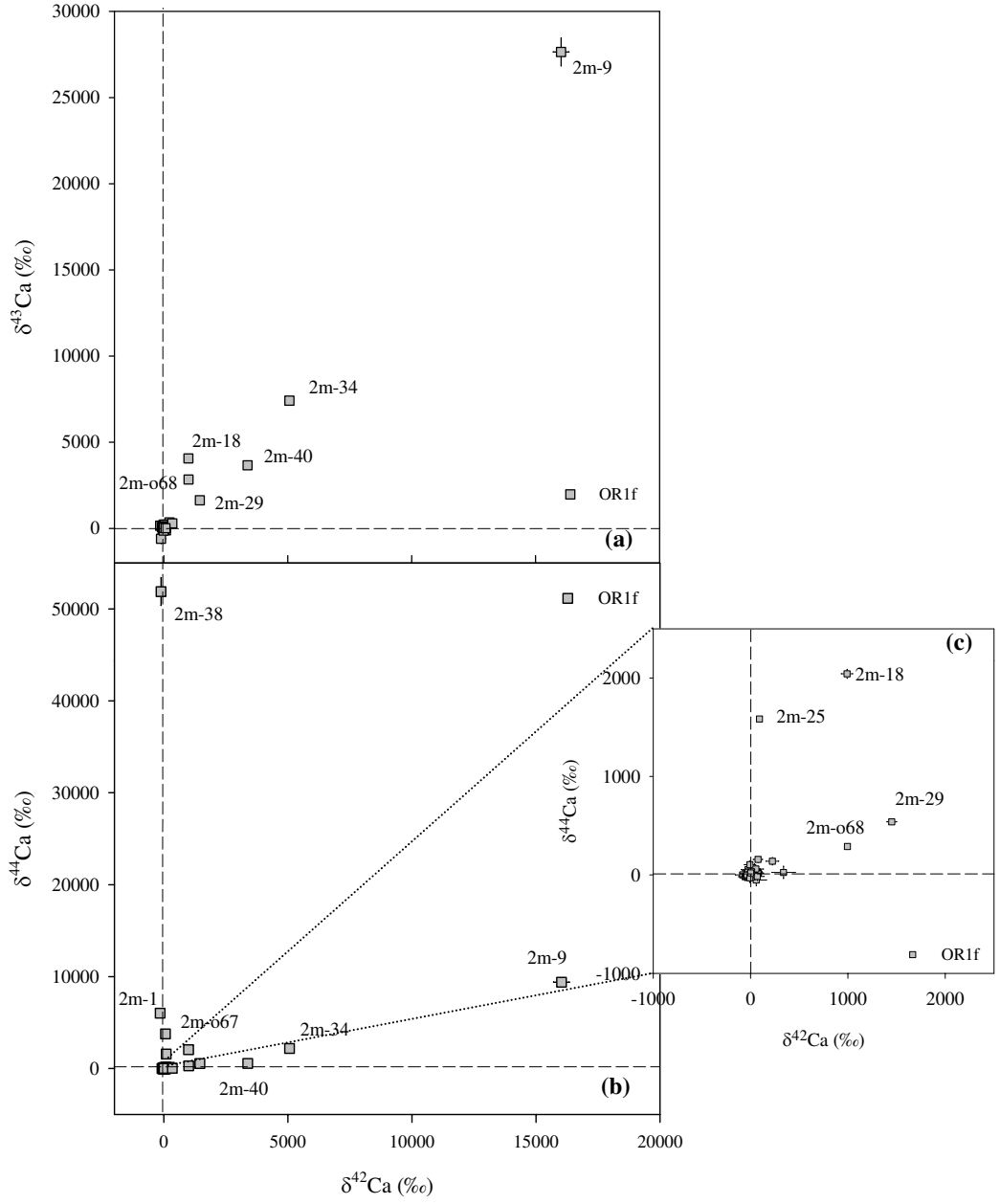

Figure 4.12 Delta-value three-isotope plots of the ^{42,43,44}Ca ratios measured in graphite grains from the HD fraction. The ratios are plotted as δ-values, deviations from the terrestrial ratios in permil (‰). Error bars are 1 σ. Dashed lines indicate solar ratios.

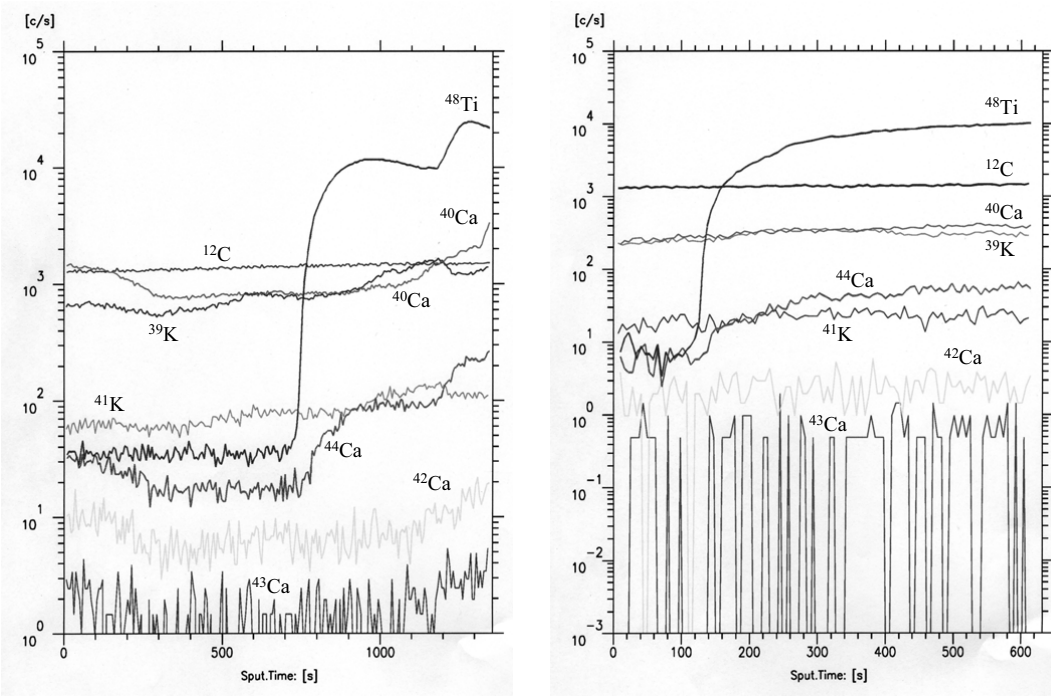

Figure 4.13 Depth profile of various ion signals during analyses indicating the correlation between the ^{44}Ca and ^{48}Ti ion signal from subgrains in the host graphites. This is evidence that ^{44}Ca excesses must originate from the decay of radiogenic ^{44}Ti.

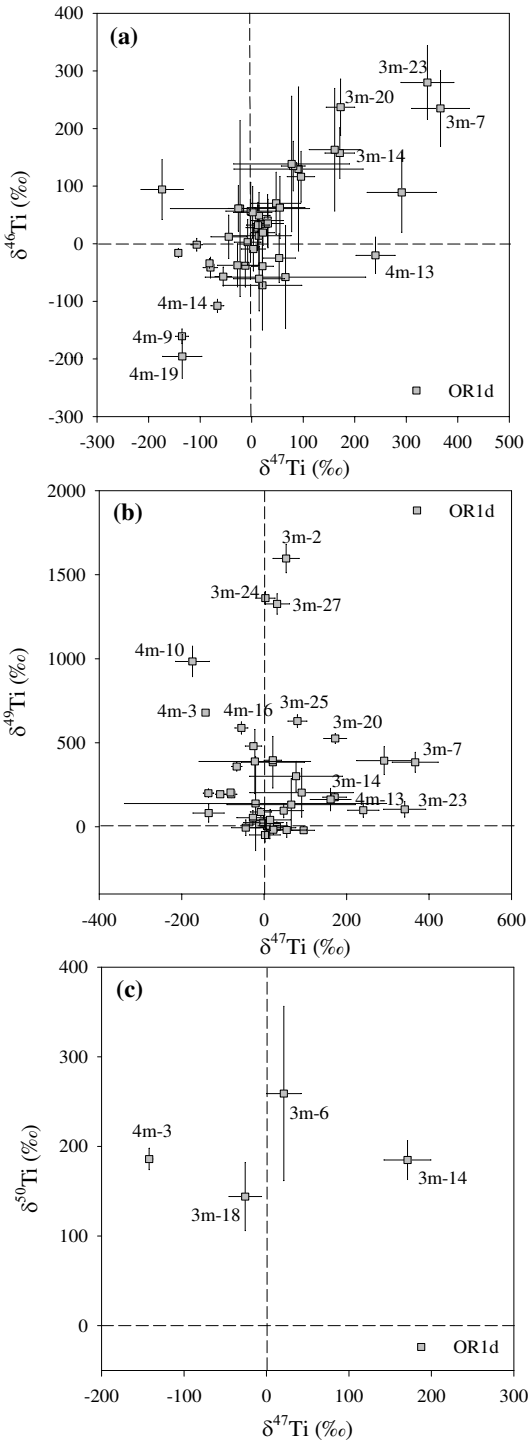

Figure 4.14 Delta-value three-isotope plots of the ^{46,47,48,49,50}Ti ratios measured in graphite grains from the LD OR1d fraction. The ratios are plotted as δ-values, deviations from the terrestrial ratios in permil (‰). Error bars are 1 σ. Dashed lines indicate solar ratios.

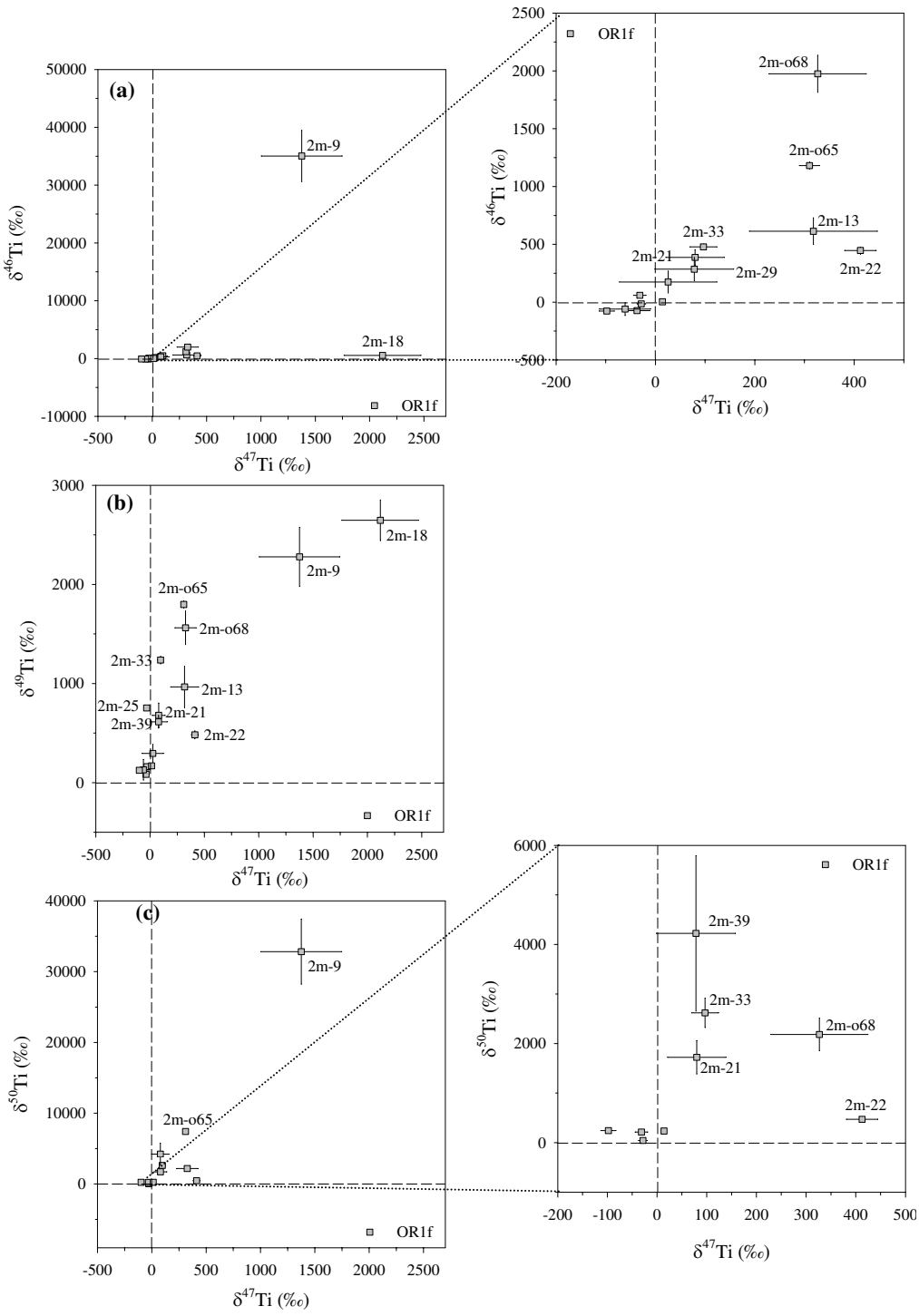

Figure 4.15 Delta-value three-isotope plots of the ^{46,47,48,49,50}Ti ratios measured in graphite grains from the HD OR1f fraction. The ratios are plotted as δ-values, deviations from the terrestrial ratios in permil (‰). Error bars are 1 σ. Dashed lines indicate solar ratios.

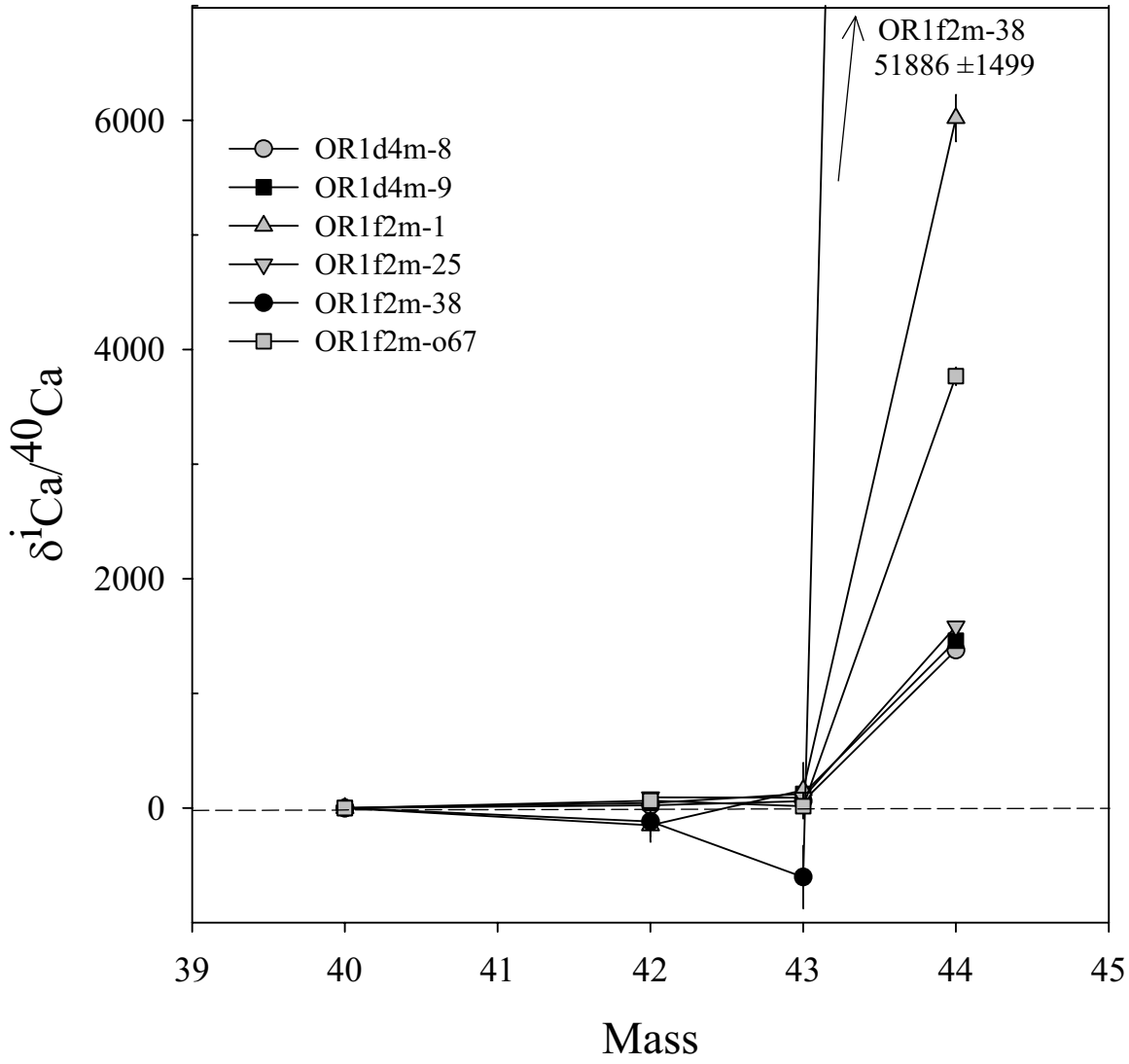

Figure 4.16 Ca isotopic pattern observed in 6 graphite grains from the LD and HD fractions. All these grains have ^{44}Ca excesses that vastly exceed the ^{42,43}Ca excesses seen in the grains, indicating the initial presence of the short-lived radionuclide, ^{44}Ti.

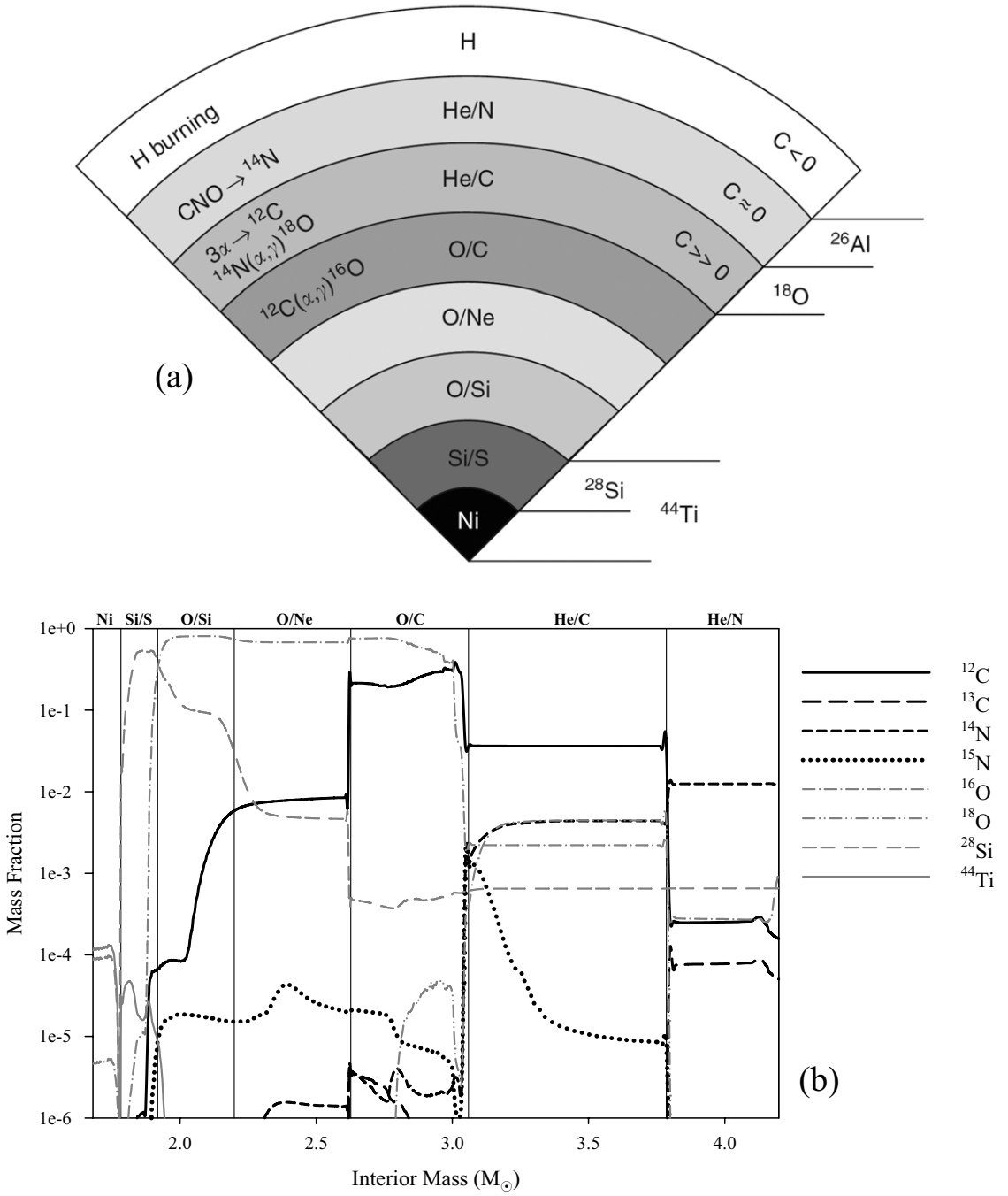

Figure 4.17 (a) Schematic diagram of the interior structure of a massive star before it explodes as a type II SN (Source: Woosley and Weaver, 1995) (b) Model abundances of ^{12,13}C, ^{14,15}N, ^{16,18}O, ^{28}Si, and ^{44}Ti isotopes in the interior of a 15 $M_{\odot}$ SN (Rauscher et al., 2002).

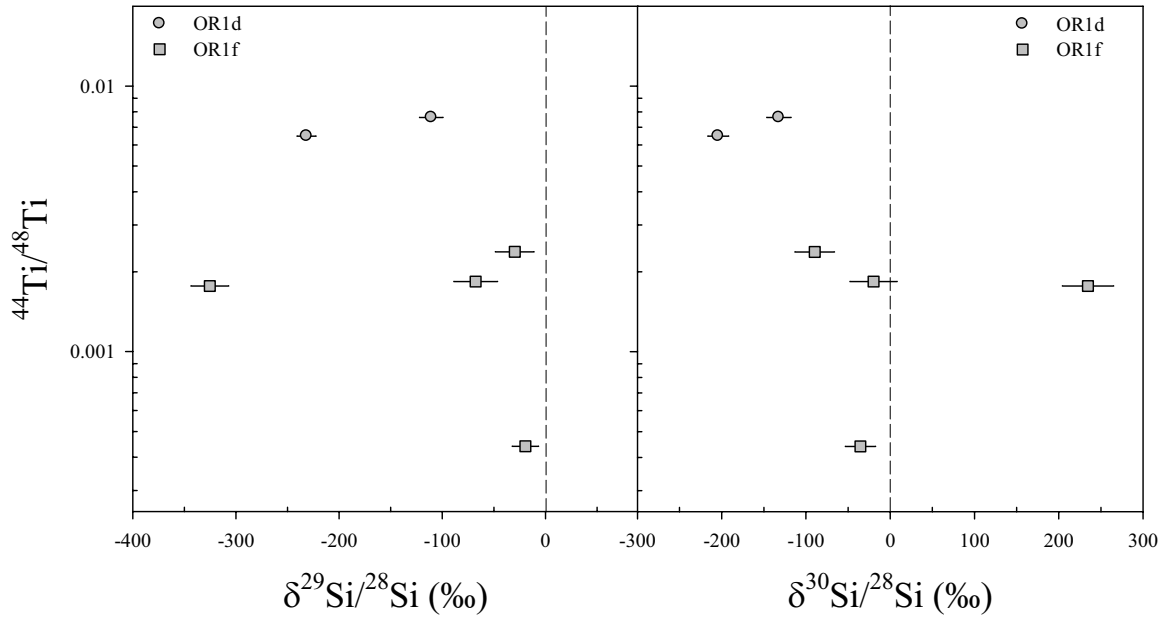

Figure 4.18 The inferred $^{44}Ti/^{48}Ti$ ratios in graphite grains from both LD and HD fractions are plotted as a function of Si isotopic ratios. Three out of the six graphites with high $^{44}Ti/^{48}Ti$ ratios do not have significant ^{28}Si excesses.

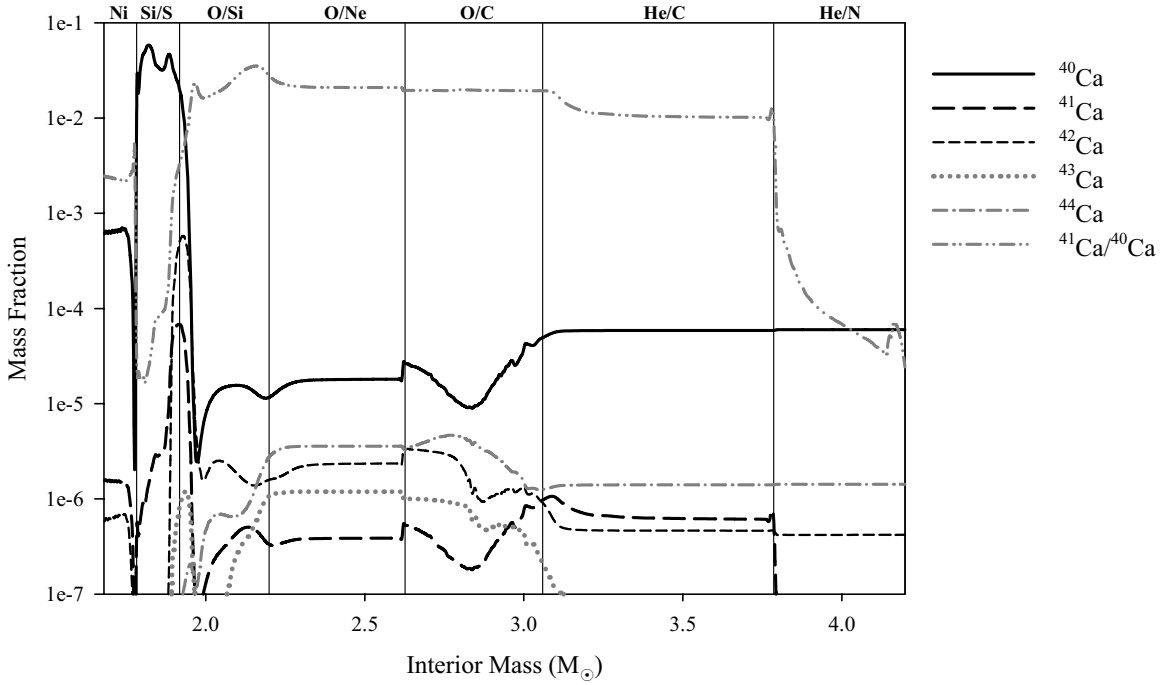

Figure 4.19 Model abundances of ^{40,41,42,43,44}Ca and the ^{41}Ca/^{40}Ca ratio in the interior of a 15 $M_{\odot}$ SN (Rauscher et al., 2002)

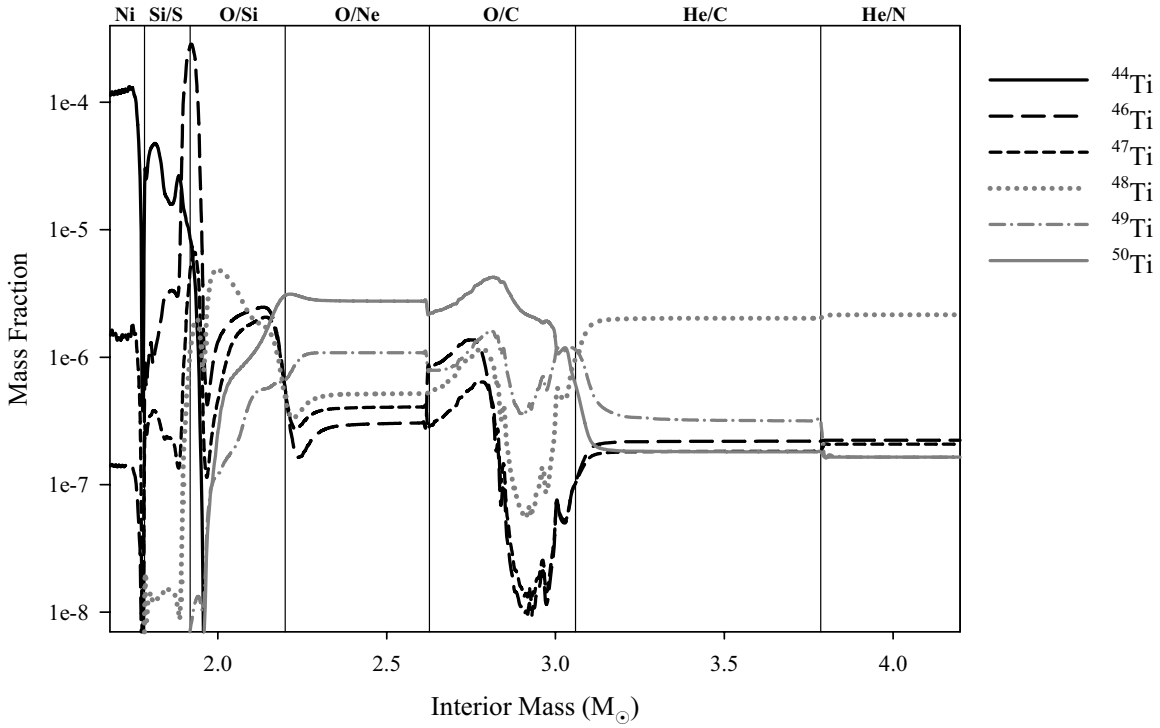

Figure 4.20 Model abundances of ^{44,46,47,48,49,50}Ti isotopes in the interior of a 15 $M_{\odot}$ SN (Rauscher et al., 2002)

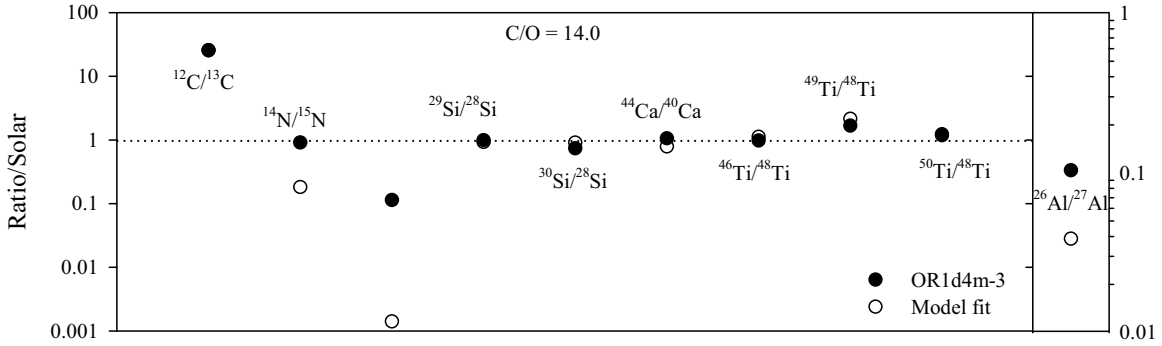

Figure 4.21 Isotopic ratio comparisons between the measured grain OR1d4m-3 with a high $^{12}C/^{13}C$ ratio and that predicted by mixing different layers of a 15 $M_{\odot}$ SN (Rauscher et al. 2002). All the ratios are normalized to solar values except the $^{26}Al/^{27}Al$ ratio. The C/O ratio of the resultant mixture is also indicated.

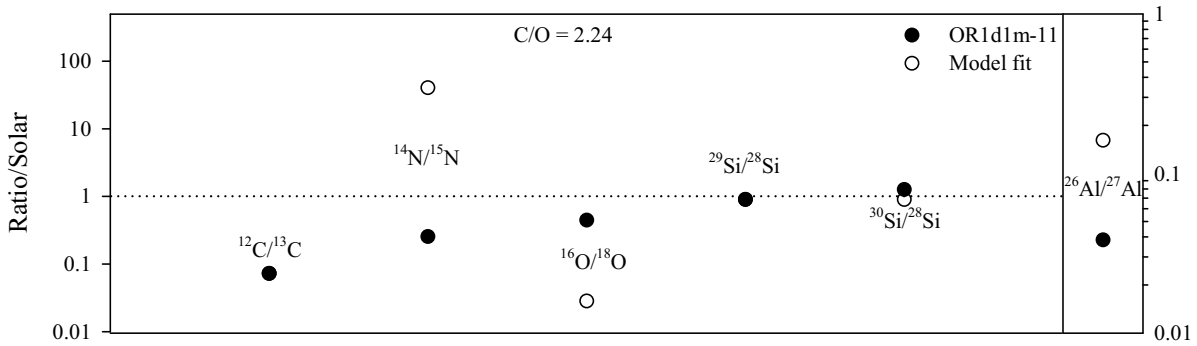

Figure 4.22 Isotopic ratio comparisons between measured grain OR1d1m-11 with a low $^{12}C/^{13}C$ ratio and that predicted by mixing different layers of a 15 $M_{\odot}$ SN (Rauscher et al. 2002). The mixing calculation was constrained to produce the low $^{12}C/^{13}C$ ratio measured in the grain. All the ratios are normalized to solar values except the $^{26}Al/^{27}Al$ ratio.

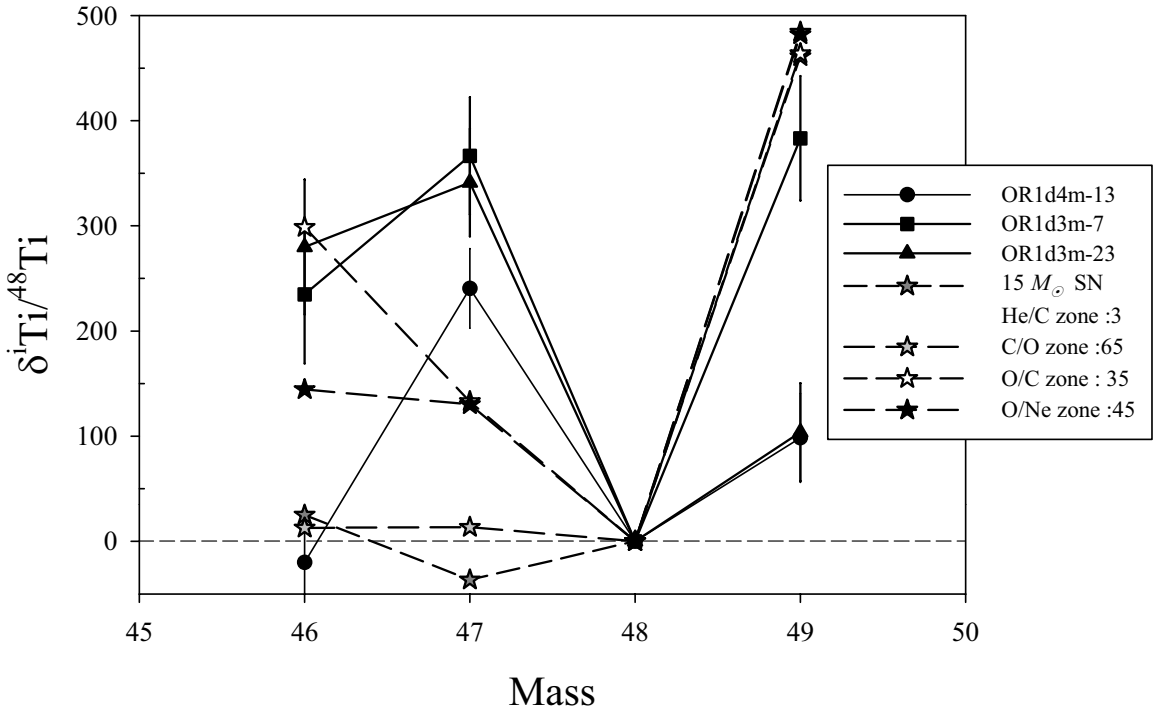

Figure 4.23 Ti isotopic pattern indicating a ^{47}Ti anomaly found in a LD graphite grain. The ^{49}Ti excess can be explained by admixture of material from O-rich zones to the He/C zone, but the source of the ^{47}Ti excess is unknown (Woosley and Weaver, 1995).

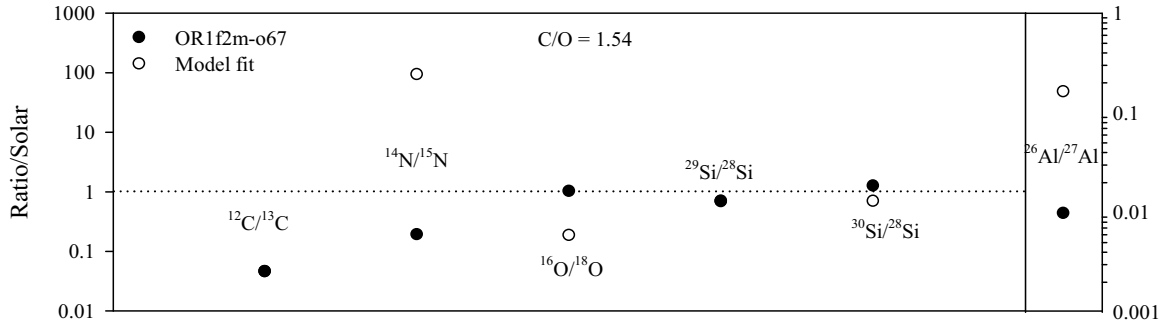

Figure 4.24 Isotopic ratio comparisons between measured grain, OR1f(1,2)m-o67, with a low $^{12}C/^{13}C$ ratio and that predicted by mixing different layers of a 15 $M_{\odot}$ SN (Rauscher et al. 2002). The mixing calculation is constrained to produce the low $^{12}C/^{13}C$ ratio measured in the grain. All the ratios are normalized to solar values except the $^{26}Al/^{27}Al$ ratio. The C/O ratios of the resultant mixture is also indicated.

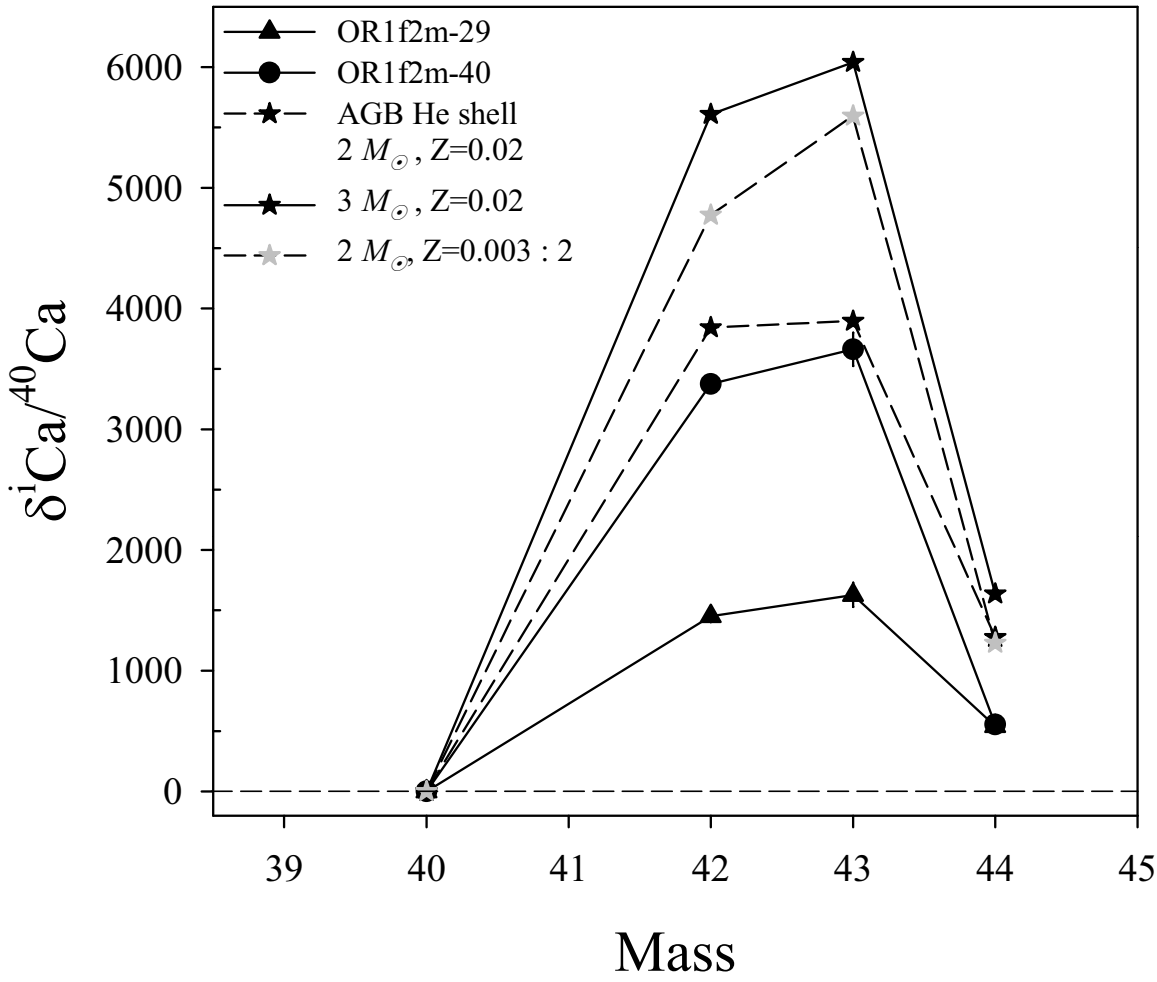

Figure 4.25 Ca isotopic pattern for grains, OR1f2m-29 and OR1f2m-40, compared to those predicted for the He shell of 2 $M_\odot$ (Z = 0.003 – 0.02) and 3 $M_\odot$ (Z = 0.02) AGB stars (Gallino et al. 1998). The predicted anomalies are scaled down by the factors indicated.

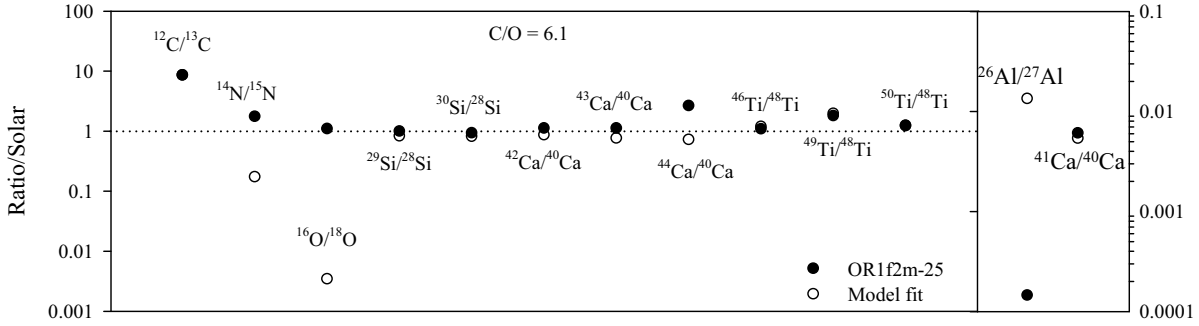

Figure 4.26 Isotopic ratio comparisons between the measured grain (OR1f2m-25) with a high $^{12}C/^{13}C$ ratio and that predicted by mixing different layers of a 15 $M_{\odot}$ SN (Rauscher et al. 2002). All the ratios are normalized to solar values except the $^{26}Al/^{27}Al$ and $^{41}Ca/^{40}Ca$ ratios. The C/O ratio of the resultant mixture is also indicated.

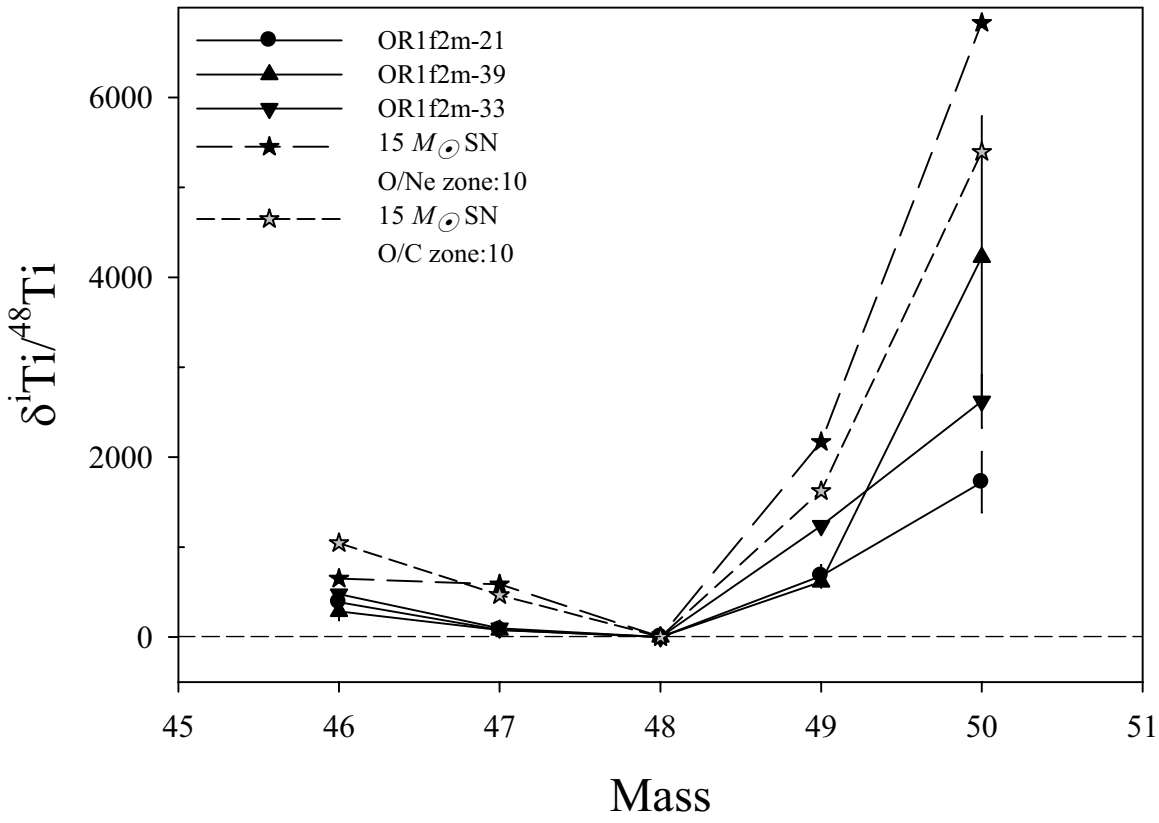

Figure 4.27 The Ti isotopic patterns of 3 ^{12}C-enriched HD grains can be matched by the patterns seen in the O/C and O/Ne zones of a type II SN (Woosley and Weaver, 1995). The anomalies in the zones are reduced by appropriate factors as indicated.

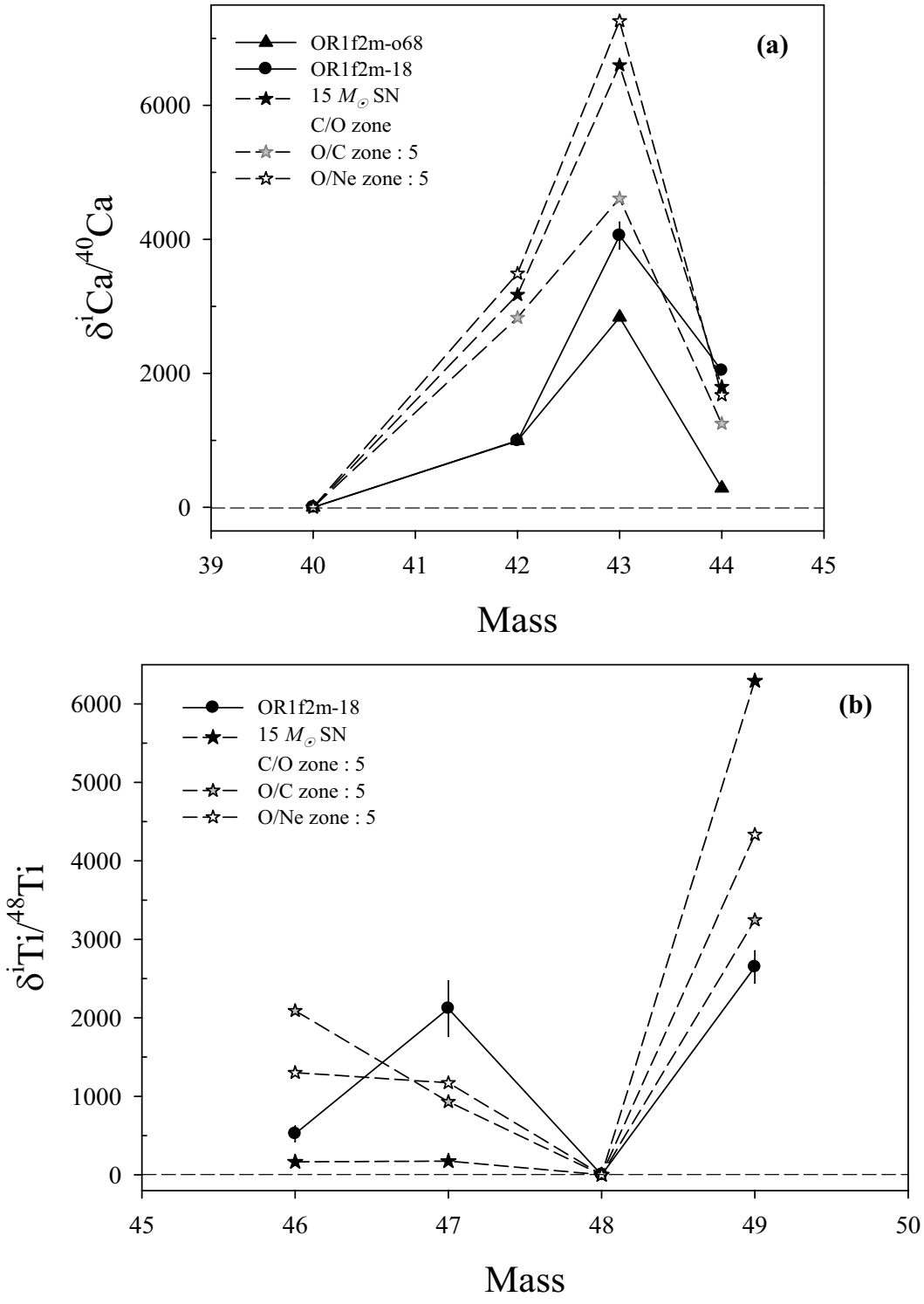

Figure 4.28 Ca and Ti isotopic patterns of HD grains can be obtained by mixing C/O[1] and O-rich zones to the He/C zone (Woosley and Weaver, 1995). Grain OR1f2m-18 has a large ^{47}Ti excess whose source is unknown.

Table 4.1: Different density fractions of Orgueil and the grain mounts analyzed

Density fraction	Density type	Density (g cm^{-3})	Mounts analyzed	Number of grains analyzed
OR1b	LD	1.59 –1.67	OR1b1m	22
OR1c	LD	1.67 – 1.75	OR1c1m	7
OR1d	LD	1.75 – 1.92	OR1d(1,2,3,4)m	128
OR1f	HD	2.02 – 2.04	OR1df(1,2)m	109
OR1g	HD	2.04 – 2.12	OR1g1m	52
OR1h	HD	2.12 – 2.16	OR1h1m	18
OR1i	HD	2.16 – 2.30	OR1i1m	9

NOTE: LD = low-density graphite grains; HD = high-density graphite grains

Table 4.2 A list of measurement phases, type of primary beam used to collect the secondary ions detected in parallel (phases 1 – 3) and combined mode (phases 4 and 5), and the isotopic ratios measured for the different density mounts of graphite grains from Orgueil

Measurement phase	Primary beam	Secondary ions detected	Isotopic ratios measured	Mounts measured
1a	Cs^+	$^{12}C^-$, $^{13}C^-$, $^{16}O^-$, $^{18}O^-$	$^{12}C/^{13}C$, $^{16}O/^{18}O$	OR1(b,c,d,f,g,h,i)1m
1b	Cs^+	$^{12}C^-$, $^{13}C^-$, $^{12}C^{14}N^-$, $^{12}C^{15}N^-$	$^{12}C/^{13}C$, $^{14}N/^{15}N$	OR1d2m, OR1f2m
1c	Cs^+	$^{12}C^-$, $^{13}C^-$, $^{28}Si^-$, $^{29}Si^-$, $^{30}Si^-$	$^{12}C/^{13}C$, $^{29}Si/^{28}Si$, $^{30}Si/^{28}Si$	OR1d(3,4)m
2a	Cs^+	$^{12}C^{14}N^-$, $^{12}C^{15}N^-$, $^{28}Si^-$, $^{29}Si^-$, $^{30}Si^-$	$^{14}N/^{15}N$, $^{29}Si/^{28}Si$, $^{30}Si/^{28}Si$	OR1(c,d,f,g,i)1m
2b	Cs^+	$^{16}O^-$, $^{18}O^-$, $^{28}Si^-$, $^{29}Si^-$, $^{30}Si^-$	$^{16}O/^{18}O$, $^{29}Si/^{28}Si$, $^{30}Si/^{28}Si$	OR1d2m, OR1f2m
2c	Cs^+	$^{12}C^{14}N^-$, $^{12}C^{15}N^-$, $^{16}O^-$, $^{18}O^-$	$^{14}N/^{15}N$, $^{16}O/^{18}O$	OR1d(3,4)m
3	O^-	$^{12}C^+$, $^{24}Mg^+$, $^{25}Mg^+$, $^{26}Mg^+$, $^{27}Al^+$	$^{25}Mg/^{24}Mg$, $^{26}Mg/^{24}Mg$	OR1(d,f)1m; OR1d(2,3,4)m; OR1f2m
4	O^-	$^{39}K^+$, $^{41}K^+$, $^{43}Ca^+$ $^{12}C^+$, $^{40}Ca^+$, $^{42}Ca^+$, $^{44}Ca^+$, $^{48}Ti^+$	$^{41}K/^{39}K$, $^{42}Ca/^{40}Ca$, $^{43}Ca/^{40}Ca$, $^{44}Ca/^{40}Ca$	OR1d(2,3,4)m; OR1f2m
5	O^-	$^{46}Ti^+$, $^{48}Ti^+$, $^{50}Ti^+$ $^{47}Ti^+$, $^{49}Ti^+$, $^{51}V^+$ $^{12}C^+$, $^{40}Ca^+$, $^{48}Ti^+$, $^{50}Ti^+$, $^{52}Cr^+$	$^{46}Ti/^{48}Ti$, $^{47}Ti/^{48}Ti$, $^{49}Ti/^{48}Ti$, $^{50}Ti/^{48}Ti$	OR1d(2,3,4)m; OR1f2m

Table 4.3: C, N, O, and Si isotopic ratios of graphite grains from Orgueil with large N, O, and Si anomalies discussed in Sections 4.3.1 and Figures 4.3-4.5. (Errors are 1σ)

Grain	Type	$^{12}C/^{13}C$	$^{14}N/^{15}N$	$^{16}O/^{18}O$	$\delta^{29}Si/^{28}Si$ (‰)	$\delta^{30}Si/^{28}Si$ (‰)
Solar ratio		89	272	499	0	0
OR1c1m-6	LD	158.1 ± 2.3	135.2 ± 2.3	127.3 ± 2.2	10 ± 12	9 ± 17
OR1c1m-7	LD	78.5 ± 1.1	272.8 ± 7.3	391.4 ± 7	– 7 ± 19	– 6 ± 24
OR1d1m-2	LD	60 ± 0.5	139.7 ± 1.6	97 ± 3.6	– 295 ± 10	– 385 ± 11
OR1d1m-3	LD	25.1 ± 0.2	139.7 ± 1.6	118.5 ± 4.4	– 189 ± 8	– 224 ± 9
OR1d1m-8	LD	72.9 ± 0.6	237.2 ± 3	196.7 ± 8.2	54 ± 12	49 ± 15
OR1d1m-11	LD	6.5 ± 0	69.3 ± 1.1	222.1 ± 10.6	– 95 ± 20	260 ± 29
OR1d1m-17	LD	117.5 ± 1.1	54.5 ± 0.8	86.8 ± 4.8	78 ± 18	– 290 ± 17
OR1d1m-20	LD	446 ± 4.9	74.7 ± 1.4	169.5 ± 7.4	– 62 ± 42	– 90 ± 49
OR1d1m-21	LD	879.8 ± 9.7	154.8 ± 2.2	97.8 ± 4	– 309 ± 19	– 572 ± 18
OR1d1m-22	LD	89.8 ± 0.7	174.8 ± 2.5	507.4 ± 23.7	– 18 ± 50	32 ± 61
OR1d1m-24	LD	150.1 ± 1.2		17.4 ± 0.6		
OR1d1m-26	LD	508.8 ± 5.3	159.8 ± 3.1	408.9 ± 14.7	– 30 ± 39	– 257 ± 39
OR1d1m-30	LD	9.7 ± 0.1	284.4 ± 6	364 ± 18	– 28 ± 15	– 31 ± 18
OR1d1m-31	LD	123 ± 1	172.8 ± 2.1	189.4 ± 7.8	68 ± 17	– 162 ± 18
OR1d1m-34	LD	169.8 ± 1.7	158.8 ± 2	16.2 ± 0.2	– 249 ± 7	– 483 ± 7
OR1d2m-2	LD	546.1 ± 7.9	234.2 ± 3.5	294.9 ± 3.7	– 7 ± 8	– 61 ± 9
OR1d2m-6	LD	117.4 ± 1.7	247.1 ± 2.2	170.2 ± 1.9	– 90 ± 6	– 135 ± 6
OR1d2m-9	LD	118.9 ± 1.7	203.4 ± 1.9	68 ± 0.7	– 295 ± 5	– 457 ± 4
OR1d2m-12	LD	93.2 ± 1.3	208.3 ± 2.3	351.7 ± 4.1	– 13 ± 7	– 79 ± 8
OR1d2m-18	LD	76.5 ± 1.1	239.2 ± 2.1	378.7 ± 4.2	– 37 ± 6	– 52 ± 7
OR1d2m-19	LD	39.1 ± 0.5	116.7 ± 1.1	59.2 ± 0.6	– 85 ± 6	– 110 ± 7
OR1d2m-20	LD	37.2 ± 0.5	214.1 ± 3.3	225.3 ± 2.6	– 61 ± 7	– 78 ± 8
OR1d2m-23	LD	31.3 ± 0.4	66.4 ± 0.9	33.3 ± 0.4	– 85 ± 8	– 128 ± 9
OR1d2m-24	LD	121.1 ± 1.7	234.7 ± 2.3	417.4 ± 4.8	– 13 ± 7	– 22 ± 8
OR1d2m-30	LD	94.5 ± 1.3	195.1 ± 1.9	374.2 ± 4.3	– 59 ± 6	– 86 ± 7
OR1d2m-35	LD	6.3 ± 0.1	246.7 ± 2.8	406.4 ± 5	– 29 ± 7	– 42 ± 8
OR1d2m-42	LD	97.4 ± 1.4	194.1 ± 2.1	59.4 ± 0.7	– 38 ± 7	– 55 ± 8
OR1d3m-2	LD	115.4 ± 0.7	182.3 ± 1.8	435.2 ± 7.9	4 ± 10	-33 ± 12
OR1d3m-5	LD	2477.9 ± 16	238.7 ± 4	535.6 ± 17.5	– 64 ± 21	136 ± 28
OR1d3m-6	LD	126.7 ± 0.7	218.3 ± 1.6	436.6 ± 7.9	– 9 ± 3	– 6 ± 3
OR1d3m-14	LD	92 ± 0.6	272.4 ± 1.4	527.8 ± 11.5	– 45 ± 49	– 79 ± 57
OR1d3m-16	LD	49.9 ± 0.3	256.3 ± 4.3	142 ± 3.1	– 22 ± 6	– 11 ± 8
OR1d3m-17	LD	91.7 ± 0.5	229.3 ± 1.8	516.1 ± 9.2	– 55 ± 10	– 99 ± 12

Table 4.3 – continued from previous page

Grain	Type	$^{12}C/^{13}C$	$^{14}N/^{15}N$	$^{16}O/^{18}O$	$\delta^{29}Si/^{28}Si$ (‰)	$\delta^{30}Si/^{28}Si$ (‰)
OR1d3m-18	LD	75.9 ± 0.4	217.5 ± 1.8	286.4 ± 5.4	– 89 ± 9	– 102 ± 11
OR1d3m-20	LD	72.9 ± 0.4	227.6 ± 1.7	298.6 ± 5	– 40 ± 4	– 55 ± 5
OR1d3m-24	LD	93.1 ± 0.5	142.3 ± 1.1	299.2 ± 5.3	45 ± 19	– 172 ± 19
OR1d3m-27	LD	95.8 ± 0.6	214.3 ± 1.3	328.2 ± 5.4	– 4 ± 12	– 76 ± 14
OR1d4m-1	LD	64.4 ± 0.6	72.7 ± 0.6	144.4 ± 2.1	– 451 ± 5	– 660 ± 5
OR1d4m-3	LD	2279.1 ± 22.9	248.9 ± 4.3	56.6 ± 0.7	– 8 ± 19	– 261 ± 20
OR1d4m-4	LD	58.1 ± 0.6	197.1 ± 1.3	197.1 ± 2.2	– 143 ± 8	– 164 ± 11
OR1d4m-7	LD	117 ± 1.1	245.5 ± 2.8	295.4 ± 4.5	– 156 ± 14	– 169 ± 18
OR1d4m-8	LD	14.3 ± 0.1	248.1 ± 2.9	324.7 ± 5.5	– 232 ± 9	– 204 ± 12
OR1d4m-9	LD	110.6 ± 1.1	259.3 ± 2.5	444.4 ± 6.4	– 111 ± 11	– 132 ± 15
OR1d4m-10	LD	108.6 ± 1.1	244.8 ± 4	145.2 ± 2.3	18 ± 12	– 45 ± 15
OR1d4m-13	LD	106.7 ± 1	161.3 ± 1.6	149 ± 1.6	– 54 ± 11	– 56 ± 15
OR1d4m-14	LD	22.9 ± 0.2	168.4 ± 1.3	250.8 ± 3.6	– 108 ± 10	– 142 ± 13
OR1d4m-16	LD	103.9 ± 1	182.6 ± 1.4	113.1 ± 1.2	– 59 ± 9	– 27 ± 12
OR1d4m-18	LD	89.6 ± 0.9	274 ± 2.8	535.3 ± 11.6	– 80 ± 14	84 ± 19
OR1d4m-20	LD	27.2 ± 0.3	165.5 ± 2.4	29.8 ± 0.3	– 230 ± 13	– 341 ± 15
OR1f1m-5	HD	13.5 ± 0.1	570.6 ± 15.1	518.8 ± 11.2	– 25 ± 22	4 ± 25
OR1f1m-o67	HD	3.9 ± 0	50.7 ± 0.8	499.9 ± 11.3	– 325 ± 18	235 ± 30
OR1f1m-o68	HD	245.1 ± 2.5	87 ± 1.3	511.8 ± 9.6	1341 ± 35	896 ± 33
OR1f1m-70	HD	158.4 ± 1.6	149.5 ± 2.4	505.9 ± 17.6	1043 ± 34	916 ± 36
OR1f2m-25	HD	743.1 ± 2.2	463.9 ± 13	530.9 ± 10.5	– 30 ± 19	– 90 ± 23
OR1f2m-29	HD	9.8 ± 0	412 ± 6.1	524.7 ± 9.1	– 34 ± 19	– 65 ± 25
OR1f2m-o67	HD	3.9 ± 0	50.7 ± 0.8	499.9 ± 11.3	– 325 ± 18	235 ± 30
OR1f2m-o68	HD	245.1 ± 2.5	87 ± 1.3	511.8 ± 9.6	1341 ± 35	896 ± 33
OR1g1m-33	HD	14.5 ± 0	1437 ± 29.9	522.8 ± 58.4	– 14 ± 42	– 13 ± 50
OR1i1m-4	HD	336.2 ± 1.6	475.3 ± 10.2	408.9 ± 9	– 168 ± 10	– 292 ± 10
OR1i1m-6	HD	6.1 ± 0	358.7 ± 8.2	484.6 ± 6.8	39 ± 10	37 ± 11
OR1i1m-8	HD	243.6 ± 1.4	374.2 ± 16	489.5 ± 5.5	48 ± 13	107 ± 16

Table 4.4: Mg isotopic compositions and the inferred $^{26}Al/^{27}Al$ ratios for LD and HD grains from Orgueil (Errors are 1σ and * denote upper limits)

Grain Label	Type	$\delta^{25}Mg/^{24}Mg$ (‰)	$\delta^{26}Mg/^{24}Mg$ (‰)	$^{26}Al/^{27}Al$
OR1d1m-17	LD	30 ± 13	1853 ± 39	0.04569 ± 0.00096
OR1d1m-11	LD	227 ± 45	4769 ± 129	0.03831 ± 0.00104
OR1d1m-8	LD	38 ± 22	520 ± 27	0.00789 ± 0.00041
OR1d1m-3	LD	2 ± 19	144 ± 20	0.00287 ± 0.0004
OR1d1m-18	LD	– 12 ± 17	47 ± 18	0.00035 ± *
OR1d2m-19	LD	1247 ± 16	130001 ± 458	0.32589 ± 0.00115
OR1d2m-30	LD	121 ± 7	22724 ± 76	0.26661 ± 0.0009
OR1d2m-42	LD	542 ± 59	340343 ± 4586	0.21076 ± 0.00284
OR1d2m-9	LD	366 ± 10	45637 ± 169	0.20882 ± 0.00077
OR1d2m-23	LD	288 ± 40	63341 ± 776	0.16347 ± 0.002
OR1d2m-18	LD	1123 ± 21	104527 ± 479	0.16117 ± 0.00074
OR1d2m-6	LD	111 ± 7	8642 ± 35	0.0988 ± 0.0004
OR1d2m-32	LD	909 ± 32	131638 ± 940	0.08453 ± 0.0006
OR1d2m-20	LD	24 ± 6	4760 ± 22	0.044 ± 0.0002
OR1d2m-35	LD	54 ± 21	13125 ± 128	0.02866 ± 0.00028
OR1d2m-2	LD	– 10 ± 15	469 ± 19	0.00811 ± 0.00033
OR1d2m-12	LD	– 8 ± 20	3342 ± 51	0.00794 ± 0.00012
OR1d2m-8	LD	4 ± 6	276 ± 6	0.00476 ± 0.0001
OR1d2m-24	LD	-3 ± 7	388 ± 8	0.00173 ± 0.00003
OR1d2m-39	LD	– 31 ± 22	62 ± 22	0.00020 ± *
OR1d3m-27	LD	391 ± 7	7649 ± 32	0.038 ± 0.00016
OR1d3m-20	LD	38 ± 16	4138 ± 71	0.03778 ± 0.00065
OR1d3m-17	LD	– 16 ± 15	1314 ± 32	0.02534 ± 0.00062
OR1d3m-24	LD	23 ± 40	6643 ± 156	0.01322 ± 0.00031
OR1d3m-2	LD	– 31 ± 15	260 ± 18	0.00378 ± 0.00026
OR1d3m-16	LD	– 13 ± 17	710 ± 26	0.00251 ± 0.00009

Table 4.4 – continued from previous page

Grain Label	Type	$\delta^{25}Mg/^{24}Mg$ (‰)	$\delta^{26}Mg/^{24}Mg$ (‰)	$^{26}Al/^{27}Al$
OR1d3m-15	LD	– 18 ± 17	79 ± 17	0.00108 ± *
OR1d3m-6	LD	– 9 ± 21	453 ± 27	0.00098 ± 0.00006
OR1d3m-4	LD	– 3 ± 16	216 ± 18	0.00095 ± 0.00008
OR1d4m-20	LD	1824 ± 46	3233134 ± 28488	0.69276 ± 0.0061
OR1d4m-1	LD	87 ± 19	83834 ± 618	0.62035 ± 0.00457
OR1d4m-16	LD	1 ± 18	613264 ± 4273	0.57218 ± 0.00399
OR1d4m-8	LD	2 ± 26	40367 ± 416	0.23546 ± 0.00243
OR1d4m-13	LD	79 ± 21	89976 ± 702	0.14137 ± 0.0011
OR1d4m-4	LD	27 ± 12	24650 ± 141	0.12086 ± 0.00069
OR1d4m-3	LD	– 44 ± 15	10147 ± 83	0.10378 ± 0.00085
OR1d4m-10	LD	– 43 ± 15	2449 ± 33	0.07776 ± 0.00105
OR1d4m-14	LD	69 ± 9	1398 ± 15	0.06937 ± 0.00072
OR1d4m-7	LD	48 ± 13	2505 ± 28	0.06483 ± 0.00072
OR1d4m-19	LD	– 45 ± 17	6219 ± 64	0.02872 ± 0.0003
OR1d4m-9	LD	– 15 ± 16	1779 ± 29	0.01052 ± 0.00017
OR1f2m-o67	HD	1 ± 78	1593 ± 140	0.00973 ± 0.00086
OR1f2m-38	HD	– 6 ± 42	336 ± 49	0.00047 ± 0.00007
OR1f(1,2)m-o8	HD	– 45 ± 19	52 ± 19	0.0002 ± 0.00007
OR1f2m-25	HD	18 ± 15	47 ± 14	0.00014 ± 0.00004

Table 4.5: K isotopic ratios and inferred $^{41}Ca/^{40}Ca$ ratios of graphite grains from Orgueil (Errors are 1σ)

Grain Label	Type	$^{41}K/^{39}K$	$^{41}Ca/^{40}Ca$ ($\times 10^{-3}$)
Solar		0.072	
OR1d3m-1	LD	0.07414 ± 0.00086	5.15 ± 1.94
OR1d3m-20	LD	0.07385 ± 0.00085	1.39 ± 0.58
OR1d4m-10	LD	0.10591 ± 0.00135	9.43 ± 0.30
OR1d4m-1	LD	0.07896 ± 0.00090	2.90 ± 0.36
OR1d4m-20	LD	0.07696 ± 0.00089	2.89 ± 0.51
OR1d4m-7	LD	0.07480 ± 0.00078	1.61 ± 0.45
OR1d4m-16	LD	0.07425 ± 0.00078	0.37 ± 0.14
OR1f(1,2)m-o68	HD	1.00093 ± 0.00716	10.18 ± 0.04
OR1f2m-18	HD	0.12613 ± 0.00191	10.65 ± 0.29
OR1f2m-25	HD	0.09429 ± 0.00085	5.98 ± 0.18
OR1f2m-9	HD	0.08031 ± 0.00184	2.26 ± 0.42
OR1f(1,2)m-o38	HD	0.07471 ± 0.00146	1.28 ± 0.61

Table 4.6 C, Ca and Ti isotopic ratios of LD graphite grains from OR1d

Grain	$^{12}C/^{13}C$	$^{41}Ca/^{40}Ca$ ($\times10^{-3}$)	$\delta^{42}Ca/^{40}Ca$ (‰)	$\delta^{43}Ca/^{40}Ca$ (‰)	$\delta^{44}Ca/^{40}Ca$ (‰)	$^{44}Ti/^{48}Ti$ ($\times10^{-3}$)	$\delta^{46}Ti/^{48}Ti$ (‰)	$\delta^{47}Ti/^{48}Ti$ (‰)	$\delta^{49}Ti/^{48}Ti$ (‰)	$\delta^{50}Ti/^{48}Ti$ (‰)
OR1d3m-2	115	[a]	36 ± 17	71 ± 25	35 ± 17	[c]	– 25 ± 42	53 ± 31	1597 ± 85	[b]
OR1d3m-5	2478	[a]	– 5 ± 22	154 ± 43	222 ± 22	[c]	-507 ± 151	– 21 ± 318	138 ± 280	[b]
OR1d3m-6	127	[a]	– 5 ± 16	– 13 ± 20	– 6 ± 16	[c]	– 39 ± 36	21 ± 21	396 ± 19	259 ± 97
OR1d3m-7	11	[a]	37 ± 18	28 ± 27	58 ± 18	[c]	235 ± 66	367 ± 56	383 ± 59	[b]
OR1d3m-14	92	[a]	– 7 ± 15	– 32 ± 18	– 5 ± 16	[c]	157 ± 44	171 ± 28	176 ± 24	185 ± 22
OR1d3m-18	76	[a]	4 ± 19	52 ± 31	29 ± 18	[c]	61 ± 40	– 26 ± 20	479 ± 20	144 ± 38
OR1d3m-20	73	1.4 ± 0.6	8 ± 16	41 ± 21	40 ± 17	[c]	237 ± 49	173 ± 28	525 ± 30	[b]
OR1d3m-23	92	[a]	3 ± 16	12 ± 23	3 ± 16	[c]	280 ± 64	341 ± 51	104 ± 47	[b]
OR1d3m-24	93	[a]	– 2 ± 16	4 ± 22	– 9 ± 16	[c]	– 9 ± 38	3 ± 23	1360 ± 37	[b]
OR1d3m-25	100	[a]	– 12 ± 16	– 234 ± 16	– 13 ± 16	[c]	135 ± 43	81 ± 23	628 ± 37	[b]
OR1d3m-27	96	[a]	– 2 ± 17	51 ± 27	– 11 ± 16	[c]	35 ± 42	32 ± 30	1326 ± 60	[b]
OR1d4m-3	2279	[a]	156 ± 22	417 ± 52	60 ± 11	[c]	– 16 ± 8	– 142 ± 4	679 ± 11	186 ± 12
OR1d4m-8	14	[a]	23 ± 31	60 ± 69	1376 ± 27	6.48 ± 0.05	– 34 ± 8	– 82 ± 6	203 ± 10	[b]
OR1d4m-9	111	[a]	43 ± 26	125 ± 59	1460 ± 22	7.61 ± 0.05	– 161 ± 13	– 135 ± 13	199 ± 25	[b]
OR1d4m-10	109	9.4 ± 0.3	477 ± 34	1534 ± 96	185 ± 17	[c]	94 ± 52	– 174 ± 41	984 ± 91	[b]
OR1d4m-13	107	[a]	– 11 ± 16	– 114 ± 31	– 21 ± 8	[c]	– 20 ± 31	241 ± 38	98 ± 42	[b]
OR1d4m-14	23	[a]	14 ± 18	139 ± 39	131 ± 10	[c]	– 108 ± 11	– 66 ± 12	358 ± 26	[b]
OR1d4m-16	104	0.4 ± 0.1	71 ± 10	202 ± 18	1 ± 4	[c]	– 57 ± 16	– 55 ± 16	587 ± 36	[b]
OR1d4m-19	9	[a]	– 11 ± 8	22 ± 13	76 ± 3	[c]	– 196 ± 38	– 135 ± 38	81 ± 54	[b]
OR1d4m-20	27	2.9 ± 0.5	103 ± 27	314 ± 65	26 ± 14	[c]	[d]	[d]	[d]	[d]

Note: Errors are 1 σ; δ values are deviations from solar ratios per mil.

[a] The Ca/K ratios for these grains were very low, making it impossible to derive a meaningful $^{41}Ca/^{40}Ca$ ratio from the ^{41}K excess.

[b] Not reported, because the ^{50}Cr contribution to the ion signal of these grains was calculated to be $\sim$ 60 %, increasing the uncertainty of the results.

[c] Did not derive $^{44}Ti/^{48}Ti$ ratios for these grains because the $\delta^{44}Ca/^{40}Ca$ values are comparable to the $\delta^{42}Ca/^{40}Ca$ and $\delta^{43}Ca/^{40}Ca$ values.

[d] Not measured because of very low Ti signal.

Table 4.7: δ^{44}Ca values and inferred ^{44}Ti/^{48}Ti isotopic ratios of graphite grains from Orgueil (Errors are 1 σ)

Grain	Type	δ^{42}Ca/^{40}Ca (‰)	δ^{43}Ca/^{40}Ca (‰)	δ^{44}Ca/^{40}Ca (‰)	^{44}Ti/^{48}Ti ($\times 10^{-3}$)
OR1d4m-8	LD	23 ± 31	60 ± 69	1376 ± 27	6.481 ± 0.050
OR1d4m-9	LD	43 ± 26	125 ± 59	1460 ± 22	7.612 ± 0.048
OR1f2m-1	HD	– 152 ± 96	156 ± 239	6018 ± 203	0.440 ± 0.004
OR1f2m-25	HD	93 ± 22	90 ± 42	1584 ± 26	2.376 ± 0.010
OR1f2m-38	HD	– 118 ± 177	– 602 ± 274	51886 ± 1499	1.837 ± 0.011
OR1f(1,2)m-o67	HD	63 ± 52	15 ± 107	3767 ± 77	1.767 ± 0.010

Table 4.8 C, Ca and Ti isotopic ratios of HD graphite grains from OR1f

Grain	$^{12}C/^{13}C$	$^{41}Ca/^{40}Ca$ ($\times10^{-3}$)	$\delta^{42}Ca/^{40}Ca$ (‰)	$\delta^{43}Ca/^{40}Ca$ (‰)	$\delta^{44}Ca/^{40}Ca$ (‰)	$^{44}Ti/^{48}Ti$ ($\times10^{-3}$)	$\delta^{46}Ti/^{48}Ti$ (‰)	$\delta^{47}Ti/^{48}Ti$ (‰)	$\delta^{49}Ti/^{48}Ti$ (‰)	$\delta^{50}Ti/^{48}Ti$ (‰)
OR1f2m-1	14	[a]	– 152 ± 96	156 ± 239	6018 ± 203	0.440 ± 0.004	– 15 ± 8	– 28 ± 9	161 ± 11	44 ± 15
OR1f2m-9	18	2.3 ± 0.4	16028 ± 316	27641 ± 805	9396 ± 151	[c]	35032 ± 4432	1376 ± 371	2278 ± 298	32827 ± 4594
OR1f2m-13	836	[a]	77 ± 48	142 ± 104	157 ± 30	[c]	613 ± 116	318 ± 129	966 ± 209	[b]
OR1f2m-18	1545	10.6 ± 0.3	992 ± 58	4057 ± 201	2042 ± 46	[c]	522 ± 98	2119 ± 354	2648 ± 204	[b]
OR1f2m-21	472	[a]	– 42 ± 46	48 ± 103	– 13 ± 28	[c]	387 ± 66	80 ± 59	679 ± 123	1722 ± 337
OR1f2m-22	94	[a]	– 7 ± 4	6 ± 8	5 ± 2	[c]	446 ± 31	413 ± 32	482 ± 39	472 ± 46
OR1f2m-25	743	6.0 ± 0.2	93 ± 22	90 ± 42	1584 ± 26	2.376 ± 0.010	58 ± 5	– 32 ± 12	754 ± 20	214 ± 23
OR1f2m-29	10	[a]	1451 ± 50	1628 ± 100	540 ± 24	[c]	[d]	[d]	[d]	[d]
OR1f2m-33	574	[a]	– 5 ± 58	9 ± 122	104 ± 37	[c]	477 ± 24	97 ± 27	1237 ± 38	2621 ± 296
OR1f2m-34	9	[a]	5064 ± 60	7410 ± 146	2179 ± 25	[c]	[d]	[d]	[d]	[d]
OR1f2m-38	4	[a]	– 118 ± 177	– 602 ± 274	51886 ± 1499	1.837 ± 0.011	– 77 ± 12	– 98 ± 15	125 ± 6	242 ± 6
OR1f2m-39	332	[a]	21 ± 38	– 30 ± 79	– 19 ± 22	[c]	285 ± 100	78 ± 79	614 ± 64	4224 ± 1568
OR1f2m-40	11	[a]	3375 ± 65	3662 ± 138	554 ± 22	[c]	[d]	[d]	[d]	[d]
OR1f(1,2)m-o65	546	[a]	340 ± 120	294 ± 252	26 ± 63	[c]	1180 ± 30	310 ± 20	1798 ± 37	7416 ± 154
OR1f(1,2)m-o67	4	[a]	63 ± 52	15 ± 107	3767 ± 77	1.767 ± 0.010	2 ± 4	14 ± 4	169 ± 5	236 ± 6
OR1f(1,2)m-o68	245	10.2 ± 0.0	996 ± 13	2839 ± 41	289 ± 7	[c]	1975 ± 160	327 ± 98	1562 ± 169	2184 ± 329

Note: Errors are 1 σ; δ values are deviations from solar ratios per mil.
[a] The Ca/K ratios for these grains were very low, making it impossible to derive a meaningful $^{41}Ca/^{40}Ca$ ratio from the ^{41}K excess.
[b] Not reported, because the ^{50}Cr contribution to the ion signal of these grains was calculated to be $\sim$ 60 %, increasing the uncertainty of the results.
[c] Did not derive $^{44}Ti/^{48}Ti$ ratios for these grains because the $\delta^{44}Ca/^{40}Ca$ values are comparable to the $\delta^{42}Ca/^{40}Ca$ and $\delta^{43}Ca/^{40}Ca$ values.
[d] Not measured because of very low Ti signal.

Table 4.9: Mix percentages of the different layers of a 15 $M_{\odot}$ SN (Woosley and Weaver, 1995) needed to obtain the isotopic anomalies observed in graphite grains. The C/O ratio of the resultant mix is also shown.

Zone	Mixing percentage			
	OR1d4m-3	OR1d1m-11	OR1f2m-o67	OR1f2m-25
Ni	0.00	0.00	0.00	0.00
Si/S	0.05	0.02	0.08	0.07
O/Si	0.00	0.00	0.00	0.00
O/Ne	0.00	0.00	0.00	0.00
O/C	0.00	0.00	0.00	0.00
He/C	82.10	0.57	0.09	67.28
He/N	15.00	99.41	99.83	0.00
H envelope	2.85	0.00	0.00	32.65
C/O ratio	14.20	2.24	1.54	6.10

Chapter 5

SUMMARY AND FUTURE PERSPECTIVES

The grains studied in this dissertation are genuine pieces of stardust. They represent individual stellar sources that supplied the presolar molecular cloud with highly refractory dust. Isotopic studies of these grains reveal more precise information about their parent stars (with precisions of a few percent) than do spectroscopic observations of circumstellar dust, which have typical errors of a factor of two. The present multi-element isotopic study of three hundred and forty-five presolar graphite grains from Orgueil represents a significant portion of the available data on this type of presolar grain. The following are the highlights of this dissertation:

- We were able to successfully carry out multi-element isotopic analyses on a large number of presolar graphite grains and still have material left over from the same grains to continue this endeavor.

- We confirmed supernovae to be the stellar source for a large fraction of the low-density graphite grains.

- High-density graphite grains seem to have originated from several types of stars: supernovae, low-metallicity, and born-again asymptotic giant branch stars.

- Presolar graphites from Murchison and Orgueil have some similarities, but also important isotopic and morphological differences.

- This study reiterates the need to further investigate sources of isotopic equilibration, either in the parent body or the laboratory.

- The chemical separation technique to isolate presolar graphites needs to be refined to eliminate or minimize contamination from insoluble organic matter.

- The isotopic data from Orgueil graphite grains pose a multitude of unanswered questions that call for significant improvements in stellar nucleosynthetic models and possibly require more accurate determination of nuclear cross sections.

Coordinated studies by resonant ionization mass spectrometry (RIMS) will enable us to extend this multi-element isotopic analysis to heavier elements, like Rb, Sr, Zr, Mo, Ba, etc. The evidence from the s-, r-, and p-process isotopes of these elements will place tighter constraints on the stellar sources of these grains, especially putative grains from born-again AGB stars.

Furthermore, Raman spectroscopy and TEM studies of Orgueil graphite grains will reveal clues to the physical and chemical properties of the circumstellar environments in which these grains formed. Properties of subgrains are often strongly indicative of their parent stars. A comparison of the morphologies of the different graphite grain populations from Murchison and Orgueil will also provide information on early solar system processes. The causes of the differences between the Murchison and Orgueil graphites are still unknown.

It is imperative to study presolar graphite (and other presolar phases) from different meteorites. Variations in the relative abundance of different types of grains in different classes of meteorites probe the properties of the protosolar nebula in which the parent bodies formed. The relative abundance is strongly dependent on the composition and temperature of the surrounding material. To further these attempts and to understand presolar graphite better, we have already begun the work to study these grains from the unique CI2 carbonaceous chondrite, Tagish Lake. Tagish Lake

is a new type of primitive meteorite whose composition was found to be intermediate between that of CI (e.g., Orgueil) and CM (e.g., Murchison) chondrites. Bulk isotopic studies by Brown et al. (2000), Nakamura et al. (2001), and Grady et al. (2002) have revealed that this meteorite is rich in presolar grains. It is believed to hail from the outer asteroid belt (Hiroi et al. 2001). We have completed the chemical separation procedure to extract presolar graphite grains from 34 g of Tagish Lake. The density separation is the last remaining step. One of the main objectives is to obtain graphite grains for detailed single grain studies but, along with graphite, we expect to produce separates containing presolar nanodiamond, SiC, and oxide grains. Analyses of graphite grains from this third type of primitive carbonaceous chondrite might reveal new populations with unique isotopic characteristics and also add to the graphite database that can help answer many important questions.

References

Brown P. G., Hildebrand A. R., Zolensky M. E., Grady M., Clayton R. N., Mayeda T. K., Tagliaferri E., Spalding R., MacRae N. D., Hoffman E. L., Mittlefehldt D. W., Wacker J. F., Bird J. A., Campbell M. D., Carpenter R., Gingerich H., Glatiotis M., Greiner E., Mazur M. J., McCausland P. J., and Plotkin H. (2000) The fall, recovery, orbit, and composition of the Tagish Lake meteorite: a new type of carbonaceous chondrite. Science 290, 320-325.

Grady M. M., Verchovsky A. B., Franchi I. A., Wright I. P., and Pillinger C. T. (2002) Light element geochemistry of the Tagish Lake CI2 chondrite: Comparison with CI1 and CM2 meteorites. Meteorit. Planet. Sci. 37, 713-735.

Hiroi T., Zolensky, M.E., and Pieters, C.M. (2001) The Tagish Lake meteorite: A possible sample from a D-type asteroid, Science, 293, 2234-2236.

Nakamura T., Noguchi T., Zolensky M. E., and Takaoka N. (2001) Noble gas iso-

topic signatures and x-ray and electron diffraction characteristics of Tagish Lake carbonaceous chondrite. Lunar Planet. Sci. XXXII, Abstract #1621.